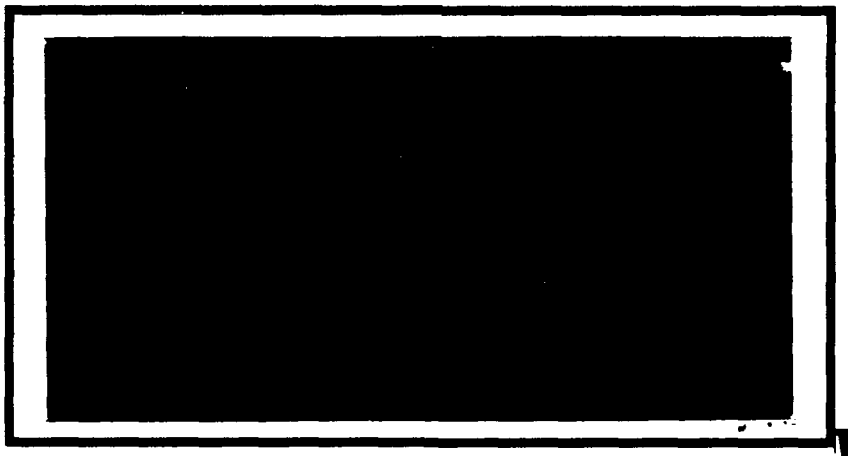

DEPARTMENT OF THE AIR FORCE

AIR UNIVERSITY

AIR FORCE INSTITUTE OF TECHNOLOGY

Wright-Patterson Air Force Base, Ohio

AFIT/GAE/AA/88D-11

INVESTIGATION OF THE FLOWFIELD CREATED BY THE INTERACTION OF A SONIC JET AND A CO-FLOWING SUPERSONIC STREAM

THESIS

Benoit J. Durand
Captain, Canadian Forces

AFIT/GAE/AA/88D-11

Approved for public release; distribution unlimited

AFIT/GAE/AA/88D-11

INVESTIGATION OF THE FLOWFIELD CREATED BY THE INTERACTION OF A SONIC JET AND A CO-FLOWING SUPERSONIC STREAM

THESIS

Presented to the Faculty of the School of Engineering

of the Air Force Institute of Technology

Air University

In Partial Fulfillment of the

Requirements for the Degree of

Master of Science in Aeronautical Engineering

Benoit J. Durand, BEng, PEng

Captain, Canadian Forces

December 1988

Preface

This experimental investigation originated with the work of Major John Traxler. Most particularly, this report describes my work towards understanding two-dimensional flow mixing and gas dynamics of dissimilar flows in the sonic and supersonic arena. Emphasis was put on flow visualization techniques as well as the graphical treatment of data.

I would like to thank Dr. William C. Elrod, my faculty advisor for showing me the ropes in experimental procedures and for supporting me technically throughout this study.

I am also greatly indebted for the help of Capt Fred Tanis and for the excellent and professional work of John Brohas and Jay Anderson, and of all technicians that participated in any way in the experimental set-up.

I wish to acknowledge my sponsor and originator of this study, Dr. Edward T. Curran, Chief Scientist of the Aero Propulsion Lab, Wright Patterson Air Force Base.

Finally, my biggest thanks goes to my wife Danielle and son Guillaume whom kept me from loosing my motivation during all the hard time we went through.

Benoit J. Durand

Table of Contents

List of Figures

List of Tables

List of Symbols

a_1	Speed of sound of fast stream
a_2	Speed of sound of slow stream
A	Area
f	Focal length
M	Mach number, Magnification (schlieren photograph)
M_c	Convective Mach number
mv	Millivolts
P	Pressure (static if no subscript), distance for schlieren system set-up
Q	Distance for schlieren system set-up
R	Gas constant for air
T	Temperature (static if no subscript)
U_c	Shear layer velocity
U_1	Free stream velocity of fast stream
U_2	Free stream velocity of slow stream
S/N	Serial number

Greek letters

δ	Delta - Boundary layer thickness
γ	Gamma - Ratio of specific heats
θ	Deflection angle

Subscript

b	Refers to base conditions
e	Refers to nozzle exit plane conditions
0	Refers to stagnation condition

Superscript

*	Refers to condition where M = 1 (sonic condition)
'	Refers to secondary flow

Abstract

The flowfield characteristics created by a sonic flow expanding freely between two supersonic streams were investigated experimentally using optical and pressure instrumentation. The base flow produced by the expansion of the streams around the base regions is compared to experimental data and theory by Chow (2).

Furthermore, the shear layer created between the sonic and supersonic stream is studied using schlieren photographs and pitot pressure profiles. The growth of the shear layer is examined in an effort to explain the observed flow phenomenon.

It was observed that a shear layer crossing a shock wave spreads and increases its turbulence level. However, an undesirable loss in total pressure results and this could be undesirable.

It appears that Chow's theory on base pressure approximates the characteristic of the flow near the end of the nozzle assembly where the two flows initially interact. The same trends were observed in the behavior of base pressure with increasing secondary total pressure as Chow observed during his experiment.

The convective Mach number concept was successfully applied to the sonic injection geometry and it was demonstrated that the convective Mach number decreases drastically as the secondary pressure is increased. This is an indication that the growth rate of the shear layer increases, giving a faster mixing rate.

INVESTIGATION OF THE FLOWFIELD CREATED BY THE INTERACTION OF A SONIC JET AND A CO-FLOWING SUPERSONIC STREAM

I. Introduction

The supersonic transport airplane is today a hot discussion item around the free world. A great amount of time and money has been spent in the USA with the National Aerospace Plane and in France with the Hermes program. With a flight Mach number between 5 and a possible 25, those aircraft will need an efficient propulsion system that does not exist today. At those speeds, a supersonic combustion ramjet (scramjet) will provide superior performance compared to a conventional ramjet engine (which burns fuel at subsonic speed). This conclusion was reached some time ago, before interest in high speed transport started to build up again (7).

Background

The performance of hydrogen-fueled engines as reviewed by Curran and others (3) indicates strongly that the ramjet cycle, using subsonic or supersonic combustion, dominates the high speed flight regime. Figure 1 illustrates the comparison between different cycles, including the liquid propellant rocket engine, using hydrogen as fuel. It also depicts the regimes for which each airbreathing engine is

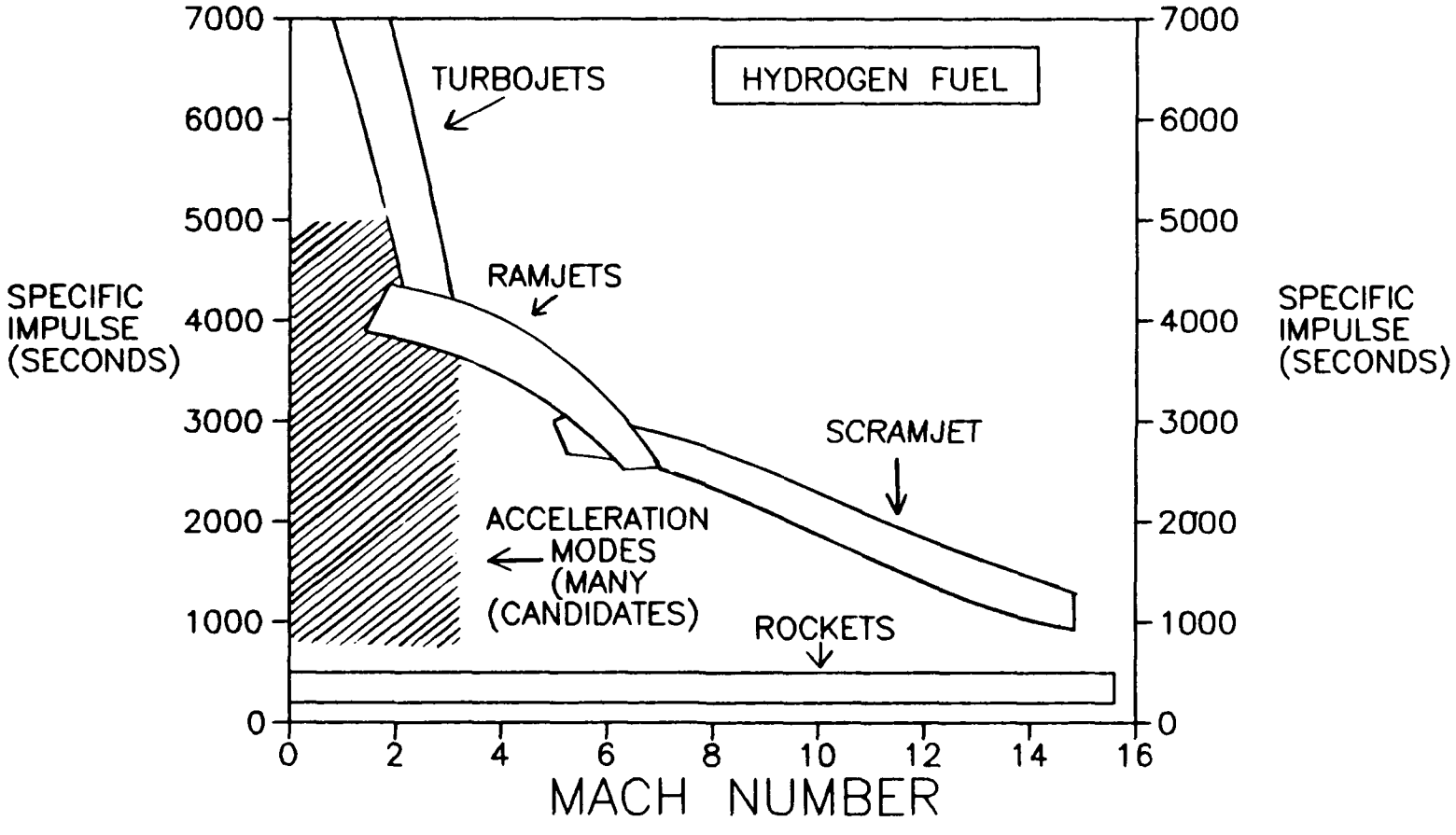

Figure 1. Performance of Hydrogen Fueled Engine (4:8)

most suited. This figure shows the scramjet "best" suited for a Mach flight of about 7 and higher. Also, it is shown that the scramjet does not satisfy the necessary low Mach number flight associated with takeoff and initial acceleration at low altitude. It is easy to prove that a conventional ramjet does not have any thrust or specific impulse below a Mach number of about 0.4. In order to provide the necessary thrust, a combined cycle idea was put forward by Billig (1) to be analyzed later by Schetz and others (13). Figure 2a) shows the boost phase configuration of the integral-rocket dual-combustion ramjet. Operating as a rocket during boost, the combustion chambers contain a solid propellant and the exit plane of the scramjet combustor is fitted with ejectable nozzles. This boost phase is characterized with high thrust and fast acceleration. When the rocket propellant is depleted, the inlet shrouds and rocket nozzles are ejected and the port covers at the entrance of both combustors are eliminated. Then, the engine works as a dual combustion ramjet. Figure 2b) illustrates this configuration. Most of the air, already compressed by the oblique shock system of the supersonic inlet, enters the supersonic combustor where it is mixed with the fuel-rich combustion products leaving the subsonic combustor. All the scramjet fuel is added in the subsonic (dump) combustor.This configuration represents sonic fuel delivery to the supersonic flow.

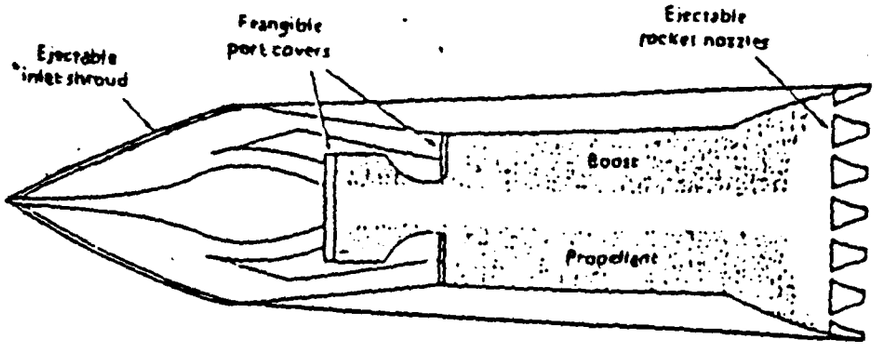

a) Boost Phase Configuration

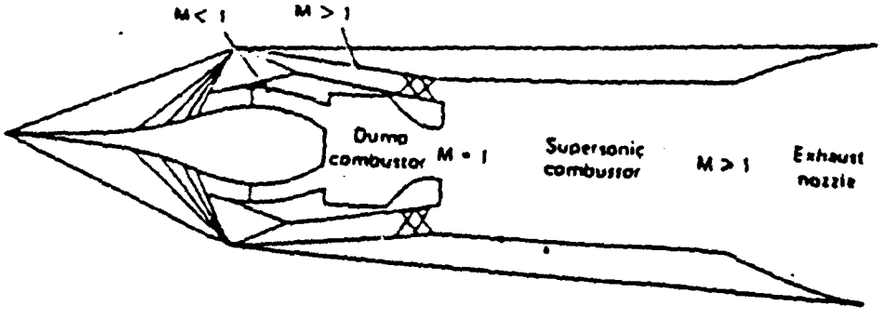

b) Dual Mode Ramjet Configuration

Figure 2. Schematic Illustration of The Integral-Rocket Dual-Combustion Ramjet. (1:417)

Another use of the scramjet was put forward by Escher and others (5) who discuss the possibility of an advanced orbital space transport propulsion system employing the combined cycle. The paper conceptualized six specific examples, one of which will be discussed here. The combination of airbreathing cycles and the rocket cycle could prove very beneficial and could provide a means to effectively put a craft in orbit while taking off from conventional runways. The specific example discussed here is a system capable of operating all modes of airbreathing cycles combined with a special rocket subsystem. Figure 3 graphically illustrates the optimum usage of each cycle, depending on specific impulse for a given flight velocity. Not shown on the figure is the cycle used to launch the craft using this new system. It is proposed to use the air augmented rocket to get the needed velocity in order to use the ramjet cycle.

This elaborate engine, diagramed by Figure 4, consists of a supersonic type inlet followed by a retractable fan subsystem. Located downstream of the fan, the rocket subsystem is placed at the exit plane of the ejector. What follows is an air liquefaction subsystem designed to produce an "Airbreathing Rocket Engine" (5:11) which gives a lightweight rocket system combined with the airbreathing cycles performance to improve overall specific impulse. The combustion products or fuel/air mixture (depending on the

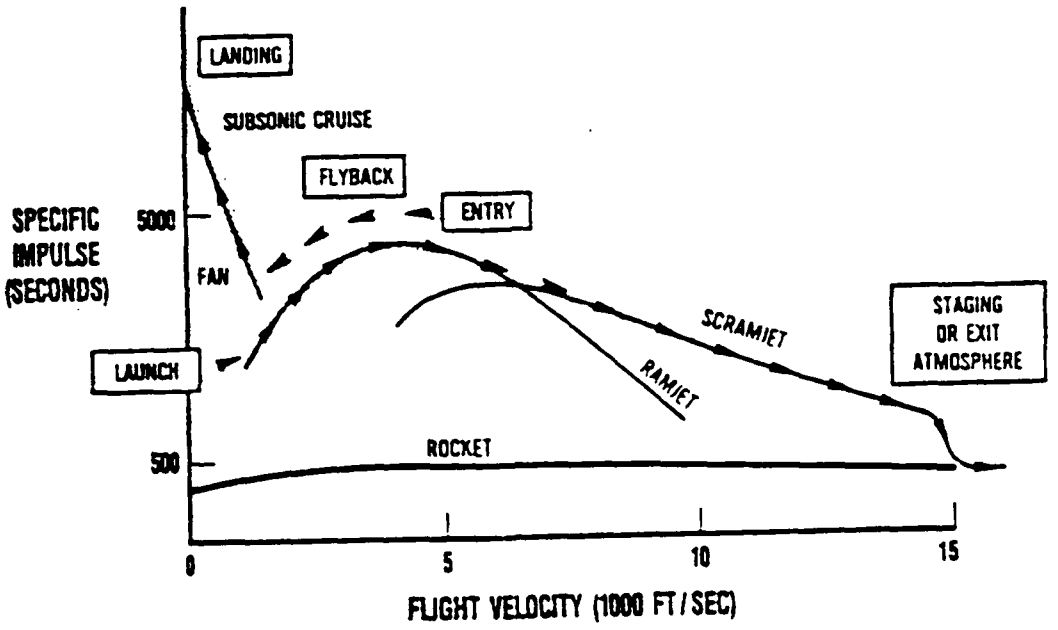

Figure 3. Performance/Flight Speed Trends (6:2)

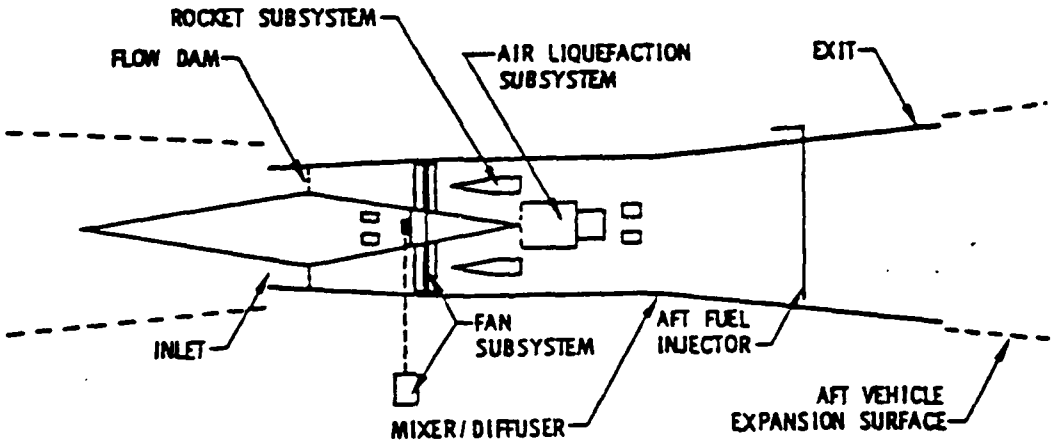

Figure 4. Representative Combined Cycle Engine (6:2)

cycle used) are then exausted. At the exit, the vehicle surface is used as an expansion surface to keep the engine to a reasonable length. The fan subsystem acts as a supercharger upstream of the ejector and provides a means to mechanically compress the air for the subsonic cruise to landing. It can be driven by an airbreathing or rocket type gas generator. This fan subsystem is stowed away at high speed to protect it from high temperature and to prevent flow blockage during the ramjet and scramjet operation. The scramjet mode is the very last airbreathing cycle used before the engine operates only with its rocket subsystem. The rocket special thrust chambers are used as a fuel injection system for the scramjet mode and both perpendicular and parallel fuel injection are used to prevent thermal choking and to enhance mixing. Once out of the atmosphere, all intakes are covered and the rocket subsystem is used for space operations. This example of airbreathing and rocket propulsion synergism may very well be the next propulsion system of the space shuttle.

With those two fascinating examples of combined cycle technology, it is easy to realize that the scramjet cycle is very important as a future propulsion system if very high speed of flight is desired. This is why studies of mixing and interaction of dissimilar flows are so important.

As it's name implies, a scramjet burns fuel in an air stream flowing at supersonic speed. The fuel can be

injected at sonic or supersonic speed. Depending on the configuration used, different gas dynamics effects such as shock waves, Mach and slip lines will develop. The fuel and air mixing process may differ greatly for parallel as compared to perpendicular injection of the fuel. For sonic parallel injection, a base region between the supersonic air stream and the fuel delivery orifice is very possible. A flow model based on two-dimensional flow past a backward facing step devised by Korst typically divides the flow into four components (10);

- the flow approaching the trailing edge
- the expansion around the trailing edge
- the mixing within the free jet boundary,
- the recompression at the end of the wake.

Experiments and studies conducted by Chow (2) using the Korst model showed that experimental data correlates with theory. Chow divided his results into three regimes based on the ratio of sonic stream total pressure to supersonic stream static pressure at the exit plane of the nozzle. This approach of studying the base pressure and downstream flowfield pressure distribution resulting from the interaction of a supersonic external stream with a sonic jet is an integral part of the present study.

Schetz and others (12) performed a theoretical and computational investigation of the same basic flow geometry as done by Chow. Their studies were based on the assumption

that a portion of the boundary layer thickness participates in the shear layer and thus in the mixing process. This assumption is consistent with the work of Donaldson (5) who studied the separation of a supersonic flow at a sharp corner. He suggested that the flow is dominated by viscous forces and that these may be sufficient to cause the separation point to be on the rear face of the step. Those viscous forces are an integral part of the mixing process.

Purpose and Scope

A lot of research has been accomplished in the past and still, the mixing process between two dissimilar flow streams is not completely understood. This mixing process is extremely important in the design of a supersonic combustor since the combustion time allowable is so low. Efficient mixing will result in a shorter combustion chamber and lighter vehicle, thus enabling a higher thrust to weight ratio.

A cold flow study of interacting flow streams was conducted. Although not effectively representing the fuel injection in the scramjet engine, cold flow studies usually provide the best start for this kind of investigation.

The main objective of this study was to investigate the interaction of a sonic flow expanding into a supersonic stream. The analysis of the shock patterns, together with the distribution of static and total pressures and Mach

number was also important. Another objective was to correlate the data with schlieren pictures to obtain an indication of mixing between the two flows.

A nozzle assembly producing sonic flow expanding into two Mach 3 flows was designed and investigated. Total and static pressure measurements were made in the region just aft of the nozzle exit plane and base pressure readings were also taken. This part of the investigation was used to understand the fundamentals of base flow. Finally pitot pressure measurements were made to get some indication of mixing and shear layer growth between the flows.

II. Experimental Apparatus

Two experimental facilities were used for this investigation. The AFIT water table was used only for flow visualization, and a steady flow air-air test section mounted on a stilling chamber was used for both flow visualization and data collection. The water table model consisted of a nozzle assembly simulating two Mach 2.85 supersonic streams flowing on each sides of a jet produced by a choked throat. A similar model was used with the gasdynamic facility. It produced the gasdynamic flow conditions which were simulated by the water table model. The supersonic streams were, however, at a theoretical Mach number of 3.0.

Water Table

The use of a water table to simulate supersonic airflow characteristics is an application of the hydraulic analogy (8). This analogy permits qualitative examination of the flow and flow visualization. Also, if used properly, the analogy can be used for quantitative approximation of supersonic airflow characteristics.

Description of Facility. The AFIT water table consists of a 4 foot (1.219 m) by 8 foot (2.438 m) glass table top between two reservoirs. The head tank provides

water upstream of the model. A gate which can be lowered to the glass floor provides a means of flow control by elevating the level of water in the head tank. The receiving tank is located at the opposite end of the table and is connected through a pipe and pump system back to the head tank, creating a recirculating flow. The flow rate can be controlled by a valve placed between the tanks and the pump. A weir is available at the receiving tank to control the water depth (back pressure) downstream of the model. An overhead projector adapted for flow visualization through the glass table top enables an image of the flow to be projected on a wall screen. Pictures of the flow characteristics can then be taken. A schematic diagram of the AFIT water table can be found in Figure 5.

The Test Section. The test section designed for the water table is made of wood and varnished to prevent water damage. The supersonic airflow conditions were simulated with water flowing through nozzles. As discussed before, this test section produced a sonic flow expanding into the center of two parallel supersonic streams. The method of characteristics was applied using a γ = 2.0 for water to design the supersonic half-nozzles. The actual wooden piece (as shown in Figure 6) is 3 feet (0.914 m) long by 14 inches (0.356 m) wide and 2 inches (5.08 cm) high and produces a theoretical primary flow exit Mach number of 2.85 when using a throat dimension of 3 inches (7.62 cm) and an exit width

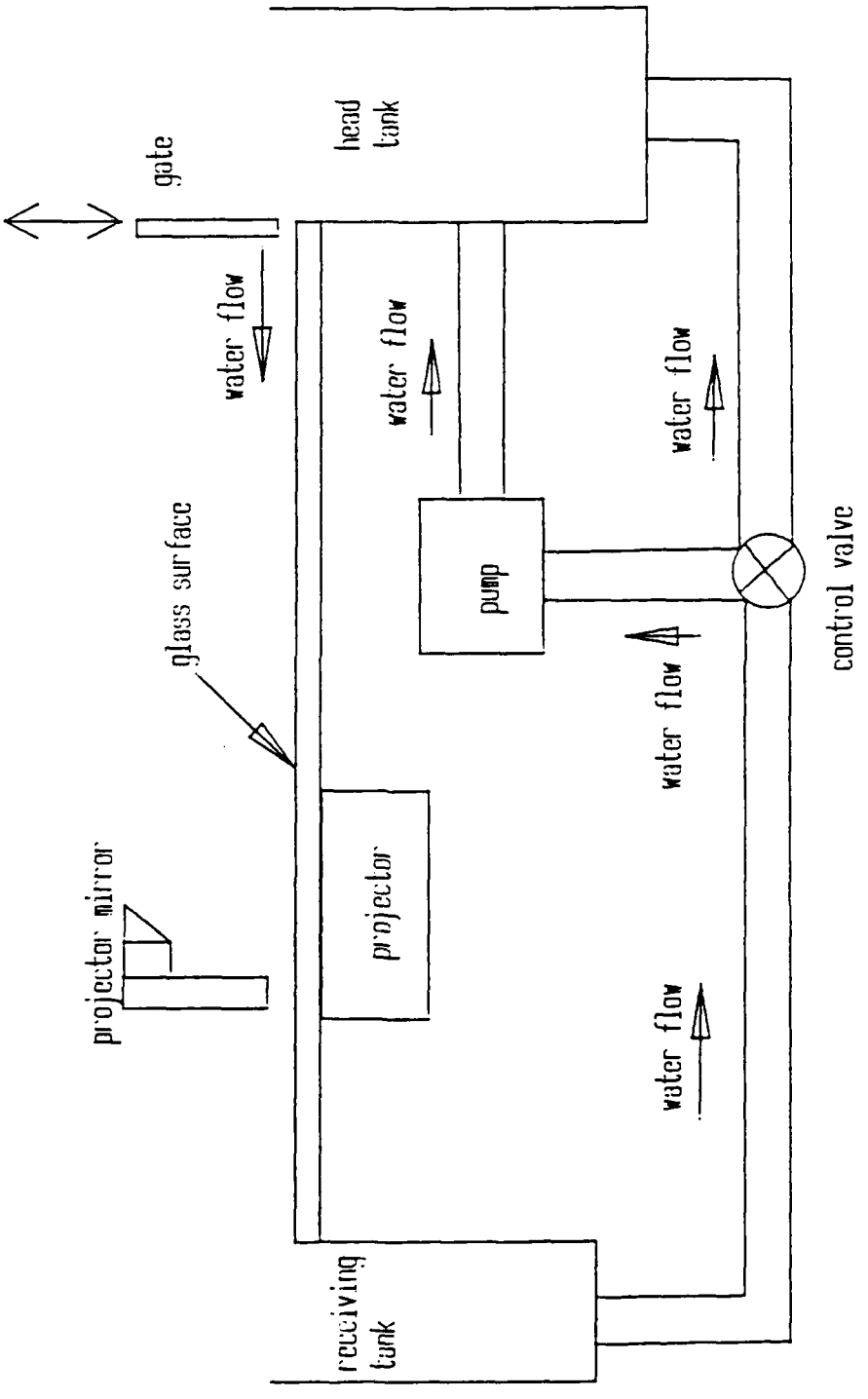

Figure 5. The AFIT Water Table

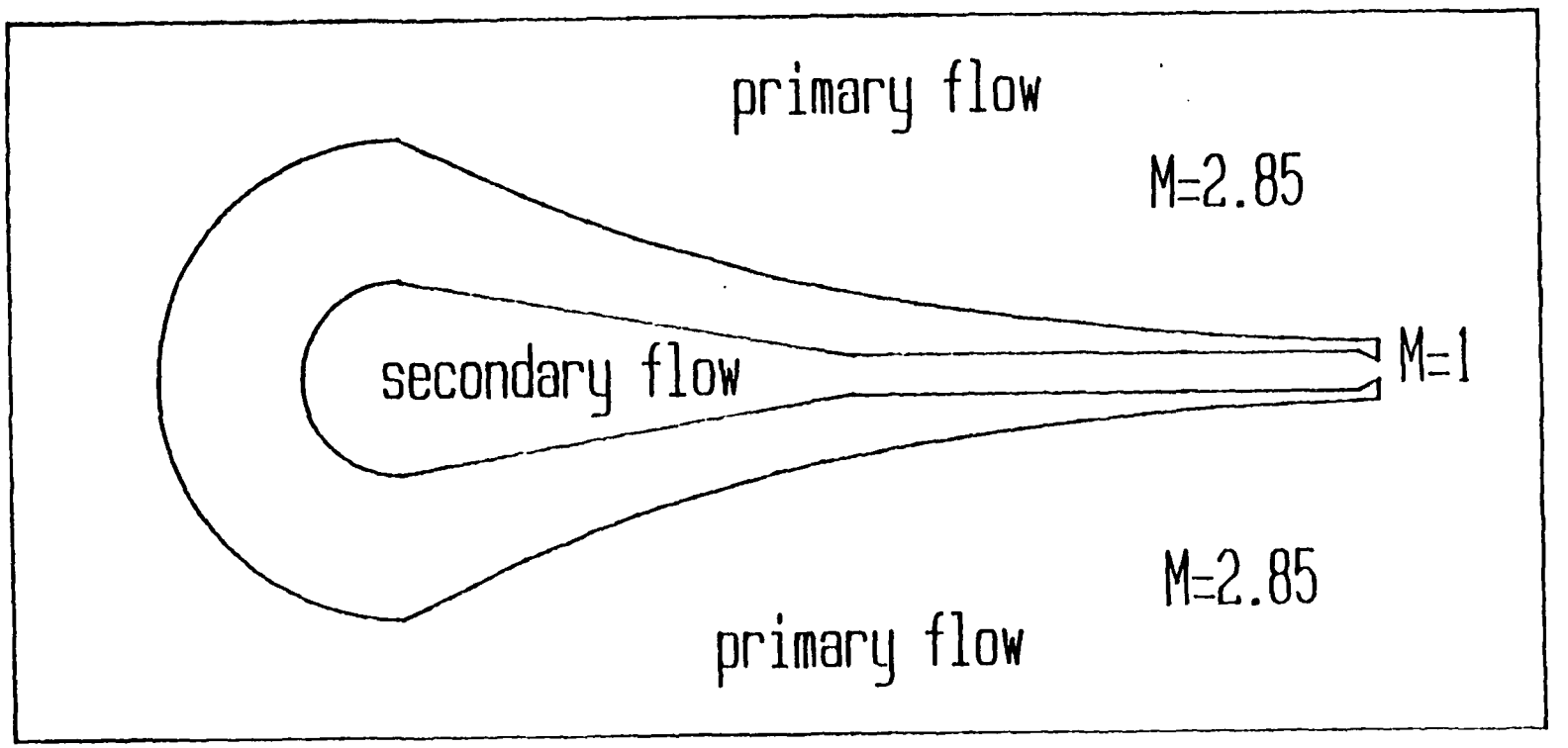

Figure 6. The Water Table Test Section

of 6.5 inches (16.51 cm). The outside nozzle flow is referred to as primary flow because the mass flow rate is higher than that for the inside nozzle assembly. The inside nozzle flow will be referred as secondary flow. The inside of the wooden nozzle assembly was designed with a throat at the exit to simulate sonic flow condition. The secondary water flow is inserted with a water hose. Since this experiment was only for flow visualization purposes, the measurement of the mass flow rate of this secondary flow was not important. The exit width of the secondary nozzle was 2 inches (5.08 cm) and produced "choked" flow when the water head inside this nozzle was high enough. An additional piece of wood of 5 by 3 by 0.25 inch (12.7 by 7.62 by 0.635 cm) was provided to be used as a gate to control water flow through the sonic nozzle. Longer pieces of straight, sealed wood provided the "sidewalls" for this model. Weights were used to hold the model down on the table surface preventing floating.

Gasdynamic Facility

Description of Facility. The steady flow gasdynamic facility was used for acquisition of experimental data and flow visualization during this investigation. Located in the AFIT School Of Engineering, it is supplied by a 100 psig (689.5 kPag) laboratory air source. The compressed air is passed through a centrifugal water and particle separator

and two sets of combination screens/filters. The last one served additionally as a baffle to straighten the airflow in the primary stilling chamber. A test section can be bolted to the end of the primary flow chamber. A second stilling chamber located underneath the primary one is fed from the same pressure source. The flow can be adjusted by a dome valve to give the desired secondary flow pressure. Four connectors are located at the end of the secondary stilling chamber and can be connected through tubes to the test section if desired. A complete schematic of the air supply can be found in Figure 7.

The Test Section. The test section was a modification of one of the test sections designed by Traxler (16). It was decided to investigate his test section in larger scale in order to give a better balance of the gas flows, shear layers and boundary layers in the flow as well as clearer indication of the mixing process between the two shear layers. The test section was made with plexiglas sidewalls 10.7 inches (27.178 cm) long, 4.375 inches (11.113 cm) wide , giving a test cavity 2.375 inches (6.033 cm) wide by 0.625 (1.588 cm) inches deep.

The nozzle assembly, shown in Figure 8, consisted of a single aluminum block centered in the test cavity. The nozzle profile for the outside supersonic nozzles was designed with the method of characteristics. An upper

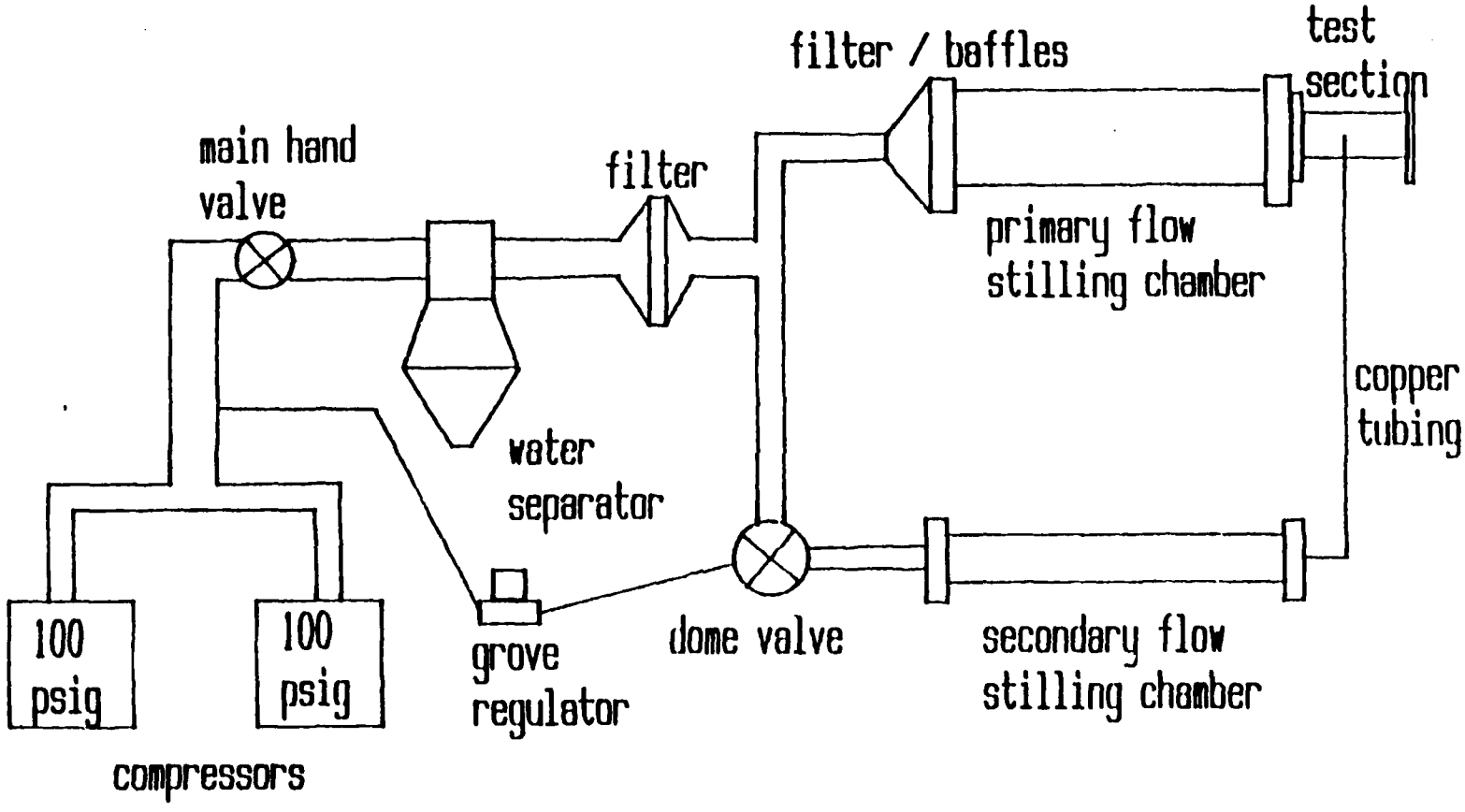

Figure 7. Schematic of Air Supply

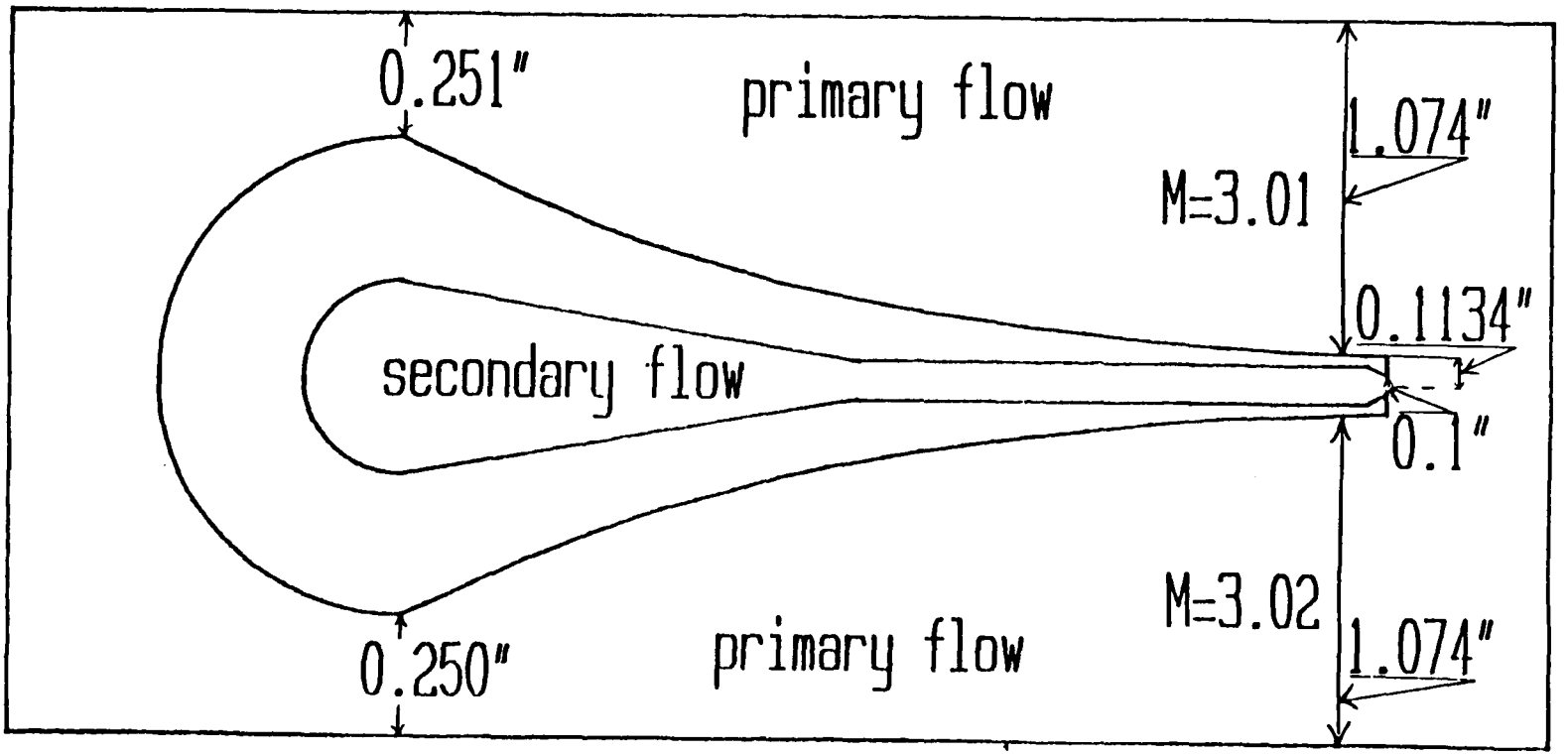

Figure 8. The Gasdynamic Test Section

throat of 0.251 by 0.625 inch (0.638 by 1.588 cm) and a lower throat of 0.250 by 0.625 inch (0.635 by 1.588 cm) together with both upper and lower exit area of 1.074 by 0.625 inch (2.728 by 1.588 cm) will give respectively design exit Mach numbers of 3.01 and 3.02. This design assumed two dimensional non-viscous isentropic flow.

The inside channel of the nozzle assembly was designed to produce a sonic secondary flow by placing a throat at the end of the straight channel. The air passed through a 0.1 by 0.625 inch (0.254 by 1.588) sonic throat with free expansion into the surrounding supersonic flow. The end or base region on each side of the nozzle assembly was 0.0634 inch (0.161 cm) high giving a total step height to centerline of 0.1134 inch (0.288 cm). The total length of the assembly was 10.7 inches (27.178 cm) with a supersonic test cavity 6 inches (15.24 cm) in length.

One of the plexiglas sidewalls was equipped with a flush mounted Endevco pressure transducer rated at 100 psia (689.5 kPa). It was located far enough upstream from the sonic exit that it gave accurate secondary flow total pressure. The other sidewall was interchangeable: a clear plexiglas wall for schlieren photography, or a wall with 67 static pressure ports for measuring the flowfield pressure distribution in the nozzles and test cavity. Twenty ports were located on the centerline from the throat to the exit of the upper supersonic nozzle. Two ports were situated in

order to give data on the nature of the secondary flow: a port just inside the throat and a port just outside the throat. Finally, 5 rows of 9 pressure ports 0.2 inch (0.508 cm) apart were located downstream of the nozzle assembly, starting 0.5 inch (1.27 cm) from the exits. The rows were one inch apart and the fifth port of each row was located on the centerline of the nozzle assembly.

The whole test section was attached to two circular aluminum plates in order to bolt it to the primary stilling chamber on one end while permitting the attachment of a diffuser on the other. This test section was designed in order to get possible correlation data with the water table test section .

Diffuser. A five inch (12.7 cm) long subsonic/supersonic diffuser was available to mount at the end of the test section. The variable ramps of the diffuser could be completely closed or opened larger than the full test cavity height. The purposes of the diffuser were as follow:

- used as straight wall to diffuse supersonic flow and lower the back pressure to the nozzle. This was needed to start the nozzles since the overall pressure ratio of the air source was limited,
- stabilizing the flow by reducing or increasing the exit area when unsteady motion was detected,
- changing the back pressure in the test cavity, and

- holding the probe traversing mechanism.

Probes. A probe holder was bolted to a one degree of freedom traversing mechanism. A probe could be placed anywhere in the test cavity but was aligned with the vertical center plane. The traversing mechanism was used for height positioning while the axial location was obtained by positioning the probe by hand.

Static Pressure Probe. A static pressure probe , built of mild steel with a outside diameter of 0.25 inch (0.635 cm) could be used for static pressure readings. The probe had a very sharp, conical nose with two pressure taps located at about 10 probe diameters downstream. It was connected to the Scanivalve or an independent pressure transducer through flexible pressure tubing.

Total Pressure Probe. A total pressure probe with the same outside diameter as the static pressure probe was used for stagnation pressure measurements. When used in supersonic flow, a bow shock is located in front of the probe and the Rayleigh Pitot tube equation must be used:

$$\frac{P_{t2}}{P_1} = \left[\frac{\gamma + 1}{2}\right] M_1^2 \left[\frac{\frac{\gamma + 1}{2} M_1^2}{\frac{2\gamma}{\gamma + 1} M_1^2 - \frac{\gamma - 1}{\gamma + 1}}\right]^{\frac{1}{(\gamma - 1)}} \quad (1)$$

where P_{t2} = Pitot total pressure

P_1 = static pressure at location of pressure measurement (upstream of the shock)

γ = ratio of specific heats

M_1 = Mach number before the shock

A pressure transducer screwed in the end of the total pressure probe permitted monitoring and recording of the pressure. This set up with sidewall static ports and total probe permitted the operator to take both static and pitot pressure measurements simultaneously at a port. Mach number of the free stream could then be calculated.

Displacement Transducer. A Research Incorporated displacement transducer S/N 3593 was mounted on top of the primary stilling chamber. The cord of the transducer was tied to the probe holding mechanism. This permitted accurate position and displacement measurements of the probe laterally and was used for pitot pressure measurements across the test section. Continuous data taking by the probe together with exact location in the test cavity produced excellent data for mixing and shear layer growth indications.

Instrumentation. The data acquisition system consisted of a QuaTech board capable of reading four channels simultaneously at frequencies up to 32000 Hz. This circuit board, which also included a digital-to-analog converter, was housed in a Zenith Z-248 micro computer. The computer

provided control of the board along with the storage of programs and data. The digital-to-analog converter was used to activate a Scanivalve S9-48. The stepping voltage coming from the computer had to be increased by a control box in order to have enough voltage to step the Scanivalve. The Scanivalve had a total of 48 ports connected to the test section pressure ports via 0.030 inch (7.62 mm) flexible pressure tubing. The QuaTech board had four different analog-to-digital converters each connected to a channel. The channels were used as follow:

Channel 0 - connected to a Druck pressure transducer, S/N 130595 for measuring pressure through the Scanivalve. The Scanivalve could be connected to static pressure ports or to probes. This channel monitored the displacement transducer when it was used,

Channel 1 - connected to an Endevco pressure transducer, S/N 94CL for measurements of the primary flow total pressure,

Channel 2 - connected to an Endevco pressure transducer, S/N WB80 for measurement of the secondary flow total pressure, and

Channel 3 - connected to an Endevco pressure transducer, S/N 29DN to measure total pressure through the total pressure probe simultaneously with static side wall pressure.

The pressure transducer used to measure total pressure of the secondary flow was installed in a clear plexiglas sidewall inside the sonic nozzle. It was placed where the area ratio A/A^* was approximately 6.5 to produce a P/P_0 of 0.9944. Effectively, the static pressure was measured but since the pressure ratio is so close to unity, it was considered to be the stagnation pressure as well.

All transducers were calibrated (see Appendix A) and were found to be linear from zero to 75% above their rated range (except the displacement transducer which has a maximum cord extension).

The resolution of the QuaTech board D/A converters was 0.244 mv. Noise in the system averaged to be 0.43 mv which translates to a maximum pressure reading error of 0.15 psia (1.034 kPa).

A diagram of the data acquisition system is shown in Figure 9.

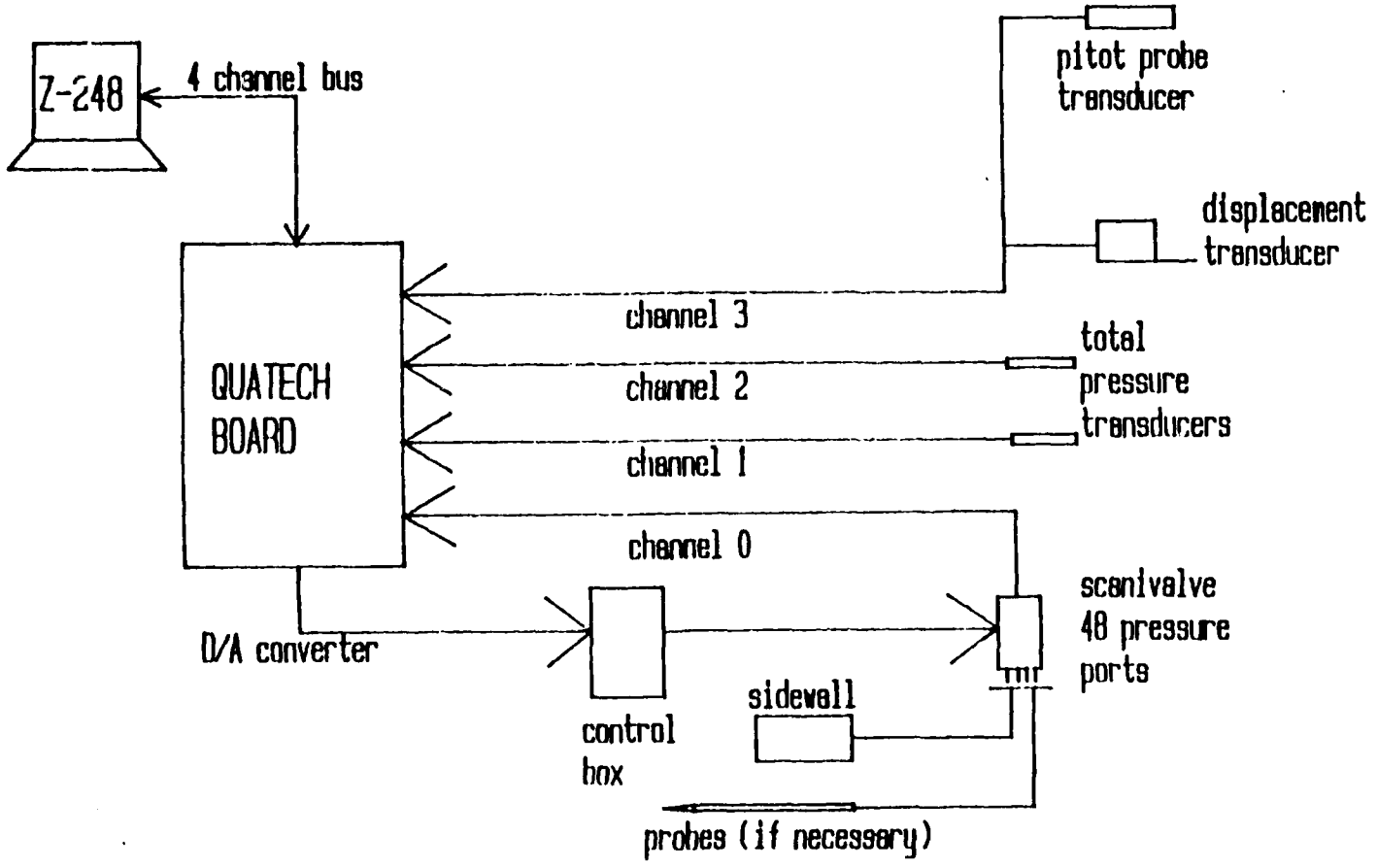

Figure 9. The Data Acquisition System

III Experimental Procedures

This chapter describes the operation of the apparatus used for the investigation. A sonic jet expanding into two supersonic air streams was simulated on the water table. Using the hydraulic analogy, supersonic air flow conditions were achieved on the water table for visualization. More detailed study was then carried out in the gasdynamic facility using a similar nozzle block designed at a much smaller scale.

Water table

Description of Operation. The operation of the water table is very simple but it is difficult to achieve a constant water flow without ripple effects at the surface of the water.

As described previously, the water table had a head tank and a receiving tank connected together through a pump and piping system. In order to start the pump, both tanks had to be filled with water. Starting the pump would then lower the level of the receiving tank and increase the water level of the head tank thus creating flow. A valve was used to control the water flow rate through the pump hence controlling the flow rate of the water on the table surface. Once acceptable flow conditions were obtained,

secondary flow could then be added to the center flow channel of the nozzle assembly. A hose connected to the laboratory water source provided the secondary flow input. Again, when acceptable conditions were met, water height readings, pictures or video could be taken.

After each run, it was nexessary to completely dry the glass top of the water table. The water was then drained from both tanks.

Flow Visualization. Many techniques exist to visualize the characteristics of the flow being simulated by the water flow on the water table. The most common is the shadowgraph method which was used extensively with success for the development of the hydraulic analogy to supersonic flow (8).

The techniques used in this investigation included shadowgraphs, normal polaroid pictures of the flow and video taping of the mixing region. A SP2000 high speed camera was used to videotape the mixing of the two flows, one of which (the secondary flow) was colored with dye. In order to see the dye on the monitor, it was necessary to place white sheets of paper underneath the glass top below the nozzle assembly. High speed video could then be taken for later studying in slow motion.

Gasdynamic Facility

Description of Operation. Operation of the steady flow test facility is fairly simple but some basic knowledge of

it is primordial for successful runs. As mentioned earlier, the gasdynamic test facility used in this investigation is connected to the AFIT 100 psig (689.5 kPa) air source line fed by two compressors hooked up in parallel. It was found that the maximum pressure available depended on the test section model used due to the compressors flow capacity. Secondary flow was obtained by opening the dome valve connected to the main line. This was done by a Grove regulator also connected to the main line. Very low and accurate secondary pressures were difficult to achieve with this system since this required operation at the extreme end of the dome valve pressure range. Therefore, a special configuration was used to obtain the very low secondary flow rates. Connections to the secondary stilling chamber were removed from the test section and replaced by a throttling valve on one side while the other was plugged. Low chamber pressure could then be attained and stabilized for the secondary nozzle with local ambient air as the source. Using this procedure, precise control of the flow was easy in the range from 2 psia (13.79 kPa) up to atmospheric pressure. It was noted that using a voltmeter to monitor the output voltage of the secondary flow total pressure transducer was very helpful. Once acceptable pressures were obtained and the flow was stabilized, pressure readings or schlieren pictures were taken.

Flow Visualization. In order to visualize the air flow conditions in the test section, a schlieren system was used. As can be seen in Figure 10, light from a Cordin model 5401 spark lamp was collimated by the top 40 inch (101.6 cm) focal length mirror. This formed a parallel light beam of 7.25 inches (18.415 cm) in diameter through the test section to a second mirror on the opposite side of the test section. This mirror was placed a suitable distance from the test section to focus the inverted image of the section on a Polaroid film. A knife edge was placed between the second mirror (at its focal point) and the film in order to produce the schlieren image. Real time viewing and video taping of the flow characteristics was feasible using a steady zirconium arc lamp and frosted glass placed at the camera film plane.

The set-up of a schlieren system is very important for clear, focused pictures. The following equation is basic to the set up for proper focus of the image in the film plane:

$$\frac{1}{f} = \frac{1}{P} + \frac{1}{Q} \qquad (2)$$

where: f = focal length of mirror

P = distance from test section centerline to mirror closest to the knife edge (bottom mirror)

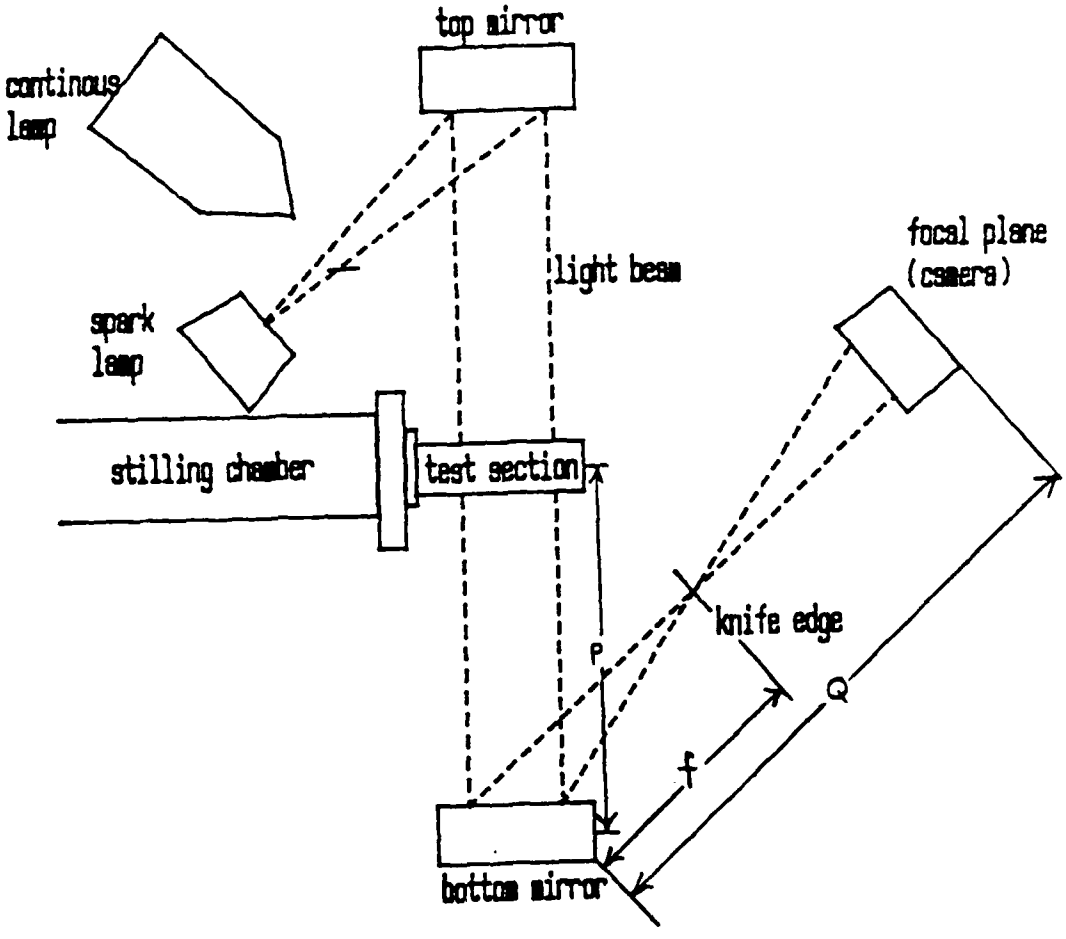

Figure 10. The Schlieren System

Q = distance from bottom mirror to film plane (screen).

Also, the distance between the top mirror and the light source had to be a focal length (f) so that parallel light passes through the test section. Bellows can be added between the knife edge and the camera to block any stray light from the film during the time that the film is exposed.

For more detailed pictures, magnification (M) can be obtained and is governed by the following equation:

$$M = \frac{Q - f}{f} \qquad (3)$$

The amount of magnification achievable was restricted by the space available in the laboratory and the type of film available. Most pictures were taken with Polaroid Type 52, ASA 400 single sheet film except for highly magnified pictures ($M \geq 2$) where Polaroid Type 57, ASA 3000 was used.

Pressure Measurements. All pressures were recorded with the data acquisition system. Since all channels of the QuaTech board had to have the same sample rate, data acquisition rate was limited by the stepping rate of the scanivalve. To ensure pressure readings were correct, the stepping rate was fixed by the computer to be about 8.5 ports per second. Accordingly it took about 5.65 seconds to complete a full scanivalve cycle of 48 ports. During this

time, each pressure was measured 50 times and the results were averaged to reduce possible errors. Very little to no decrease in total pressure was noted in the main line under the flow conditions of this investigation. Different pressure reading combinations were used depending on the analysis being performed. When necessary, pitot pressure was measured simultaneously with wall static pressure. The static pressure was read through the scanivalve while the pitot pressure probe was connected to a different channel. The pitot probe could be positioned vertically with the traversing mechanism but had to be manually positioned in the axial direction. Base pressures were also measured with the total pressure probe by positioning it a few thousandths of an inch from the backward facing step of the nozzle block. At this location, velocity in the base region is very low and the pressure read is assumed to be the base static pressure.

For more precise location of pitot pressure measurement points across the test cavity, the displacement transducer was used in conjunction with the pitot pressure probe. For this special pressure measurement, a different data acquisition rate could be utilized since the scanivalve was not used. Rates from 10000 to 32000 samples per second were used for this part of the investigation reducing the averaged error in the data acquisition system.

IV. Theoretical model

Chow's Flow Model

As discussed before, the test section represents parallel sonic injection to a supersonic stream. To fully understand the flow created by such a geometry, it is necessary to describe Chow's flow model of base bleed into the wake of blunt trailing edges (2). His model was found to be the most appropriate for the geometry of this test section. As can be seen by Figure 11, the main difference between the two experiment configurations is that our set-up investigate the interaction of two supersonic streams with the sonic flow while Chow's model has only one supersonic nozzle. The flow geometries shown in this section have been adapted to our experimental configuration, assuming that the flow is symmetrical with the centerline of the sonic nozzle.

The first region described by Chow (2:178) is for $P_0'/P_1 \leq 1$ as shown in Figure 12. The flow has been adapted to the present test section geometry. In this particular flow, secondary total pressure is very low and it is possible to create the condition where there is no mass transfer across the sonic throat. At this condition, P_0' will have a value close to the base pressure P_b. The primary flow, with $M_1 \geq 1$, expands around the sharp corner and produces a Mach number $M_2 > M_1$ and static pressure $P_2 <$

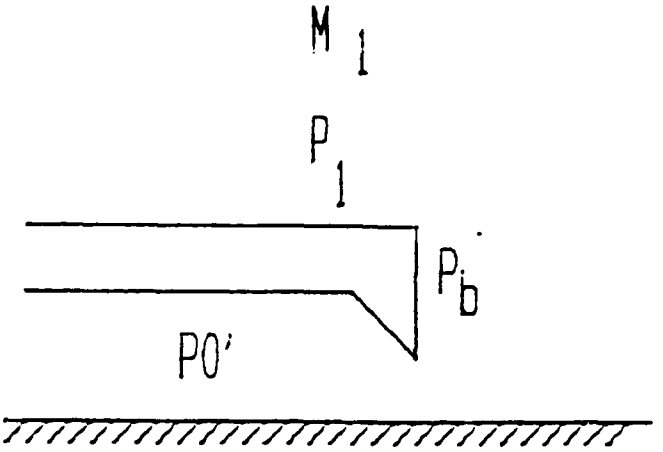

Chow's Experimental Configuration

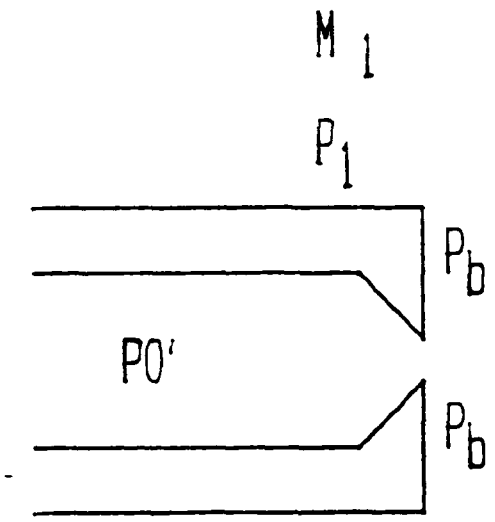

Present Experimental Configuration

Figure 11. The Difference Between Chow's (2) and the Present Experimental Configuration

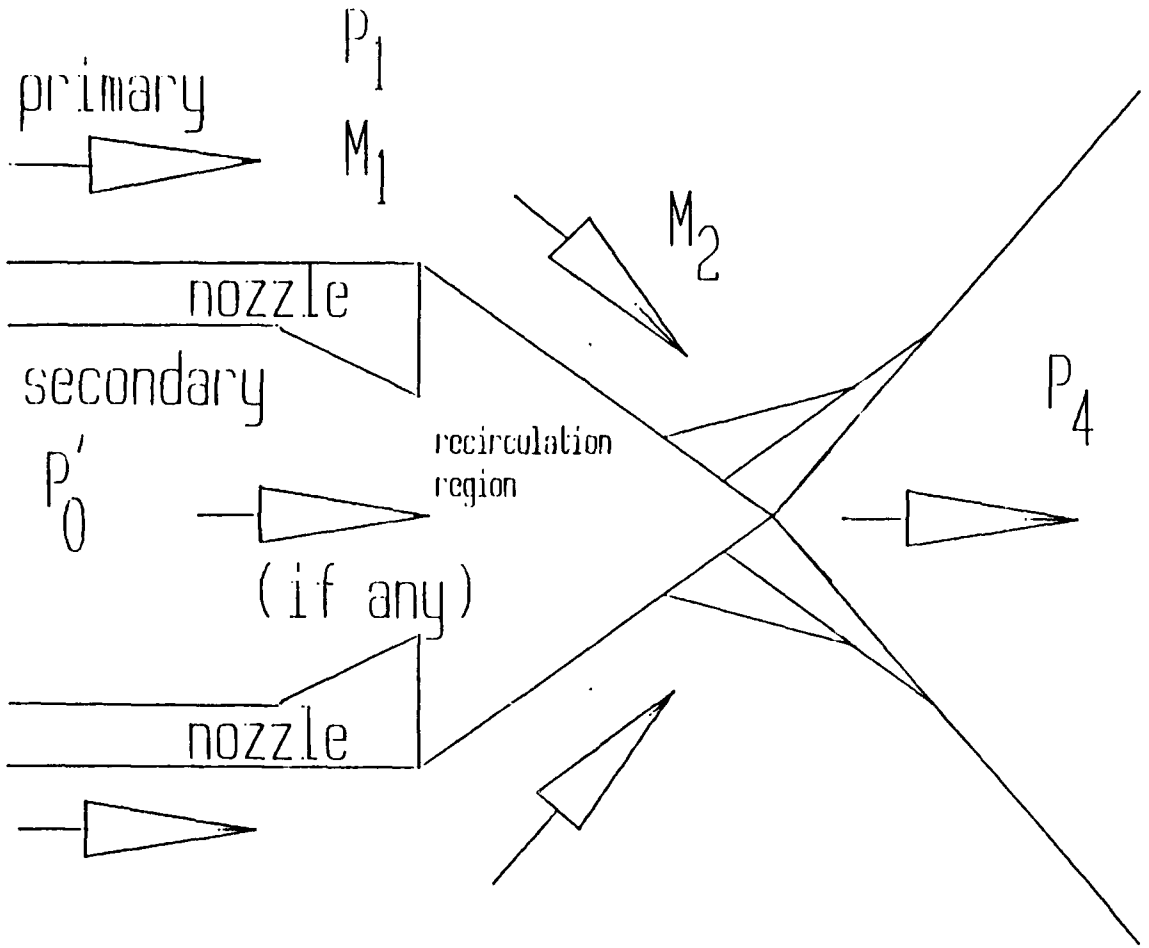

Figure 12. Chow's Flow Model - Region I

P_1. The flow deflection angle can be calculated with ideal Prandl-Meyer flow equations together with isentropic relationships. The static pressure P_2 is assumed to be equal to P_b since both regions are assumed to be at constant static pressures. If any mass flow is present through the sonic nozzle, the mass which was added to the recirculation region is pumped out by the external stream through the jet boundary streamlines, at the same rate that it was added. Figure 13 represents the relation between normalized base pressure and normalized secondary total pressure. This figure uses the experimental data gathered by Chow (2) since his experiment correlated almost perfectly to theory. The base pressure is shown to increase sharply with increasing secondary pressure P_0' in the region where $P_0'/P_0 \simeq 1$ on Figure 13, showing an almost linear relationship. At the end of the recirculation region, an oblique recompression shock redirects the flow to a path parallel with the centerline. Again, determination of the flow characteristics can be obtained by gas dynamic relationships for this region. It is of interest to note that Chow's theory predicts a relative high of the base pressure P_b at the value $P_0'/P_1 = 1$.

The term "recompression shock" will be used in this study to describe shocks formed from the interaction of the flows downstream of the nozzle. This term was also used by Korst (10) and Chow (2).

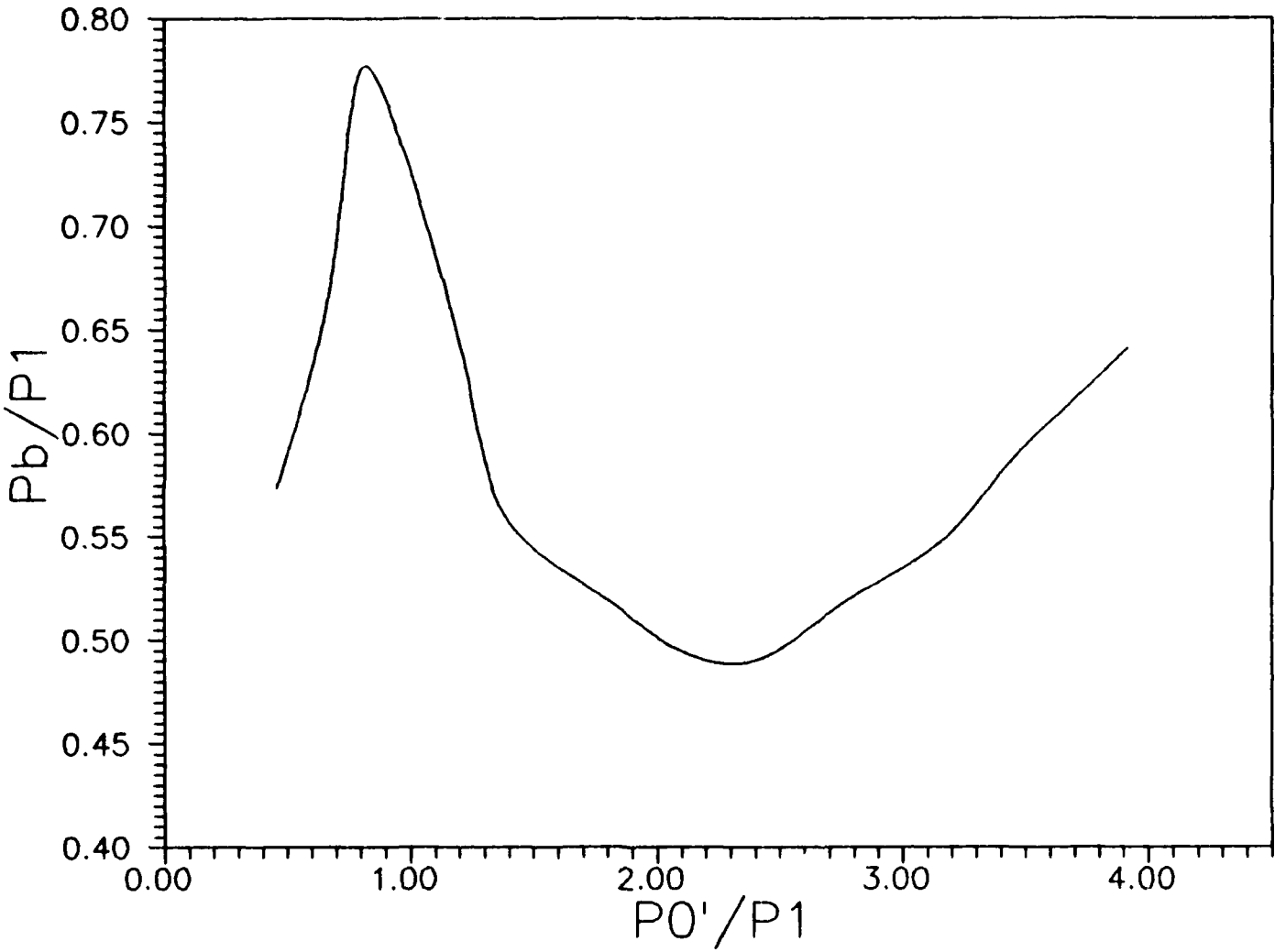

Figure 13. The Relation Between Normalized Base Pressure and Secondary Total Pressure (2:177)

Chow's region II (2:178) is described as $1 \leq P_0'/P_1 \leq \approx 2.35$ (Figure 14). The primary flow undergoes the same pattern as the flow in region I but there is enough secondary flow injected to create a subsonic jet in the center of the test cavity at the exit of the sonic nozzle. The base pressure decreases in this region as shown on Figure 13. A simple and plausible explanation would be that the subsonic jet located at the very center of the test cavity would cause the base pressure to decrease. Furthermore, since the subsonic flow static pressure is lower than the base pressure and that the conservation of mass and momentum must be satisfied between the recirculation region and the co-flowing streams, the base pressure tends to decrease when subsonic conditions exist at the exit of the sonic nozzle. At the end of the recirculation region, the flow compresses and interacts with the jet stream, creating a slipline parallel to the test cavity centerline. The shear layers between the flows initially are oriented with this slipline.

Chow's region III (3:177) is the most complicated to understand and exists for $P_0'/P_1 \geq \approx 2.35$. At those pressure ratios, the sonic nozzle flow is choked and there is a Mach number of unity at the throat. Then, the flow expands abruptly around the sharp corners and the Mach number increases dramatically. As can be seen by Figure 15, both flows expanding around the base region form a recirculation

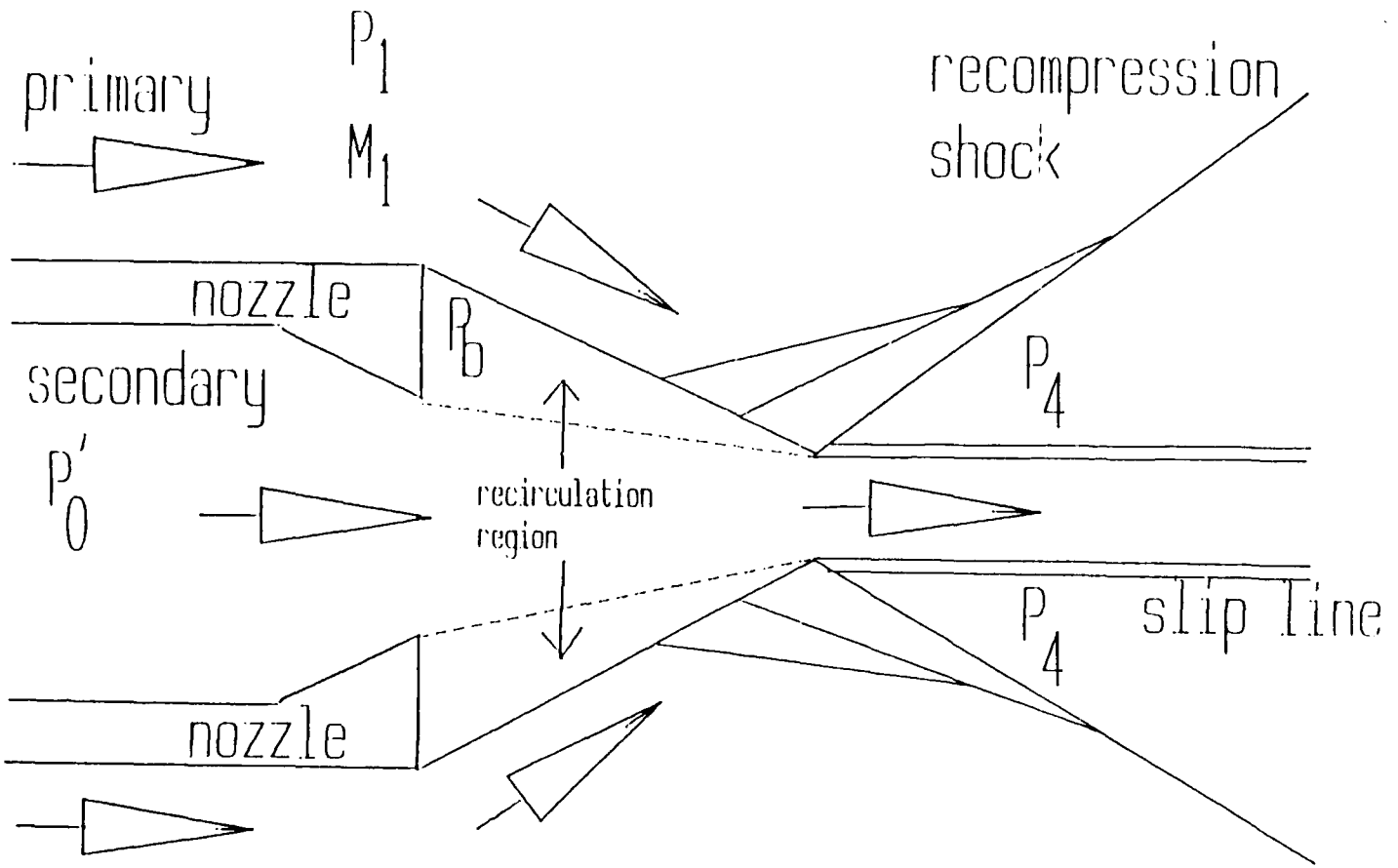

Figure 14. Chow's Flow Model - Region II

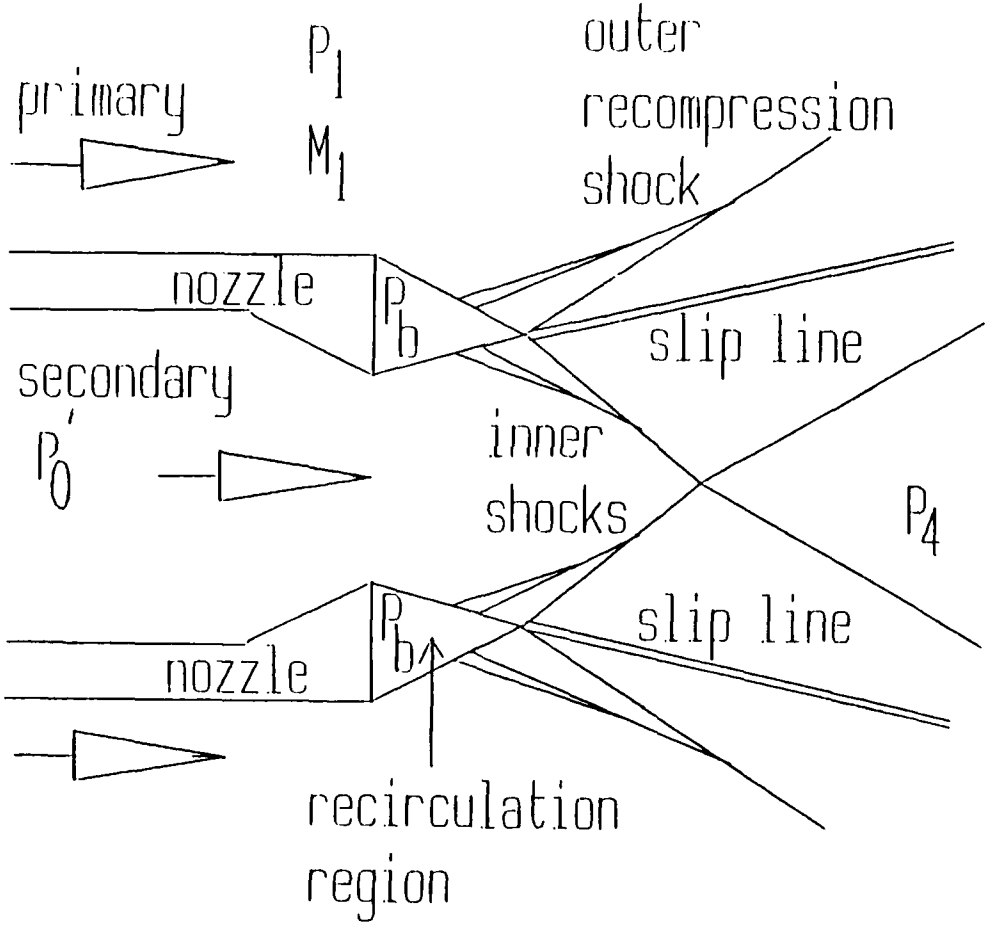

Figure 15. Chow's Flow Model - Region III

region of triangular form. The mixing process occurring at the end of the base region is at constant static pressure. Recompression of the flow happens through two oblique shocks. It is important to note that the resulting slipline always has a positive deflection angle, as shown on the figure. The slipline represents the direction of the shear layer or free mixing region.

Mathematical Model for Shear Layer Growth Rate

The development of a new mathematical model to approximate the growth of the shear layer is a complicated task and is not the aim of this investigation. However, it is interesting to use an already developed model used with a different experimental configuration.

Assuming that the shear layer is turbulent and that total temperature is conserved in the mixing process, a model was developed by Papamoschou (11) and is based on a concept of convective Mach numbers.

The convective Mach number is defined by Papamoschou as "the Mach number in a frame of reference convecting with the real phase speed of the disturbances..." (11:59) and is used as a compressibility-effect parameter throughout his study. This convective Mach number is in fact the Mach number "felt" by the shear layer caused by the co-flowing streams, one on each side of the shear layer. The important point here is the assumption that "the growth rate of the

turbulent region of the shear layer decreases drastically with increasing convective Mach number." (11:86) This result, obtained by Papamoschou, is the basis of the following development which was extracted in most part from his doctoral thesis.

The convective Mach number for two co-flowing streams is defined as

$$M_{c_1} = \frac{U_1 - U_c}{a_1} \tag{4a}$$

$$M_{c_2} = \frac{U_c - U_2}{a_2} \tag{4b}$$

where $M_{c_{1,2}}$ = convective Mach number of respective streams

U_1 = velocity of fast stream

U_2 = velocity of slow stream

U_c = velocity of shear layer

$a_{1,2}$ = speed of sound of respective stream.

In this definition, a new term, U_c is introduced and is defined as "the velocity of the dominant waves of structures" (11:72) in a compressible shear layer. For two co-flowing streams with similar ratios of specific heats,

$$U_c = \frac{a_2 U_1 + a_1 U_2}{a_1 + a_2} \qquad (5)$$

where U_c = velocity of shear layer

$U_{1,2}$ = velocity of respective stream

$a_{1,2}$ = speed of sound of respective stream.

The velocity of the streams can be calculated with known experimental values of the Mach number using gas dynamics relationships and the definition of the speed of sound for a perfect gas. One obtains

$$U = M\left\{\frac{\gamma R T_0}{\left[1 + \frac{(\gamma-1)}{2} M^2\right]}\right\}^{\frac{1}{2}} . \qquad (6)$$

where U = velocity of jet or stream

γ = ratio of specific heat

R = gas constant for flowing medium

T_0 = stagnation temperature

M = Mach number

Furthermore, it can be shown (11) that $M_{c_1} = M_{c_2}$ for co-flowing streams with similar ratios of specific heats. The convective Mach numbers can now be calculated and a relation can be established between M_c and the total pressure ratios. As the convective Mach number decreases, the growth rate of the shear layer increases as shown in Papamoschou's thesis.

V. Results and Discussion

Water Table

The water table was exclusively used for flow visualization purposes. Using the hydraulic analogy, the supersonic airflow can be qualitatively simulated with water flowing on a water table at much lower velocity.

Once the configuration of figure 6 was set up on the water table, the flow was established. Using no secondary flow, shocks forming according to Chow's flow model region I (2:178) were readily apparent with waves forming at the appropriate locations. Using tap water as a source of secondary mass injection, flow was established creating the secondary jet of Chow's flow model II (2:178). Secondary water flow was not large enough to simulate a choked sonic nozzle. To create a fully expanding flow downstream of the sonic orifice, the sonic nozzle had to be blocked to fill the cavity inside the nozzle block. Upon release of the water, the flow would be established for a short period of time and the formation of all simulated oblique shocks was visually observed. This was considered to be Chow's flow model for region III (2:177).

Three techniques were tried to record the flow characteristics. First, shadowgraph using the adapted projector was tried. It was discovered that the lighted

area of the flow was much too small to get a good appreciation of the flow. A more elaborate shadowgraph system should be used and was beyond the scope of this study. Then, a normal Polaroid picture of the water table taken from the top of the flow was tried and the shock formation on the water could not be detected accurately on film. Finally, examination of the mixing process was tried using a SP2000 high speed camera. Once the extensive lighting system was in place, die was injected in the secondary water flow. The bottom of the glass table top was covered with white paper in order to see the die on the monitor. The problem encountered here was that the ripple effect on top of the water was amplified extensively with the intense lighting. The result was that no mixing process nor flow characteristics could be recorded using this apparatus.

Good visualization of flow formation from the water table experiments was obtained. This helped to analyze the gasdynamic facility results.

Gasdynamic Facility

The analyses presented here are mostly based on static and total pressure measurements correlated with schlieren photographs. Because the flow is bounded by the test cavity sidewalls, care must be taken when analyzing data. Boundary layer effects and shock reflections become important

factors.

Steady State Assumption. The first important factor to analyze is the assumption that the flow is at a steady state. The assumption of steady flow is important, implying that there is no change of properties with time once the flow is established in the test cavity.

Figure 16 shows the total pressure of the main stilling chamber for a specific condition versus time. This particular figure illustrates a test run of about 6 seconds, the total time for a complete scanivalve cycle to be executed. As can be seen by the figure, the pressure change is less than 2 Psi (13.79 kPa), implying steady flow from the compressors for those particular tests. Figure 17 shows the stagnation pressure in the secondary stilling chamber but for a test time of about 12.5 minutes. This indicated that the airflow through the test section could be assumed to be at steady state for all tests.

Supersonic Nozzles Analysis. The investigation of the supersonic nozzles flow was started by taking schlieren pictures at different secondary flow conditions. The pictures, shown in Figure 18, were taken with the knife edge parallel and perpendicular to the flow direction. An oblique shock is present in each nozzle which may result in nonuniform exit flow conditions.

Static pressure measurements were taken on the top

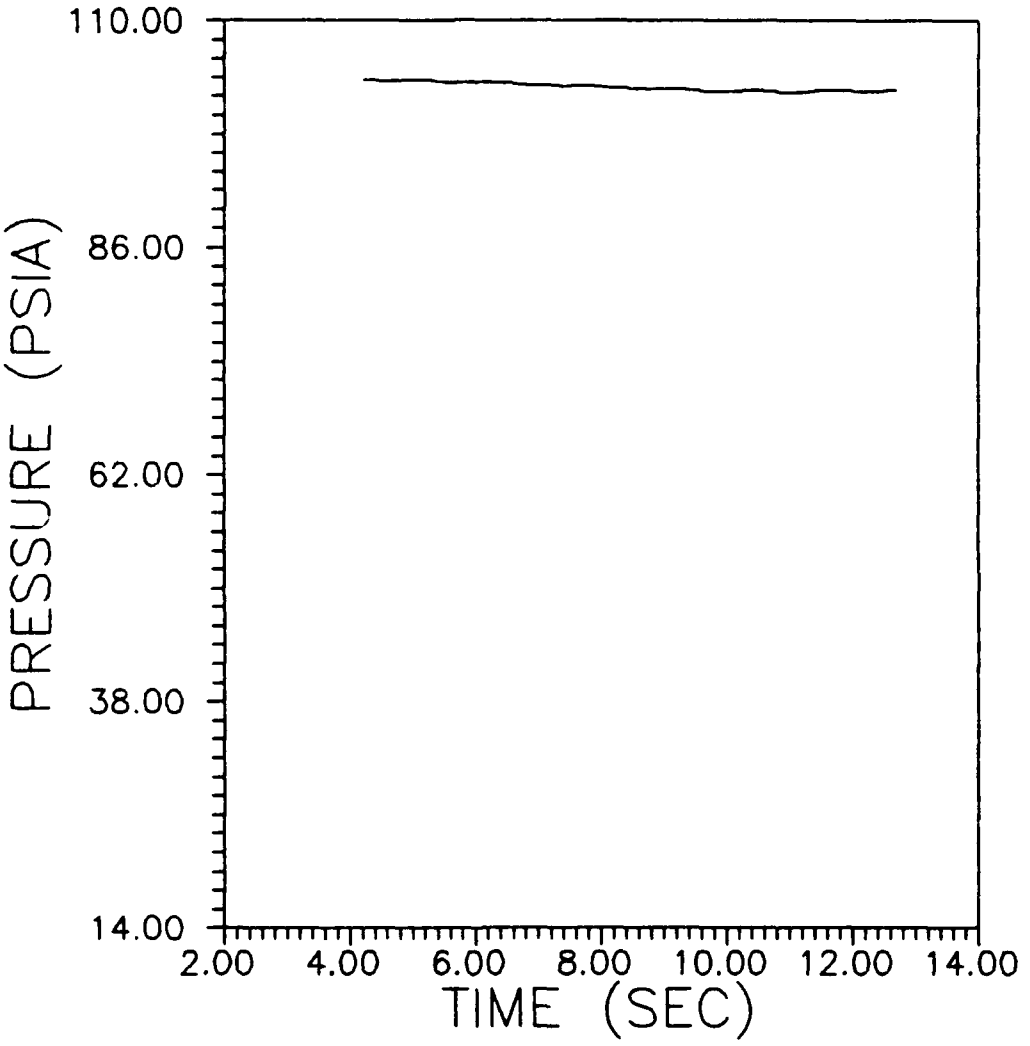

Figure 16. Primary Chamber Total Pressure VS Time

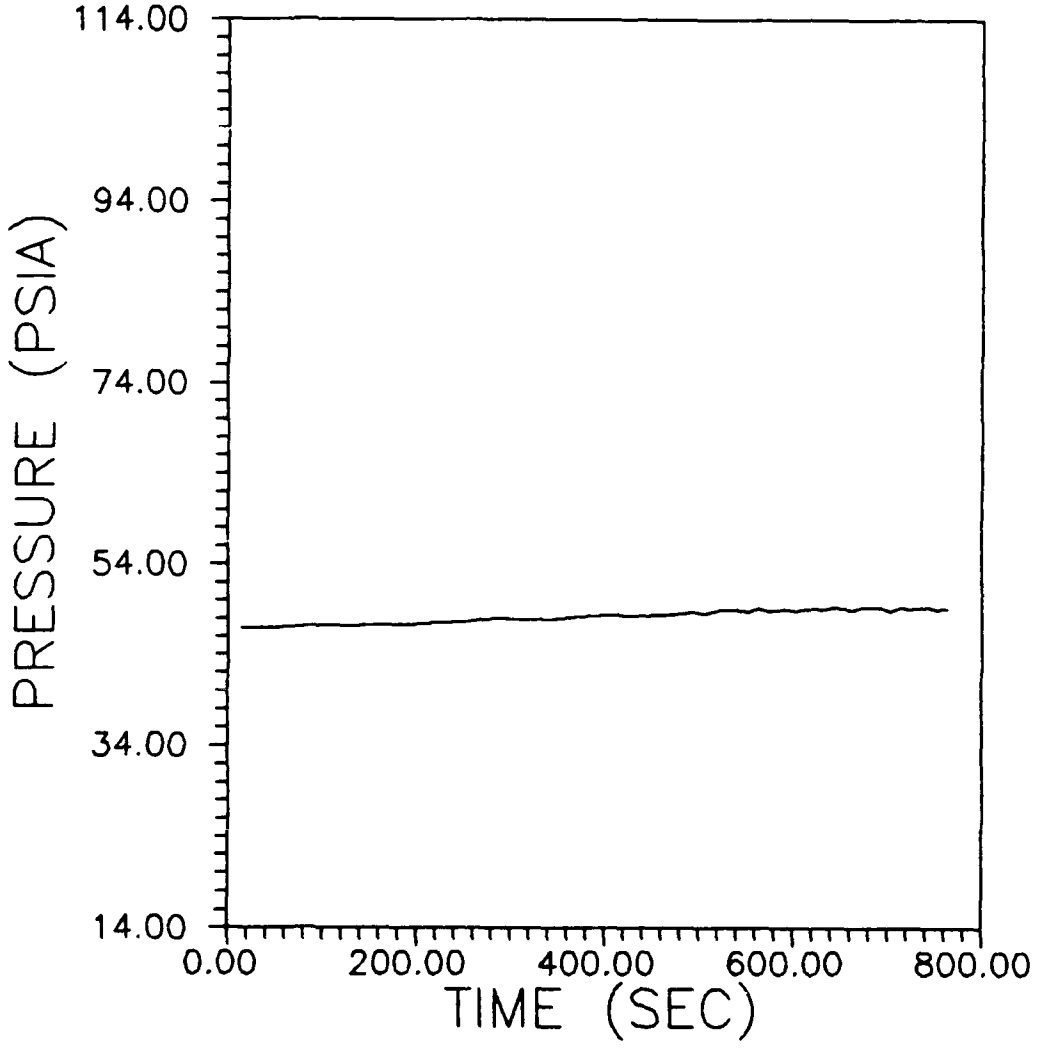

Figure 17. Secondary Chamber Total Pressure VS Time

a)

b)

Figure 18. Schlieren Photographs of Nozzle Block with
a) P_0'/P_0 = 0.02, parallel knife edge
b) P_0'/P_0 = 0.48, perpendicular knife edge

half-nozzle centerline starting from the throat to the center of the exit plane. To correlate data with photographs, more pictures of the test section were taken with the static pressure ports installed. Ten runs were made with five different secondary flow pressures and a graph of exit static pressure over primary flow total pressure versus normalized distance, where X/L = 0 at the throat, is shown in Figure 19. Since the graph shows a smooth curve with no sharp peaks, it is evident that the oblique shock visible on the schlieren pictures is a weak one and does not seem to interfere with the uniformity of the exit flow. Also, the nozzles were choked at $X/L \approx 0.02$ since the pressure ratio at that location is the one for a Mach number of one. This indicates that the first static pressure port was not located exactly at the throat but slightly upstream.

The nozzle can then be divided into four distinct regions to explain the flow conditions. For $0.02 \leq X/L \leq 0.30$, region one, the flow went through an extreme Prandl-Meyer expansion. The white region at the throat on Figures 18a) and 18b) and the large negative slope on Figure 19 clearly show this. This expansion existed mostly because the supersonic nozzles were made with a sharp throat. This design forced the flow to expand rapidly causing an extreme drop in static pressure. Region two, represented by $0.30 \leq X/L$ 0.60 was a typical expansion region. The flow expands

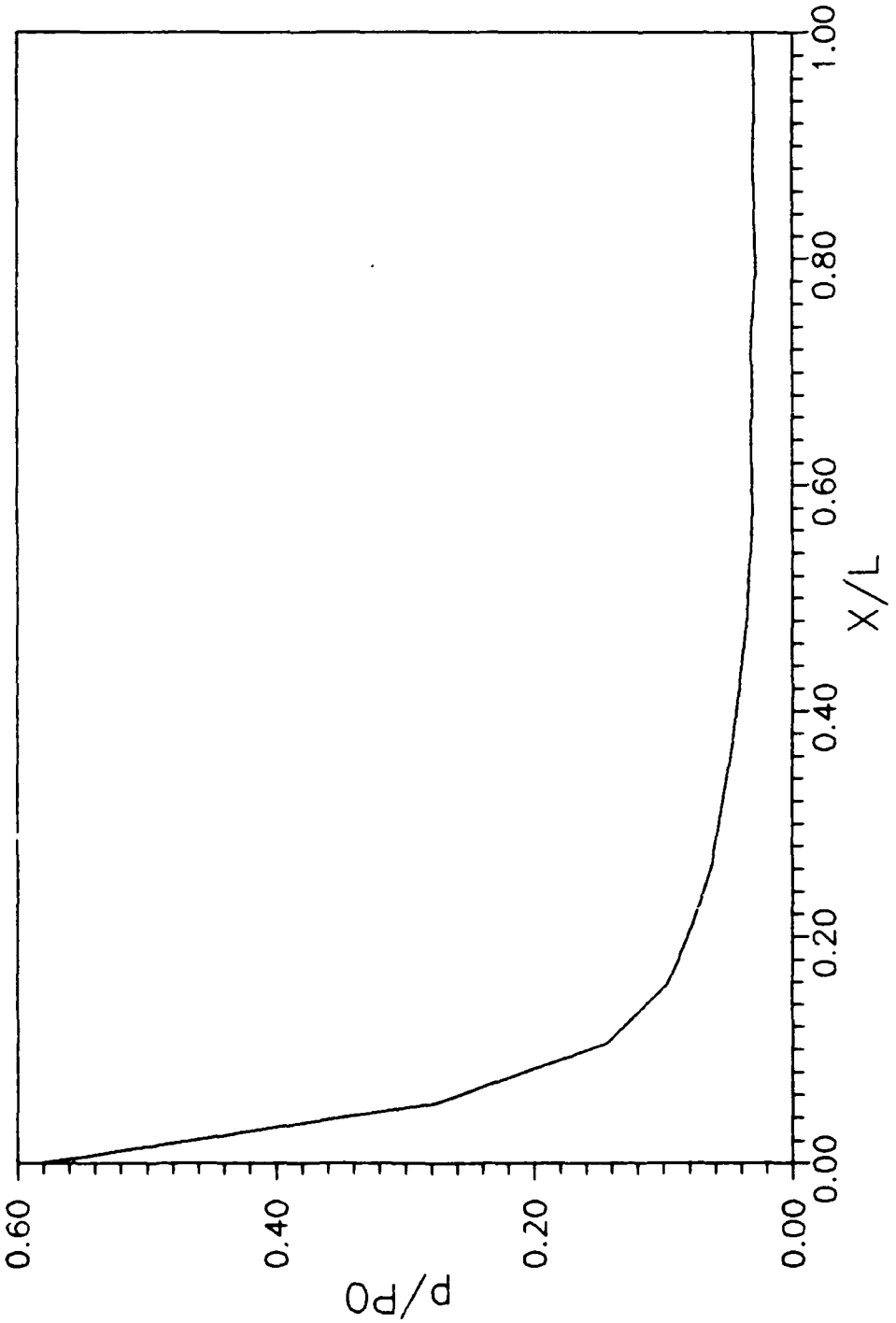

Figure 19. Supersonic Nozzles Pressure Gradient

according to the nozzle contour based on the method of characteristics. However, Figure 18a) shows a region where black and white lines alternate downstream of the lower half nozzle expansion (white region). Those lines, called Mach waves, represent alternating compressions and expansions of the flow. This could have been caused by the extreme expansion where the flow did not matched the method of characteristics, expanding more than expected. This extreme expansion caused the creation of the compression waves produced by the surface of the nozzle. Figure 19 does not show this phenomenon because static pressure ports were too far apart (0.2 inch or 0.508 cm)) and only recorded a slight drop in pressure.

Region three, $0.60 \leq X/L \leq 0.80$, is where the shock is located. Figure 18b) shows the shock as a black line and is much lighter in shade than the shocks downstream of the nozzle block which are stronger shocks. This is a partial indication that the oblique shock located in the supersonic nozzle is indeed a weak one. Furthermore, study of the graph and data collected indicate a very slight increase in static pressure at $X/L \cong 0.71$. The increase, about 0.1 psia (0.69 kPa), shows that the shock is weak. The last region, $X/L \approx 0.8$ continuing to the center of the exit plane, showed static pressure increasing and decreasing. This could be caused by the nozzle surface roughness and the way the surface was machined. Variations in pressure are small and

are not important for this present discussion. For all runs for which stagnation pressure in the main chamber was 96 Psia (661.92 kPa), the exit conditions averaged a Mach number of 2.93. It is important to note that the shock locations and pressure readings were the same for all secondary flow conditions. This is as it should be since the flow is supersonic and changes of the secondary flow would not affect conditions inside the primary nozzles.

A Mach number of 2.93 yields a ratio A_e/A^* of 3.961. Compared with the actual upper nozzle, which has a A_e/A^* = 4.275 giving a M = 3.01, it was estimated that the boundary layer occupied close to 7.5% of the exit area. Figure 18b) clearly shows boundary layers at the top and bottom of the test cavity and on the nozzle block. The boundary layer thickness δ was measured to be approximately 0.075 inch (19.05 mm) thick from the schlieren pictures. The boundary layer thickness, however, is not the same as the displacement thickness of the boundary layer, which is about three times smaller (18:291). The area lost is effectively occupied by the displacement thickness of the boundary layer. The boundary layer might be desirable for the mixing region, downstream of the nozzle. The velocity in the boundary layer, ranging from the free stream value to zero at the nozzle surface, creates a slower region at the point where both flows initially interacts which each other. This in turn can cause the initial formation of the shear layer

of a slower velocity.

Flowfield Analysis. Using a field of 45 static pressure ports, measurements of the flow static and pitot pressures were done simultaneously. The 5 columns by 9 rows array of pressure ports created a field of 1.6 inch (4.064 cm) in height by 4 inches (10.16 cm) in length centered vertically in the test section. Recorded measurements were normalized according to the following:

- axial and vertical distances by the height of the sonic nozzle orifice (0.1 inch or 0.254 cm),
- static pressures by the static pressure at the exit plane of the upper supersonic nozzle, and
- total pressures by the primary flow stilling chamber stagnation pressure.

The flowfield created by the expanding streams were studied for six different total secondary to total primary pressure ratios. Figure 20 shows schlieren photographs of the whole test cavity and Figure 21 illustrates the nomenclature used for flowfield description throughout this entire study. All photographs show a similar flow development and Figure 21 was drawn using the fully expanded sonic jet in order to show and define the complex flow characteristics observed at higher pressure ratios. Reference will also be made to Figure 22 which are schlieren pictures of the nozzle exit area magnified 2.5

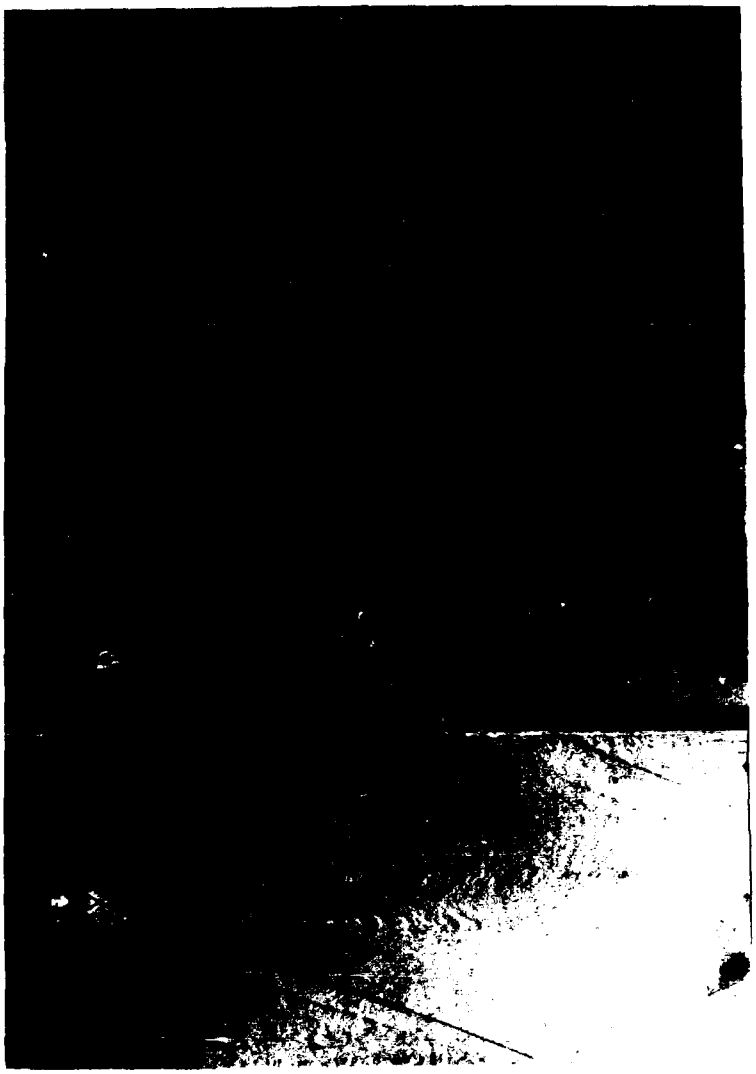

a)

b)

c)

Figure 20. Composite Schlieren Photographs with Knife Edge Perpendicular to the Flow with P_0'/P_0 of:

a) 0.02 b) 0.13
c) 0.30

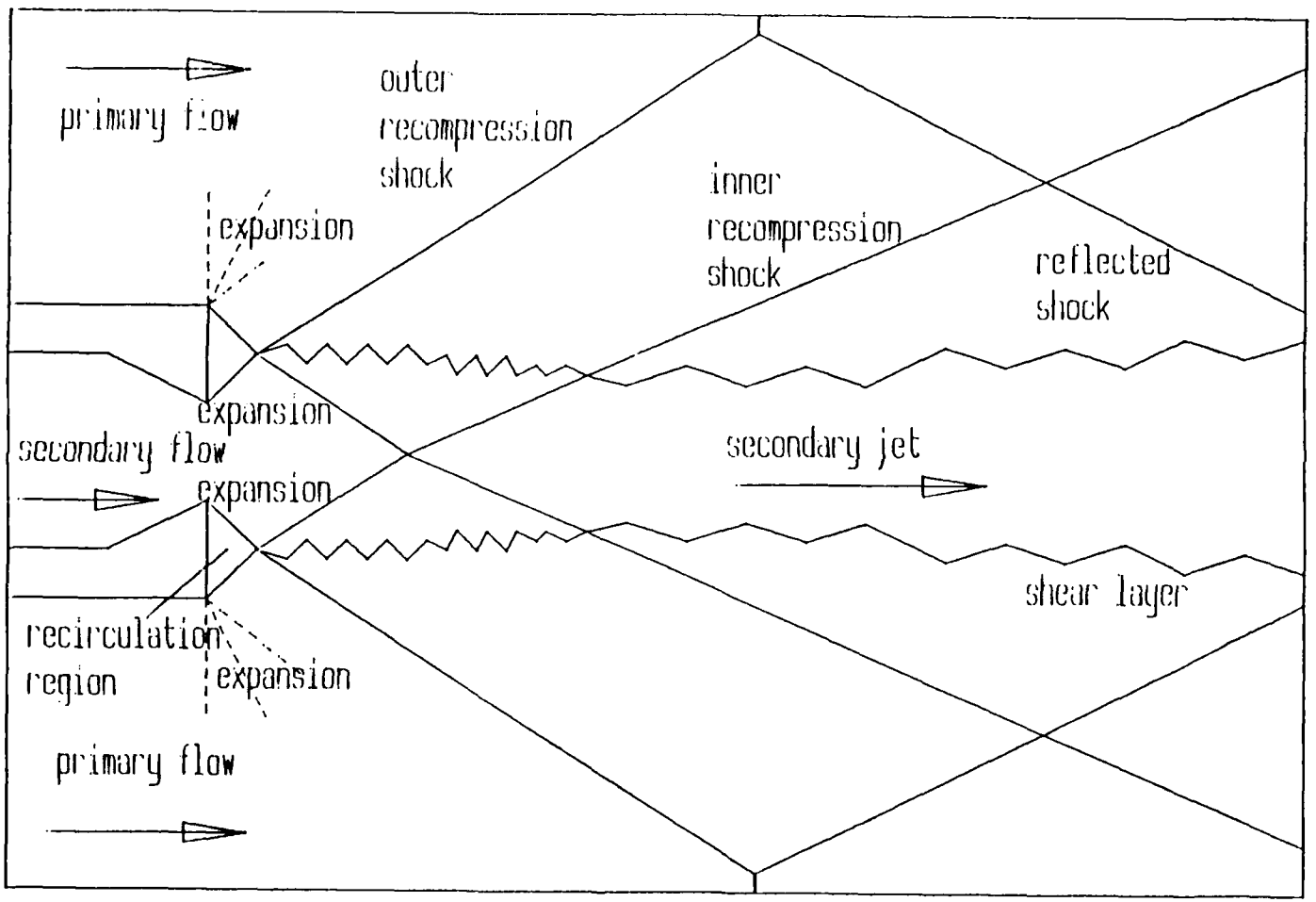

Figure 21. Nomenclature for Schlieren Photographs

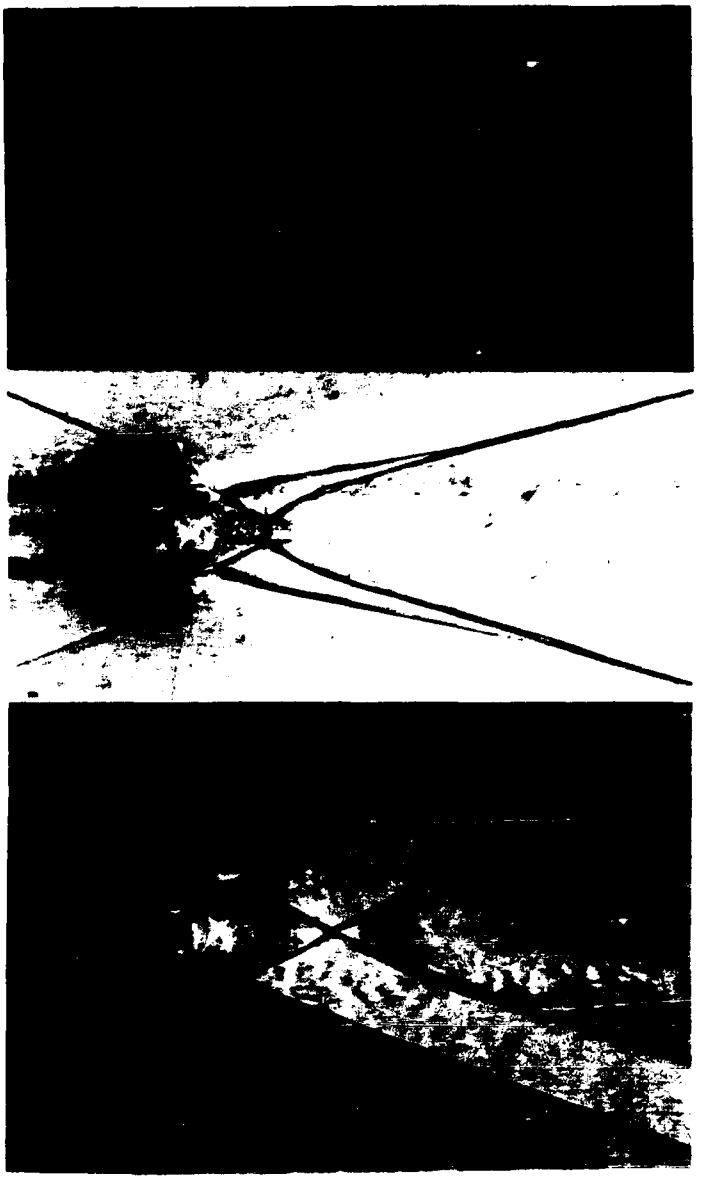

a)

b)

c)

Figure 22. Composite Schlieren Photographs with Knife Edge Perpendicular to the Flow and Magnification Factor of 2.5 with P_0'/P_0 of:

a) 0.02 b) 0.13

c) 0.30

times to give a better visualization of the flow characteristics.

As discussed previously, static and pitot pressures were taken simultaneously and the pitot Rayleigh equation was used to calculate corresponding Mach numbers. The pitot probe was manually positioned in the axial direction while the flow was established. The total pressure for each point was then calculated using the stagnation pressure relationship for a perfect gas. Static pressure measurements were repeated without the pitot probe in place. Both sets of static pressure recordings were similar but the static pressure recorded with the pitot probe in place showed consistently higher values. Therefore, values of static pressure used for calculation were the ones recorded without the probe.

Total Pressure Ratio of 0.02. The first operating condition was set at a pressure ratio of $P_0'/P_0 = 0.02$, the smallest possible pressure ratio attainable with the present set-up. Figure 23 represents the static pressure profiles for this test condition. It represents profiles of static pressure across the flowfield at specific axial locations indicated by the *'s. Profiles of total pressure and Mach number are plotted the same way for each test conditions.

As shown on the Figure 23, the Y axis represents the normalized height in the test cavity with y/d = 0.0 being

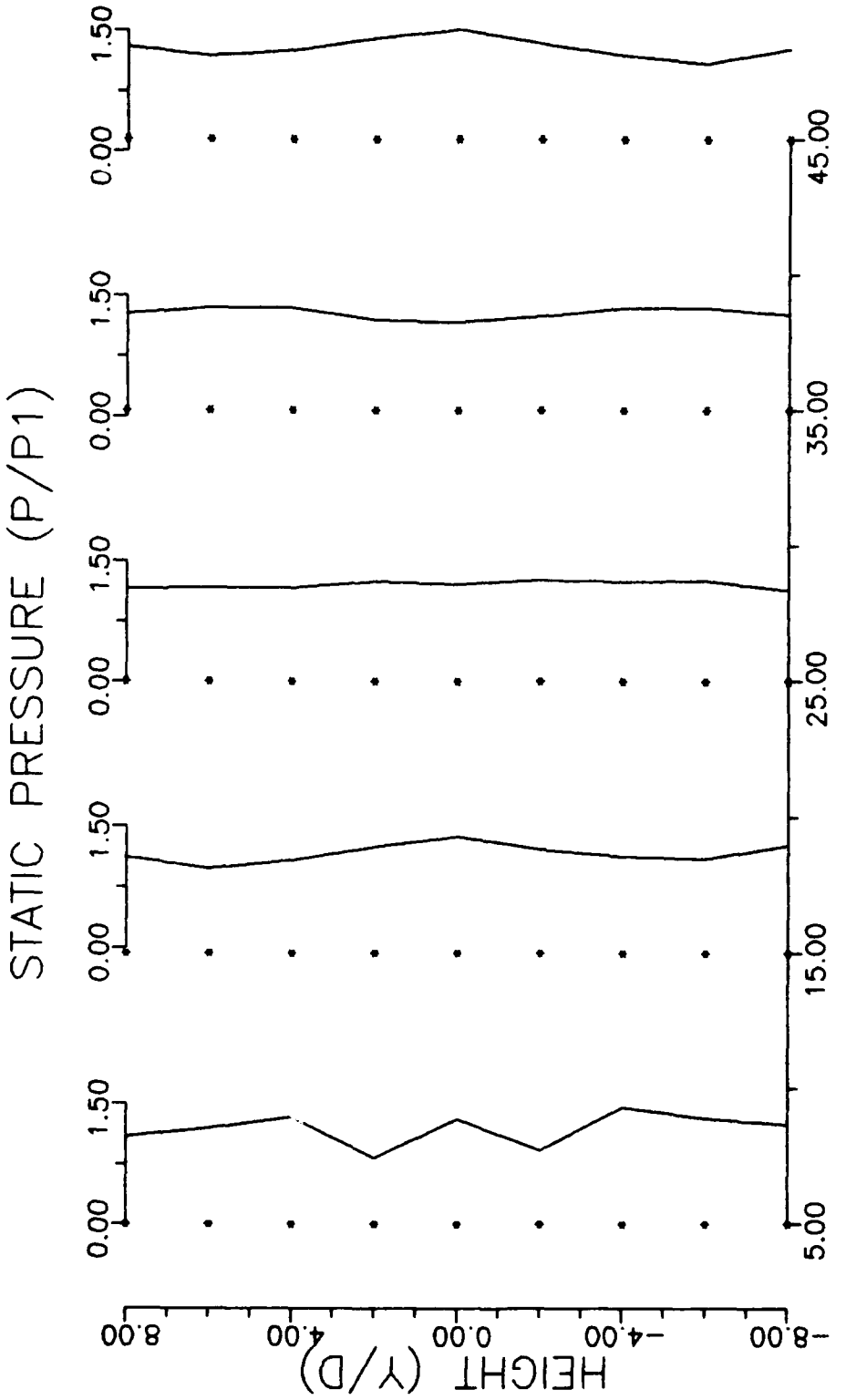

Figure 23. Static Pressure Profiles of Flow with Pressure Ratio of 0.02

the centerline of the test section. The lower X axis represents the normalized axial distance downstream of the exit plane of the nozzle assembly. For example, a value of x/d = 35 represents a location 3.5 inches (8.89 cm) downstream of the nozzle assembly exit plane. The upper X axes show the normalized static pressure and are used to plot the pressure profiles. Finally, at each of the five axial instrumentation stations the nine static port locations are represented by the symbol "*" shown at the zero pressure location for that axial station. Furthermore, a template showing shock locations (solid lines) and secondary jet boundaries (dashed lines) was produced for each test condition to be discussed by observation of schlieren photographs of the test section with pressure ports installed;the first of these shown in Figure 24. These templates were used in conjunction with the profile figures to help in the development of this discussion.

Flow for P_0'/P_0 = 0.02 is represented in Figures 20a) and 22a). Since this case is a special one, with no mass flow from the secondary nozzle, no mixing nor shear layers are present. Figure 20a) shows a wake corridor where mass from both flows diffuses in the center of the test cavity.

Close study of Figure 23 and 24 reveals that static pressure is fairly constant at locations far from the nozzle assembly and away from shocks. The sharp increase in static pressure at x/d = 5 and centerline is mainly due to the

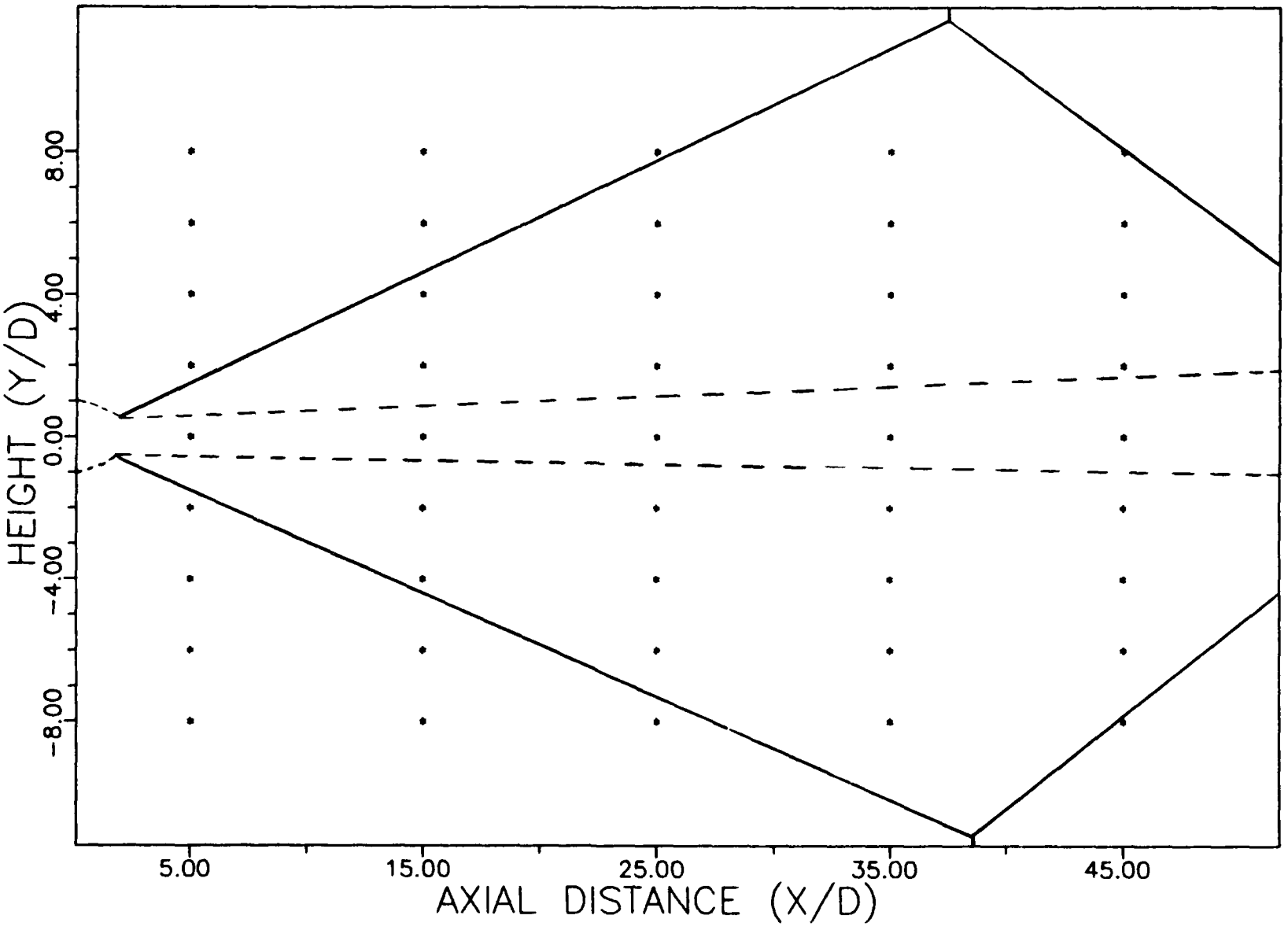

Figure 24. Template for Pressure Ratio of 0.02

subsonic jet flow at this location.A noticeable decrease in static pressure at location x/d = 5 and y/d = +2 and -2 represents the expansion of the supersonic primary stream around the nozzle assembly. The port situated at the same height location but a distance x/d = 15, has increased static pressure since the flow has been through the oblique shock. Another interesting phenomenon visible on this figure was also observed by Traxler (16). The ports at location x/d = 5 and y/d = -4 and +4 show a rise in static pressure for no apparent reason. These ports, located just upstream of the oblique shock, actually "see" a pressure higher than they should be. This is due to the pressure rise from the shock diffusing upstream through the subsonic boundary layer near the sidewall. Reffering to the pressure rise across a shock, Schlihting explained "that the pressure gradient parallel to the wall must be much more gradual in the neighborhood of the wall than in the external stream" (15:359). This observation applies as appropriate for all graphs of static pressure and the same explanation stands for the other pressure ratios.

Using static and pitot pressure measurements, Mach numbers were calculated and are plotted on Figure 25. It is very obvious that the center of the test section has a lower Mach number than the main stream. This shows that both supersonic streams are diffusing to the center of the cavity. The constant Mach number line at x/d = 5 outside

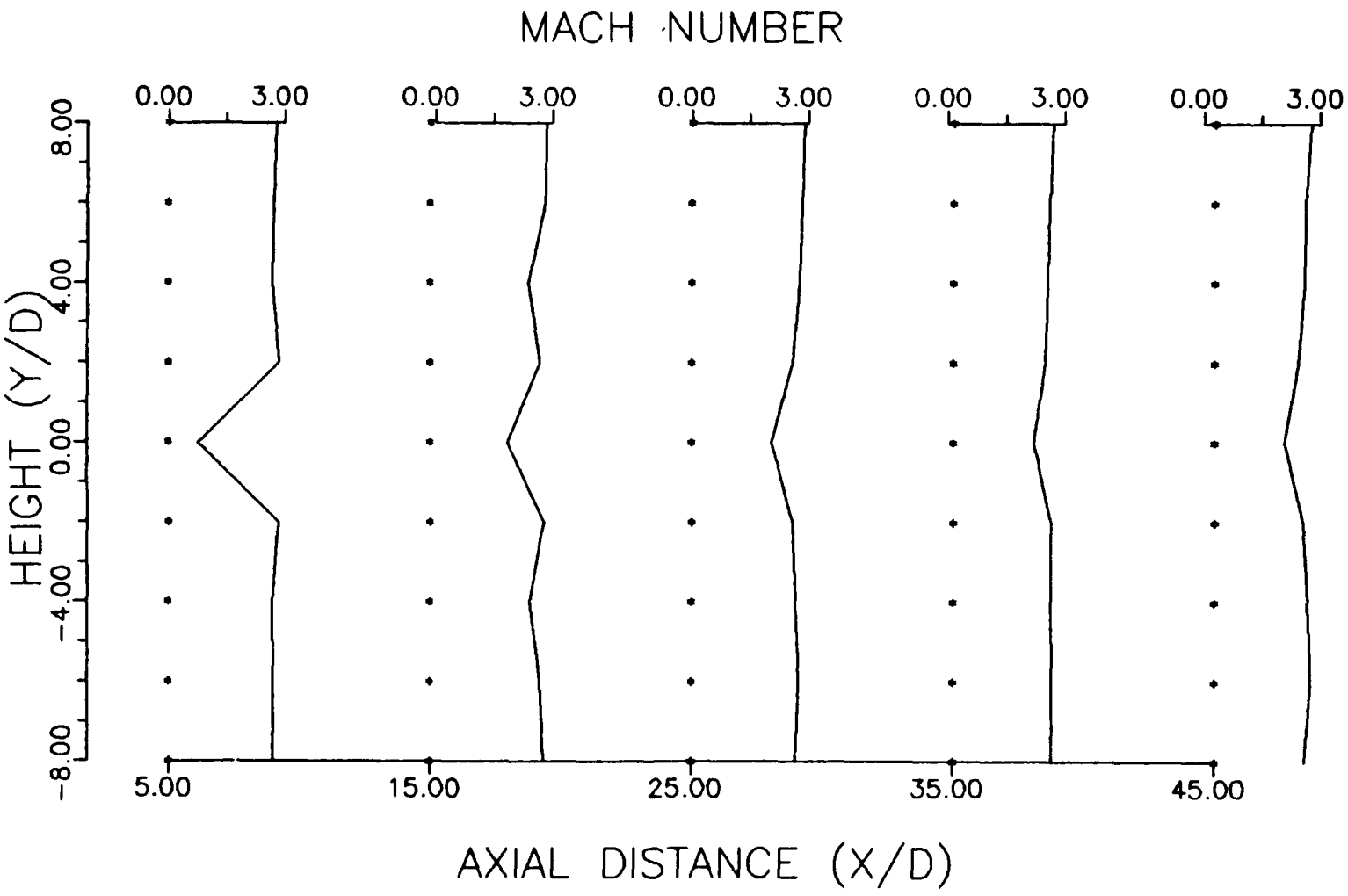

Figure 25. Mach Number Profiles of Flow with Pressure Ratio of 0.02

of the y/d = +4 and -4 shows that the flow is acceptably uniform at it's exit of the supersonic nozzles. The Mach number at x/d = 5 and y/d = +2 and -2 experiences an increase relative to the primary flow Mach number showing the expansion of the flow around the nozzle corners but is lower than the exit Mach number (2.93) because this port is close to a shock, indicating a possible error in static pressure. Last, the rise in Mach number on each side of the center port at x/d = 15 could represent an effect of the wake flow for this test condition. At the same axial location,at y/d = +4 and -4, decrease of the Mach number is due to an oblique shock.

Figure 26 represents the Mach number along the axial direction of the test cavity for the upper and lower nozzles centerlines and the test section centerline. A maximum difference of 9% in Mach number was experienced between the two main streams. The flow in the center of the cavity is shown to start subsonic but accelerates very rapidly without marked effect on the outside streams. The center wake peaked at about M = 2.25 achieving close to 87% of the outside stream Mach number at this location. This figure also illustrates that the center wake will never achieve the velocity of the outside primary streams for this flow geometry. Before any conclusions can be made, other flow conditions must be studied.

The total pressure profiles across the test cavity for

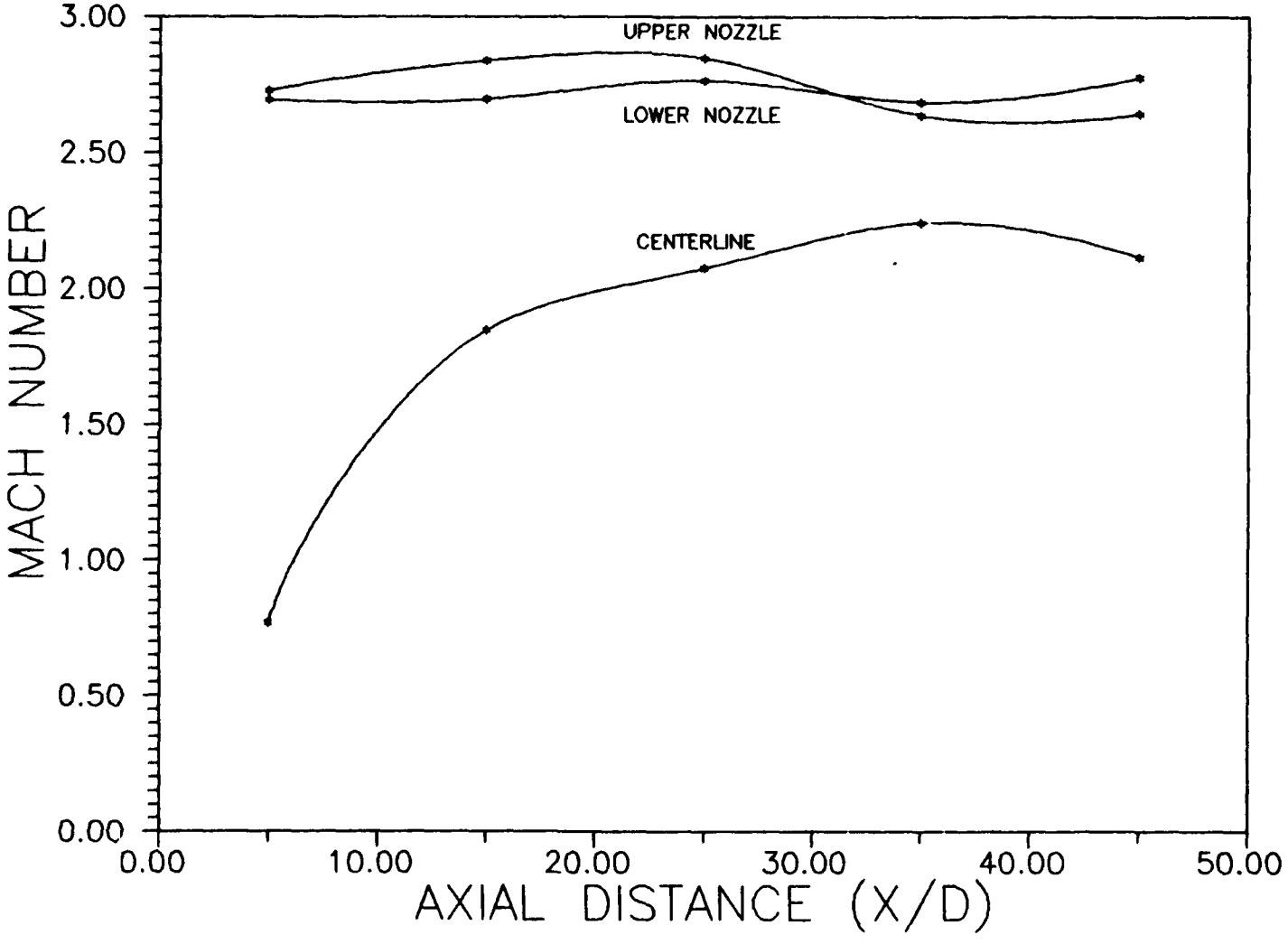

Figure 26. Mach Number VS Axial Distance on Centerlines of Flow with Pressure Ratio of 0.02

this case with no secondary flow are shown in Figure 27. Once again, the effect of the center wake is easily seen. The lower total pressure in the center represents lower velocity compared to the outer streams downstream of x/d = 15 since the static pressure was found to be fairly constant across the height of the test section. A sharp rise in total pressure is noticed at x/d = 15 and y/d = +2 and -2. Those ports are located between the center wake flow and oblique shocks (see Figure 24). These rises in total pressure could be the effect of turbulence at the edge of the wake which could affect the pitot pressure measurement. Close examination of figure 20a) shows that both recompression shocks do not intercept the upper and lower wall at the same axial location. This indicated that the nozzle block was not exactly symmetrical. As discussed before, the upper supersonic half-nozzle had a designed Mach number of 3.01 while the lower on had M = 3.02. This small difference in the nozzles created a slight upward curvature of the center wake region. This had an insignificant effect on the velocity, Mach number, and pressure in the flowfield.

Total Pressure Ratio of 0.13. With secondary flow and P_0'/P_0 = 0.13, Figure 20b) shows that the flow is still characterized by only two recompression shocks. However, Figure 22b) gives more details on the flow at the exit of the sonic nozzle. A normal shock at the centerline is clearly visible. The normal shock formed at this location

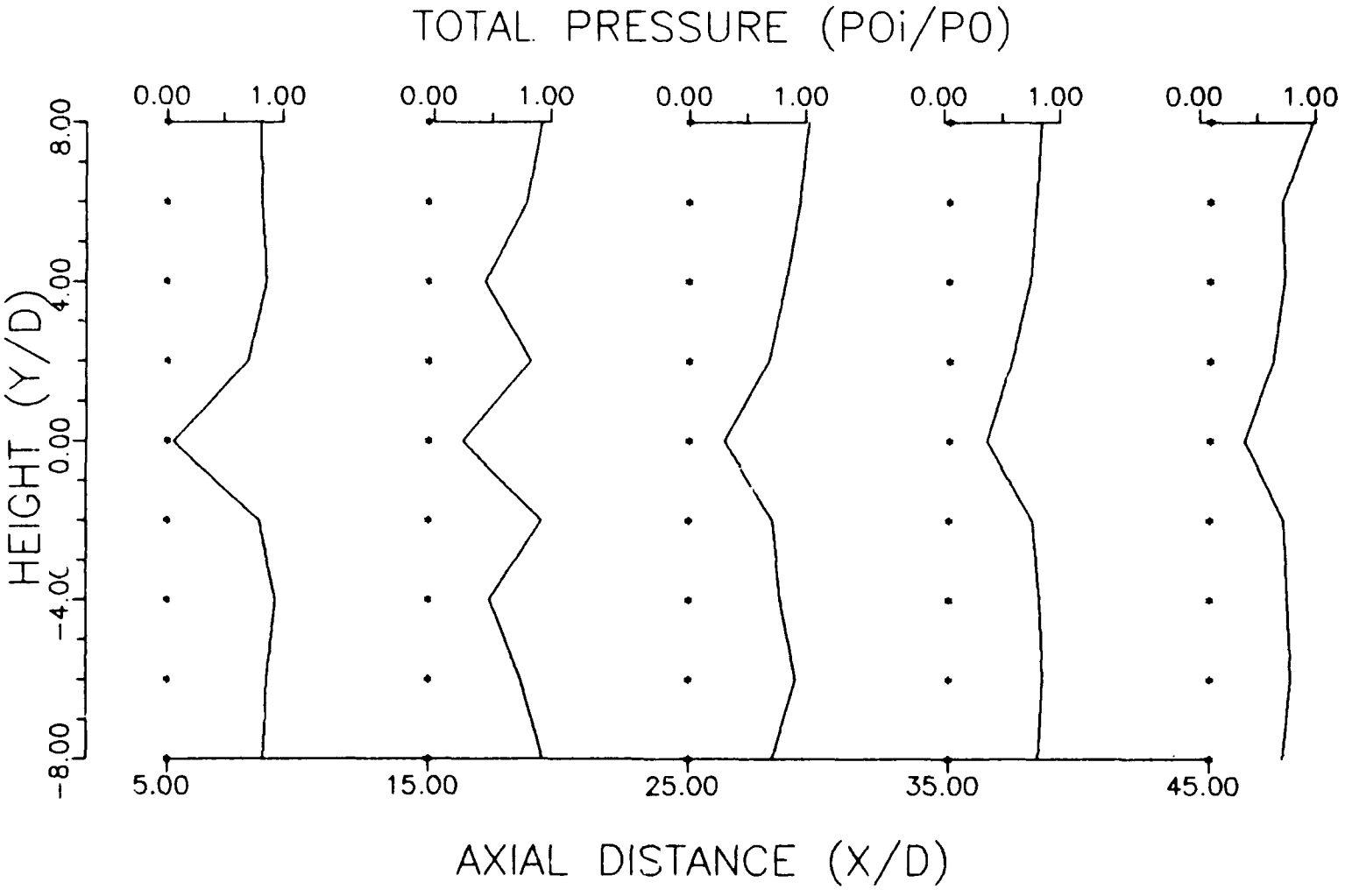

Figure 27. Total Pressure Profiles of Flow with Pressure Ratio of 0.02

could be due to a convergent pressure "wall" effect created by the two expanding streams. At a P_0'/P_0 = 0.13, the sonic nozzle is choked and the secondary flow is now expanding in a region where the Mach number is larger than unity. Also from this figure, a second compression shock formed at the end of the expansion region of the sonic jet. Figure 20b) shows a schlieren photograph of the whole flowfield and all shocks show clearly as black lines. The shear layers between the streams are visible on the photograph as two turbulent layers with the small low turbulence secondary stream between.

Figures 28 and 29 (template) show that the static pressure is fairly constant across the test section except close to the nozzle exit and shocks. This is an interesting effect since mixing between the streams is assumed in Chow's theory to be at constant pressure (2). Obviously, this condition happens at some distance downstream of the nozzle block where the flow is independent of the base region and mixing in the shear layer between the streams can be investigated. A good example of nozzle dependent flow is shown on Figure 28 at x/d = 5 and y/d = +2 and -2 where the Prandtl-Meyer expansion of the primary flow around the corners of the nozzle block caused the drop in the static pressure, accelerating the flow.

Figure 30 represents the Mach number profiles

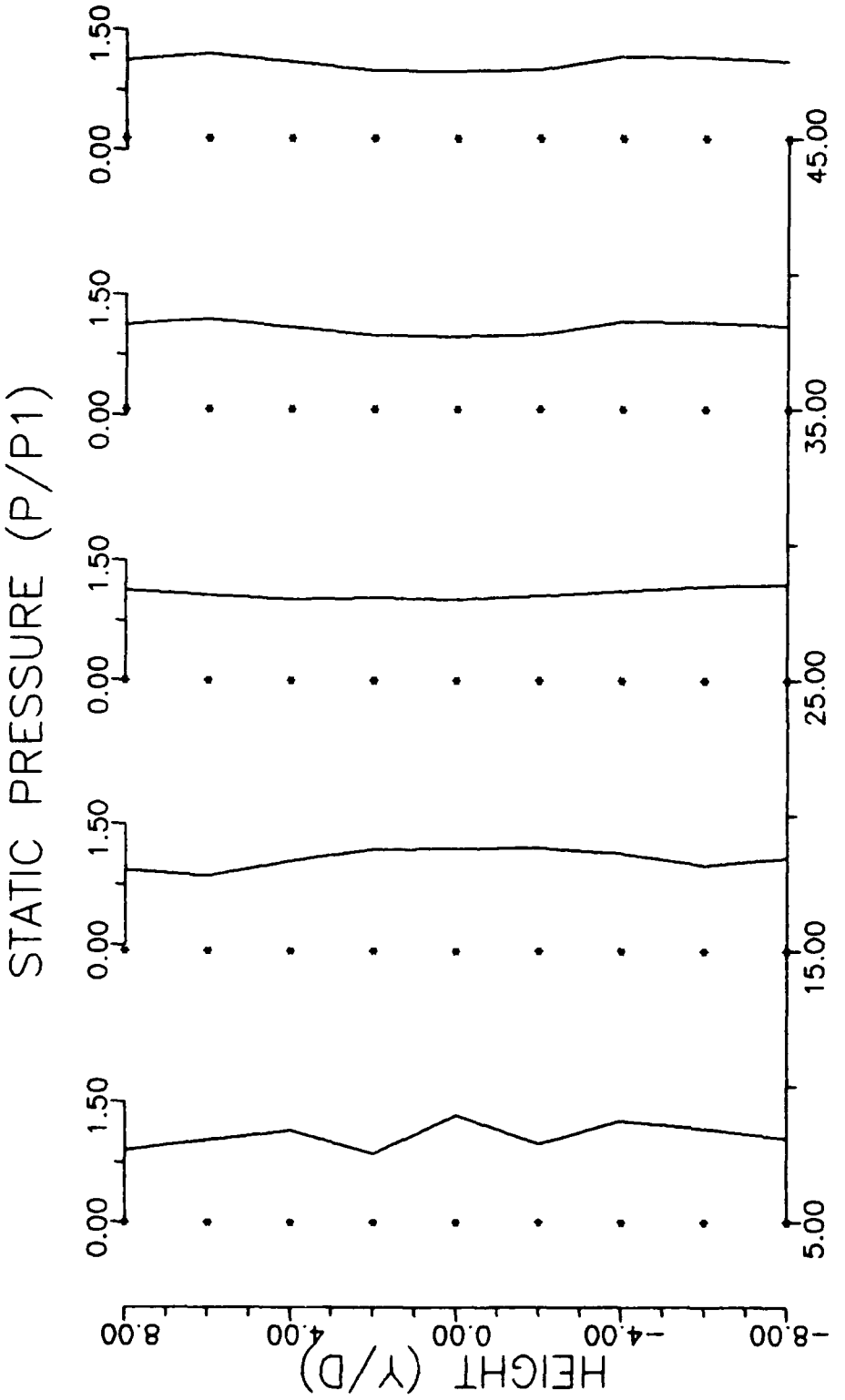

Figure 28. Static Pressure Profiles of Flow with Pressure Ratio of 0.13

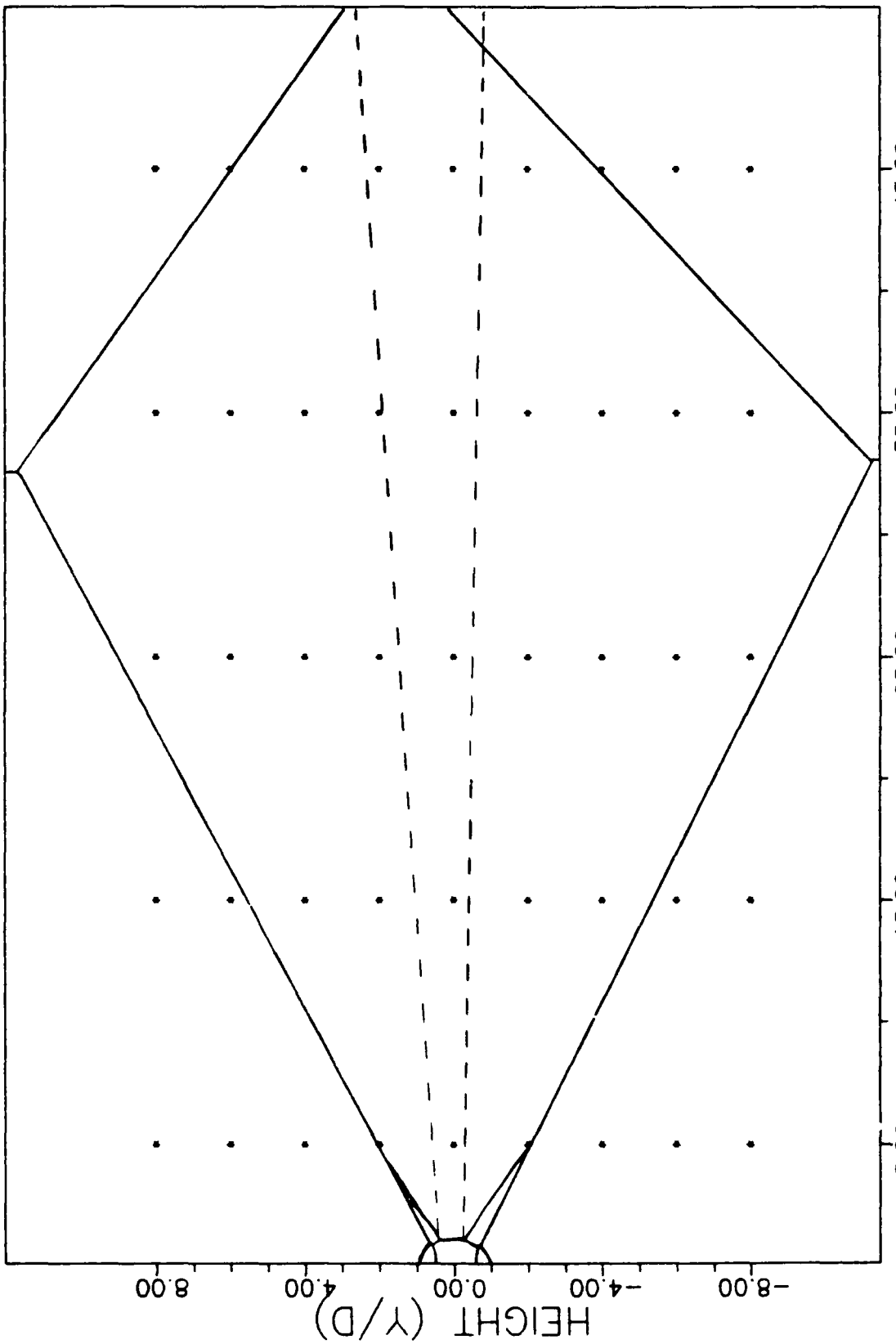

Figure 29. Template for Pressure Ratio of 0.13

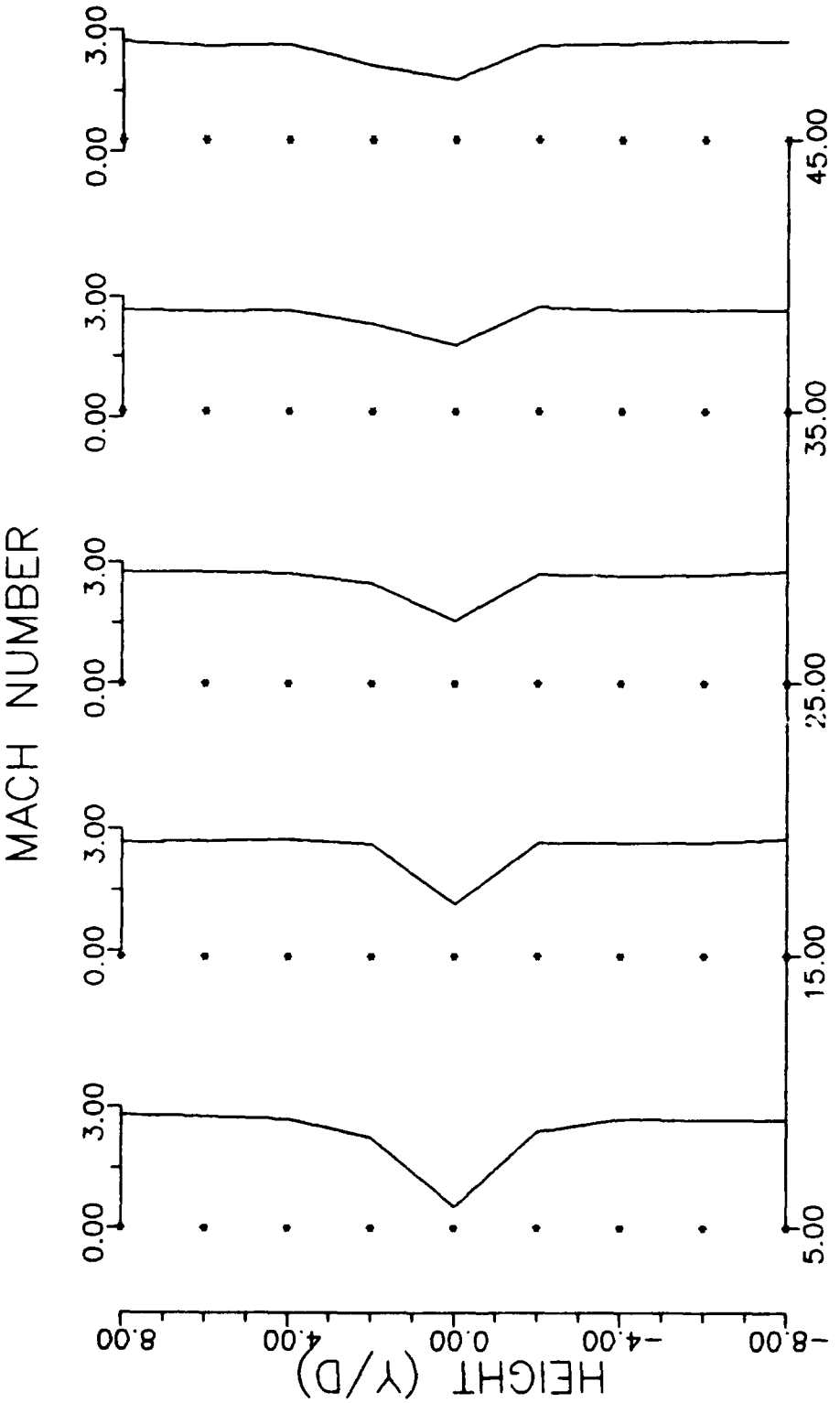

Figure 30. Mach Number Profiles of Flow with Pressure Ratio of 0.13

calculated with static and pitot pressures. The secondary jet corridor is easy to see and has a lower Mach number than the outer streams. Uniform conditions near the exits of the supersonic nozzles at x/d = 5 is evident outside of the shocks where the Mach number is constant. Figure 20b) shows that the shocks do not interact with the secondary jet and this is supported by data since no drastic decreases in Mach number are seen. Surprisingly, no large changes in Mach number are experienced across any oblique shocks for this test condition. This could mean that the amount of flow turning required is small, creating weak shock waves Next referring to Figure 31, the centerline curve shows the Mach number to be very low (0.513) at x/d = 5. This is due to the normal shock (see Figure 29). Taking this Mach number to be the value after the normal shock gives an upstream Mach number of about 2.5 in the expanding region behind the sonic nozzle. Again, the expected rise in centerline Mach number is noticed and the maximum value corresponds to about 72% of the outer stream Mach number at this location. Both upper and lower stream centerline Mach numbers act similarly. The total pressure profiles for this test condition are shown in Figure 32. Papamoschou (11:45) explained that a deficit in the total pressure may be due to the mixing process. The template (Figure 29) clearly shows the secondary jet and Figure 32 shows a decrease in total pressure on each side of the jet flow. This would give a

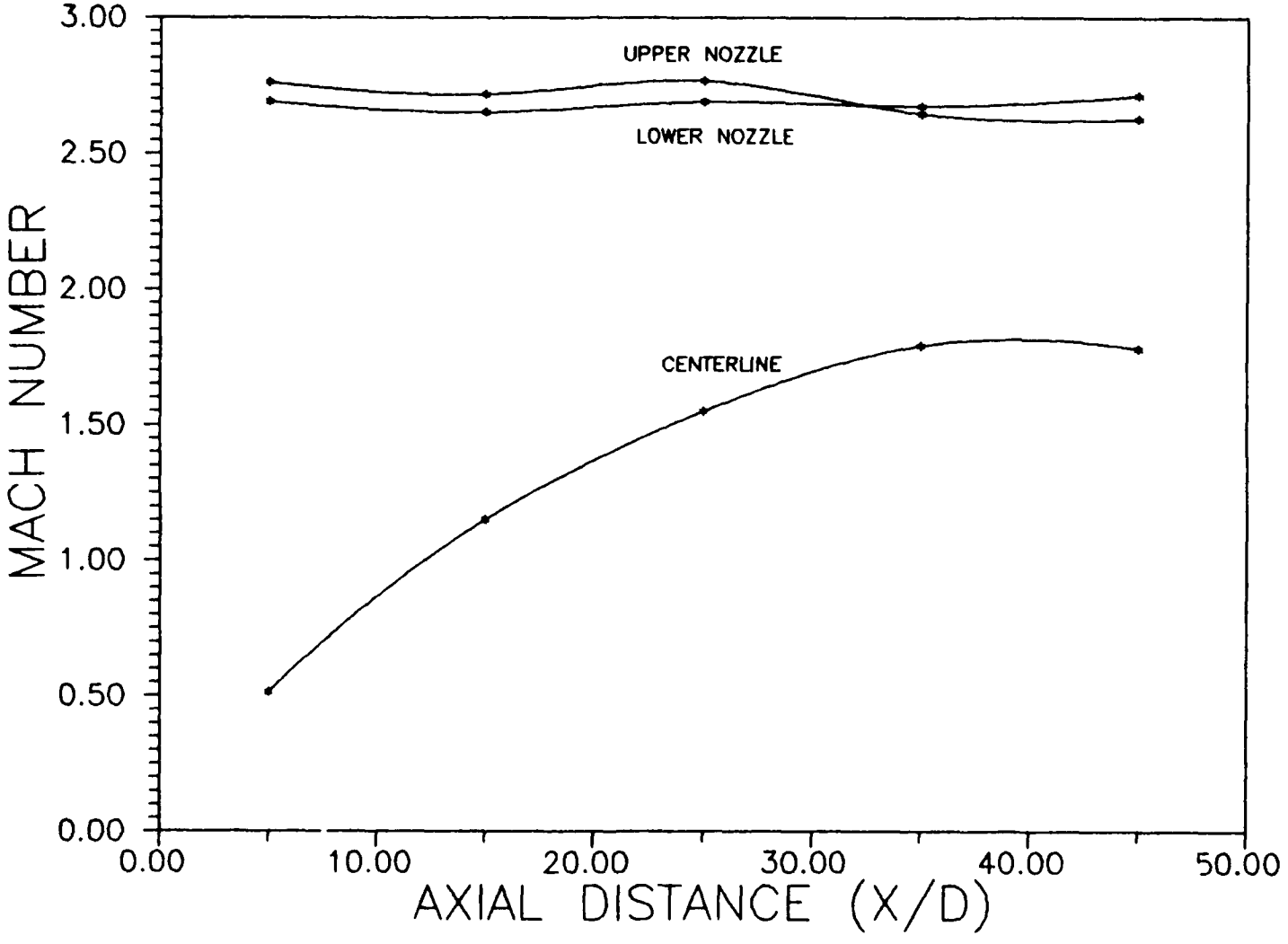

Figure 31. Mach Number VS Axial Distance on Centerlines of Flow with Pressure Ratio of 0.13

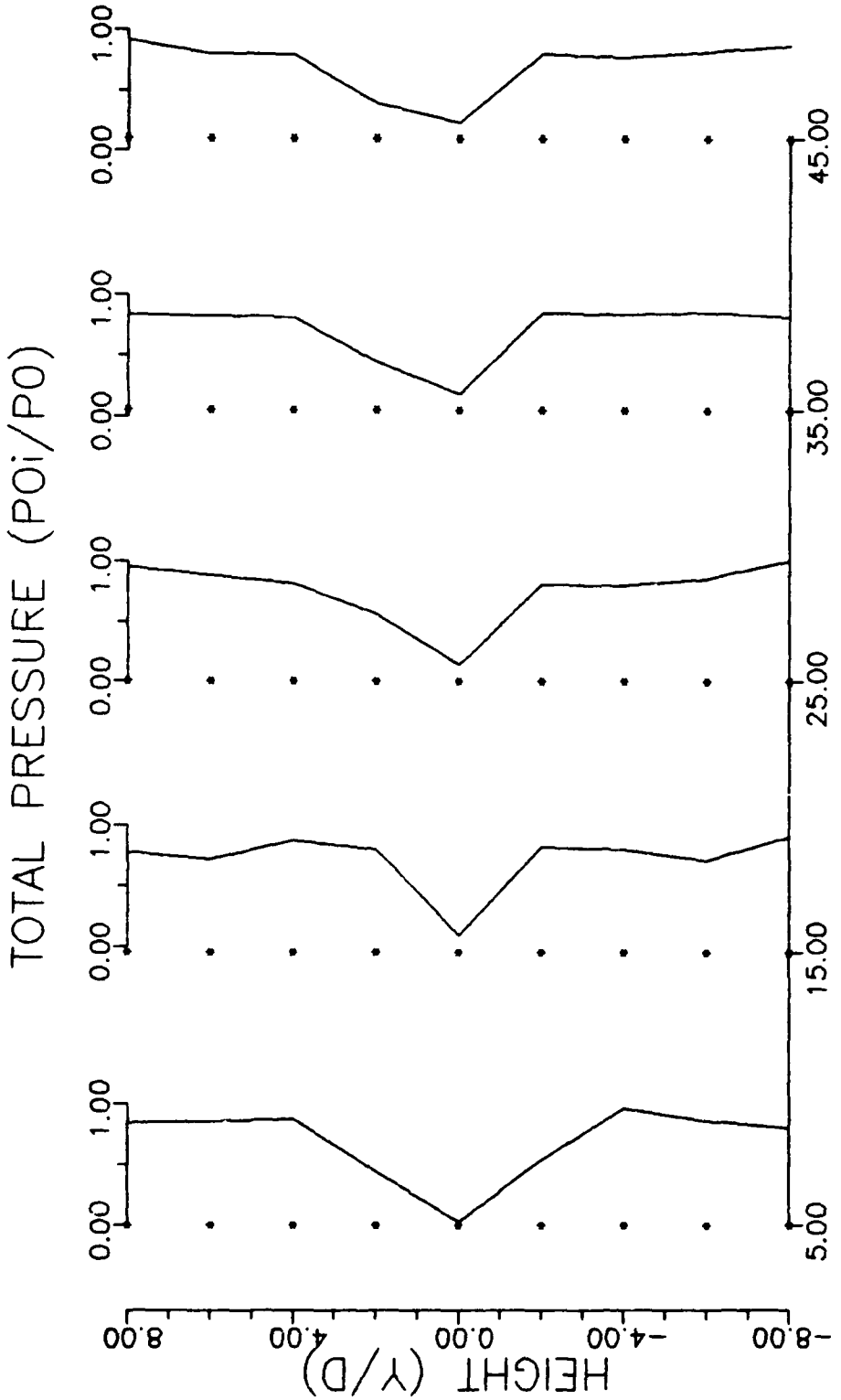

Figure 32. Total Pressure Profiles of Flow with Pressure Ratio of 0.13

coarse indication about the shear layer thickness. More results on shear layer data will be presented later.

Total Pressure Ratio of 0.30. The secondary total pressure for the next test conditions was set at P_0'/P_0 = 0.30. From Figures 20c) and 22c), the first noticeable change is the complete formation of the second recompression shocks. Four recompression shocks are now present in the test cavity and will interact with the flow. As the secondary pressure was increased, the secondary jet is easier to see (Figure 20c)). It was also noticed from Figure 22c) that the wake flow spreads evenly when it goes through a shock. Figures 33 and 34 (template) show the static pressure far from the nozzles is constant for this run. A rise in static pressure is also observed as the flow moves downstream. Static pressure at the first axial location is high since it is located behind the intersection of the inner recompression shocks. The Mach number profiles, Figure 35, shows that the secondary jet and mixing layers combined are larger than at lower secondary pressures. This can also be seen by comparing Figures 20b) and 20c). The Mach number of the first port in the centerline shows the flow to be supersonic. The normal shock seen in Figure 22b) and experienced at P_0'/P_0 = 0.13 has transformed to two interacting oblique shocks (Figure 22c)). It may also be seen from the same figures that the outer and inner recompression shocks have a larger angle

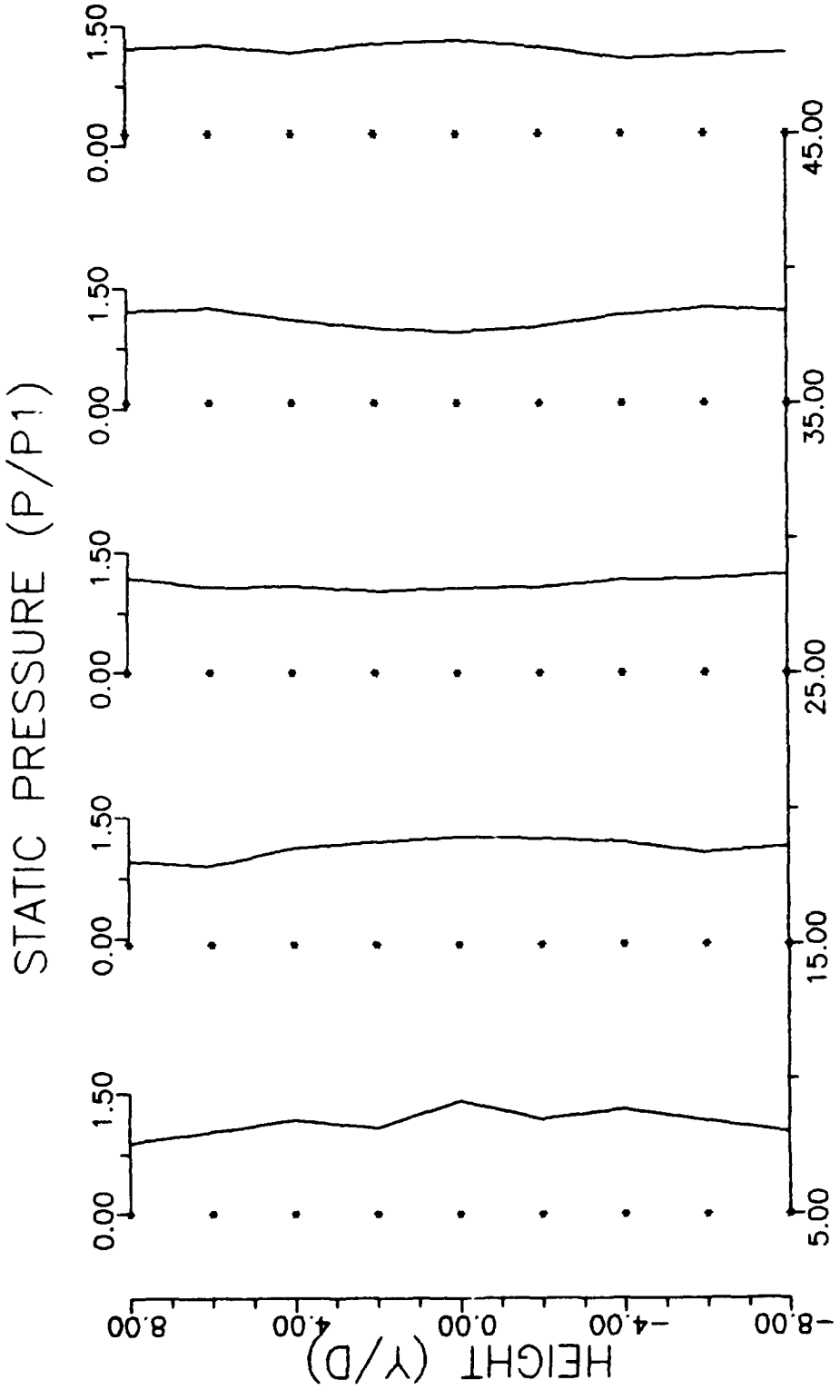

Figure 33. Static Pressure Profiles of Flow with Pressure Ratio of 0.30

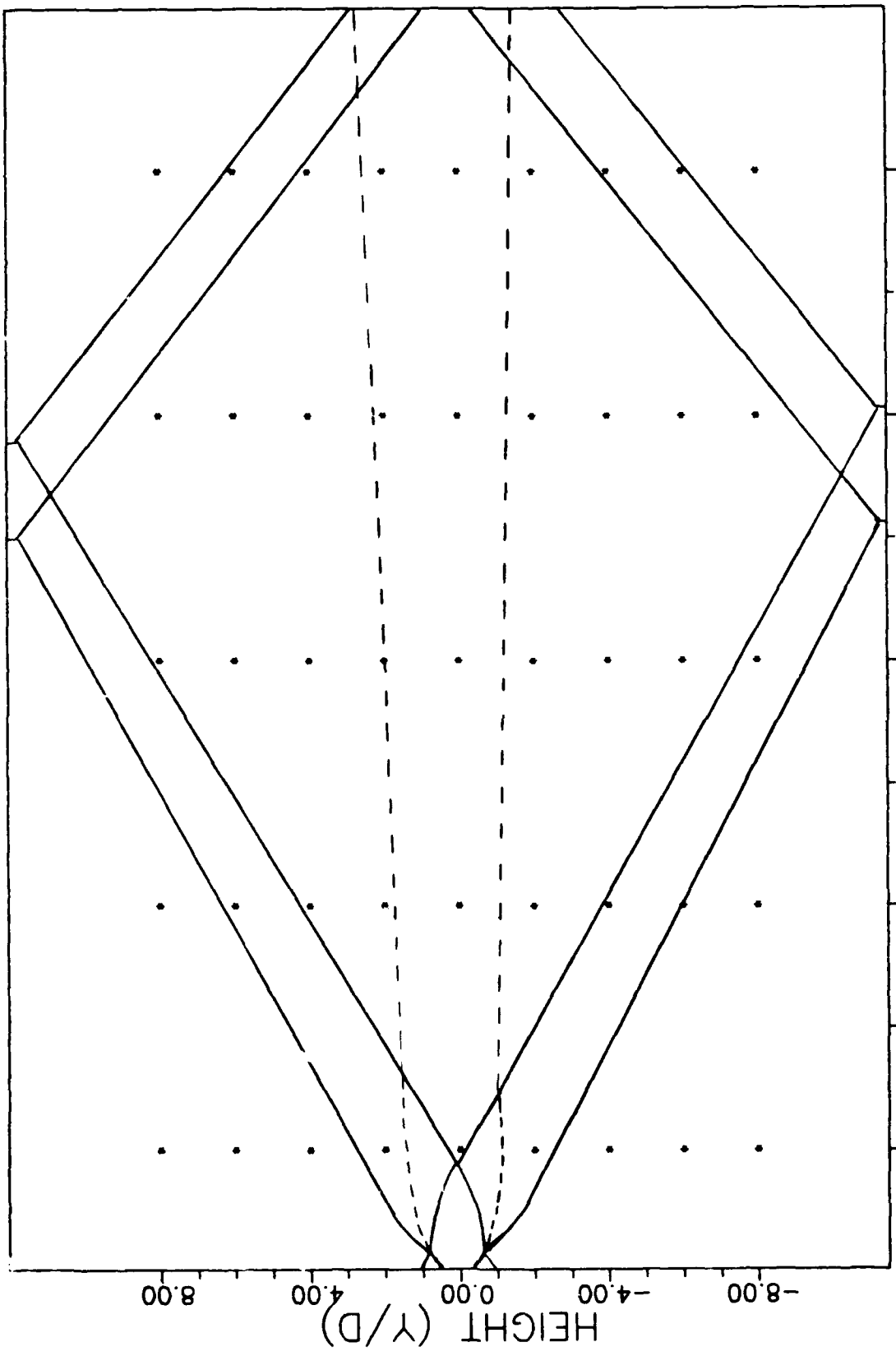

Figure 34. Template for Pressure Ratio of 0.30

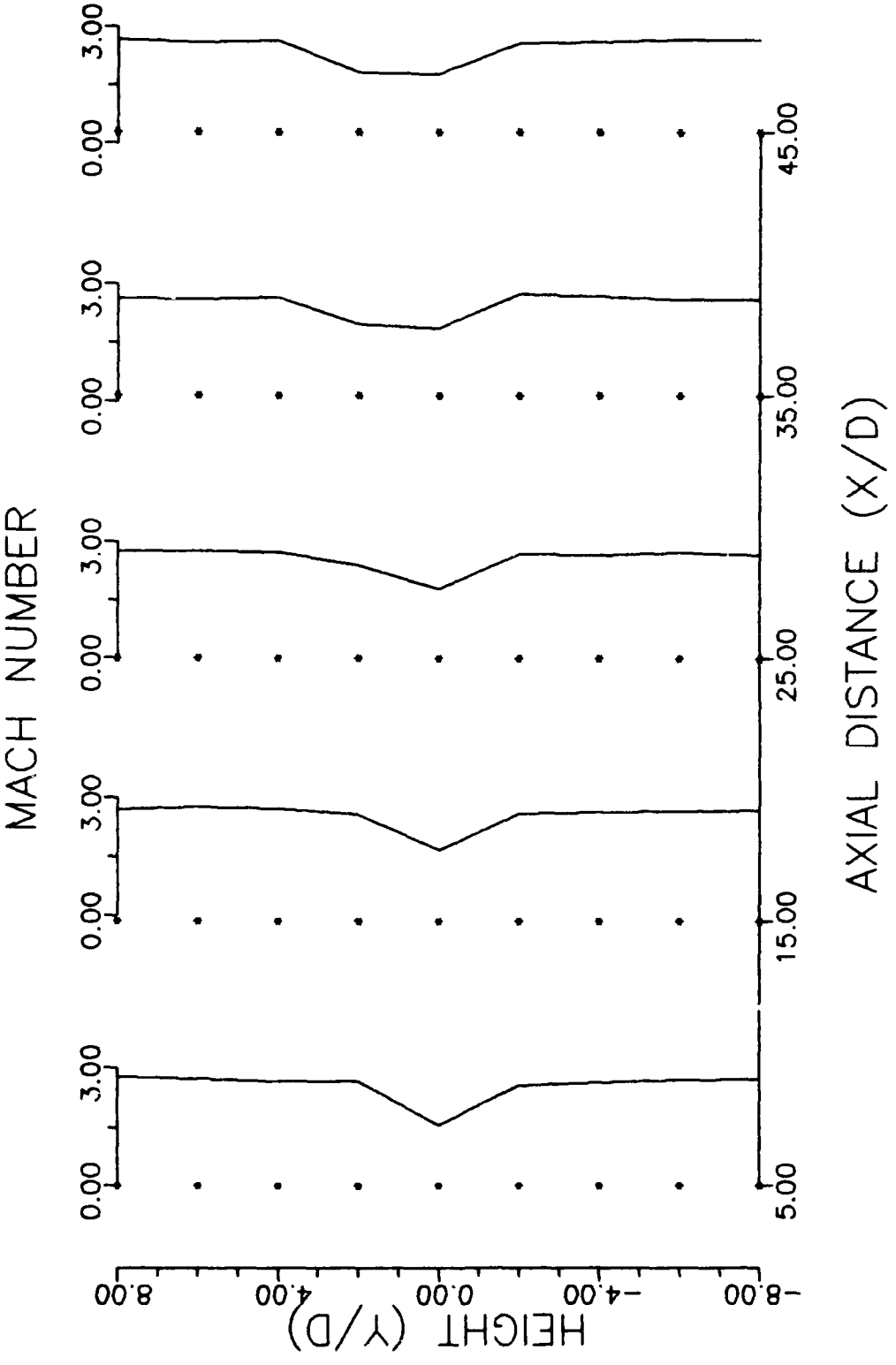

Figure 35. Mach Number Profiles of Flow with Pressure Ratio of 0.30

thus are stronger. Still, no marked step changes can be seen in the Mach number profiles, showing fairly constant Mach number away from the center jet. Figure 36 shows that both outside streams are acting similarly with no important difference in Mach number between the two (< 5%). The centerline Mach number was 1.55 at x/d = 5 and peaked at about 1.9, attaining close to 73% of the outer stream Mach number. Also worthy of mention is that the center jet accelerates less than before due to interaction with the primary streams.

For the total pressure ratio of 0.30, total pressures in the flowfield calculated from Mach numbers and static pressures are plotted in Figure 37. This time, it is clearly evident that the secondary jet plus mixing layers are growing with increase of secondary pressure. Gradual variations in total pressure are also observed on each side of the jet flow indicating the presence of the shear layer. Slight decreases in total pressure are apparent when the data point is downstream of an oblique shock.

Total Pressure Ratio of 0.48. As the secondary total pressure is raised some more, larger shock angles are noticed. At $P_0'/P_0 = 0.48$, the reflected shocks start to interact with the secondary jet after reflecting off the outside walls. Figures 38a) and 39a) are schlieren photographs of this test condition. The shear layers are now well defined and the growth of the secondary jet is

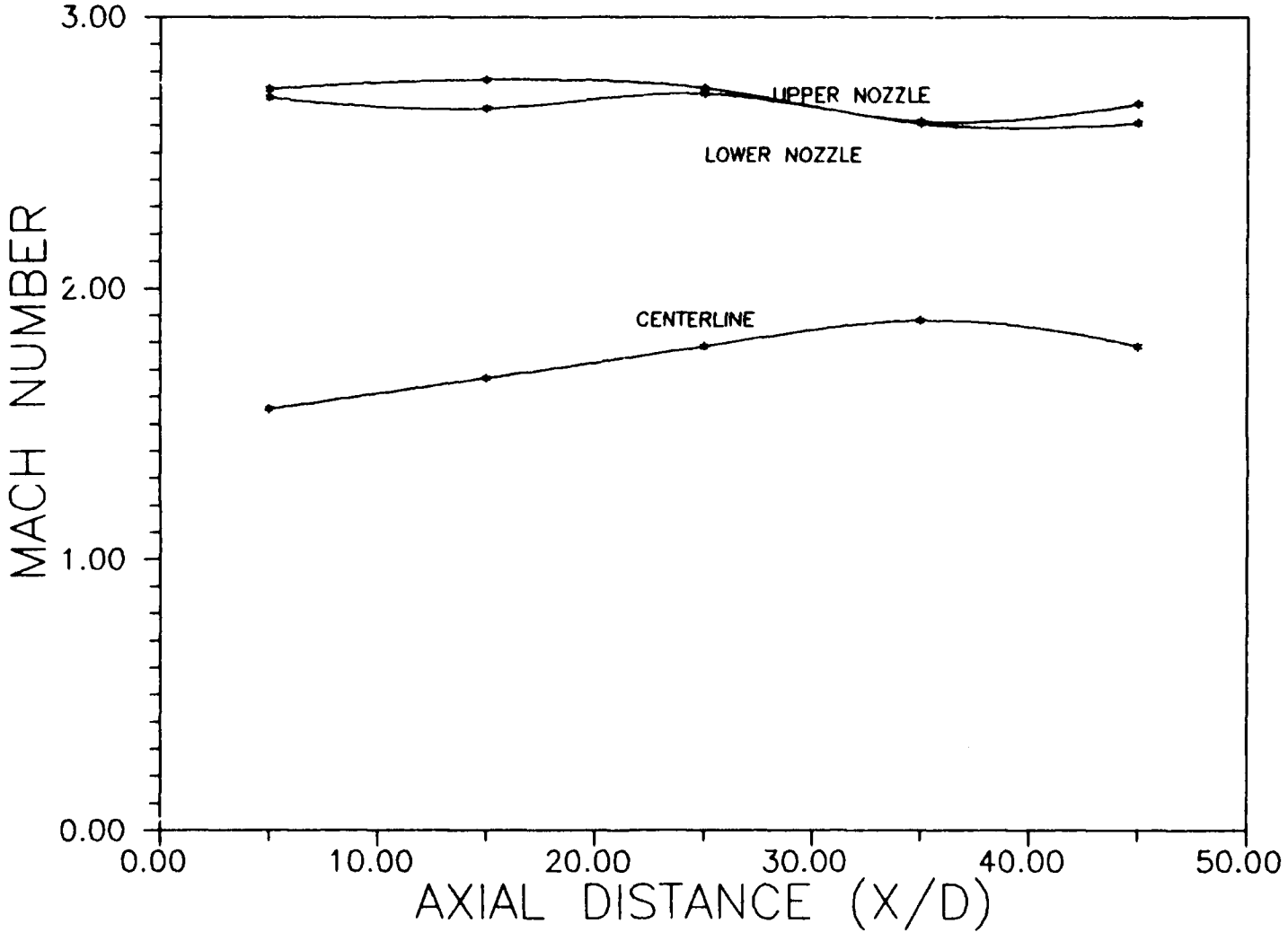

Figure 36. Mach Number VS Axial Distance on Centerlines of Flow with Pressure Ratio of 0.30

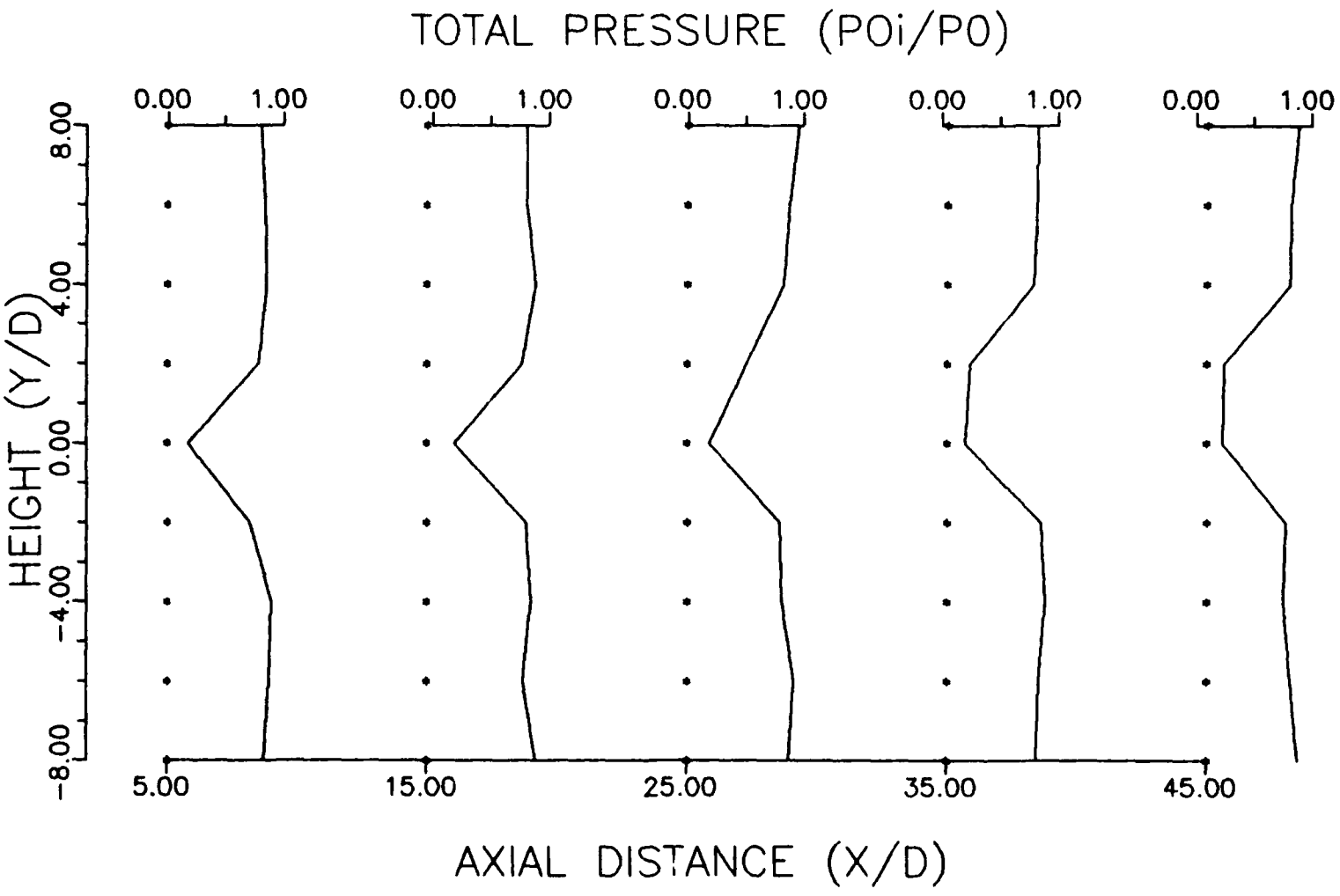

Figure 37. Total Pressure Profiles of Flow with Pressure Ratio of 0.30

a)

b)

c)

Figure 38. Composite Schlieren Photographs with Knife Edge Perpendicular to the Flow with P_0'/P_0 of:

a) 0.48 b) 0.66

c) 0.73

a)

b)

Figure 39. Composite Schlieren Photographs with Knife Edge Perpendicular to the Flow and Magnification Factor of 2.5 with P_0'/P_0 of:

a) 0.48 b) 0.66

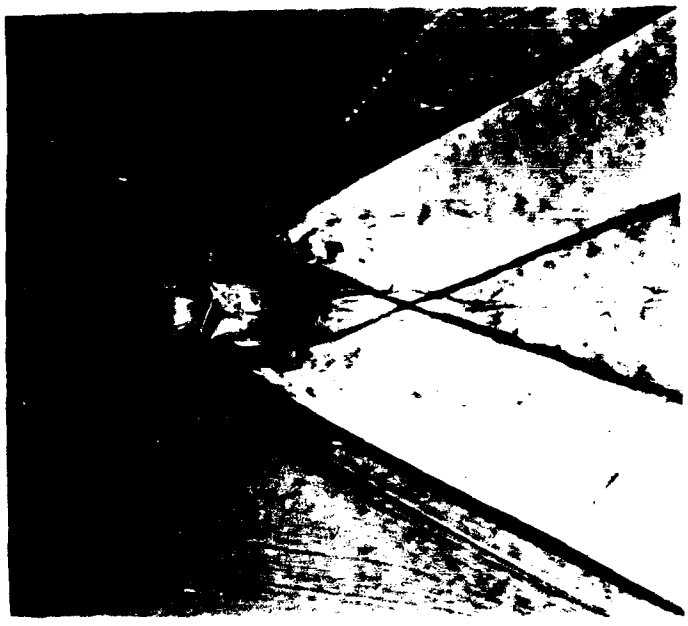

Figure 40. Composite Schlieren Photographs with Knife Edge Perpendicular to the Flow and Magnification Factor of 2.5 with P_0'/P_0 of 0.73

highly noticeable. The expansion region of the secondary flow grows larger and longer. Figure 41 shows static pressure profiles and Figure 42 shows the template for this test condition. First noticed is the absence of the wavering static pressure line at x/d = 5. The centerline pressure tap at this location is now at the intersection of the inner recompression shocks and has a high static pressure. Also at this axial location, once the static pressure has risen due to the oblique shocks, it stays fairly constant across the height of the channel. Everywhere else, the static pressure is relatively constant throughout the height of the test cavity except at x/d = 45 at centerline where two ports are located behind two oblique shocks interacting with each other.

After calculating the Mach numbers, a plot was produced and is shown in Figure 43. At this secondary pressure setting, the upward curvature of the secondary jet along the length of the channel is more noticeable. Figure 38a) also shows this effect. Once again, the shocks are growing stronger. Figure 44 represents the centerline Mach numbers. It is first observed that the test cavity centerline Mach number starts at a high supersonic value and practically stays constant up to x/d = 35. The maximum Mach number achieved was about 2.1 being 84% of the primary flow Mach number at that location. The Mach number curves of the supersonic nozzles centerline seem to be growing apart

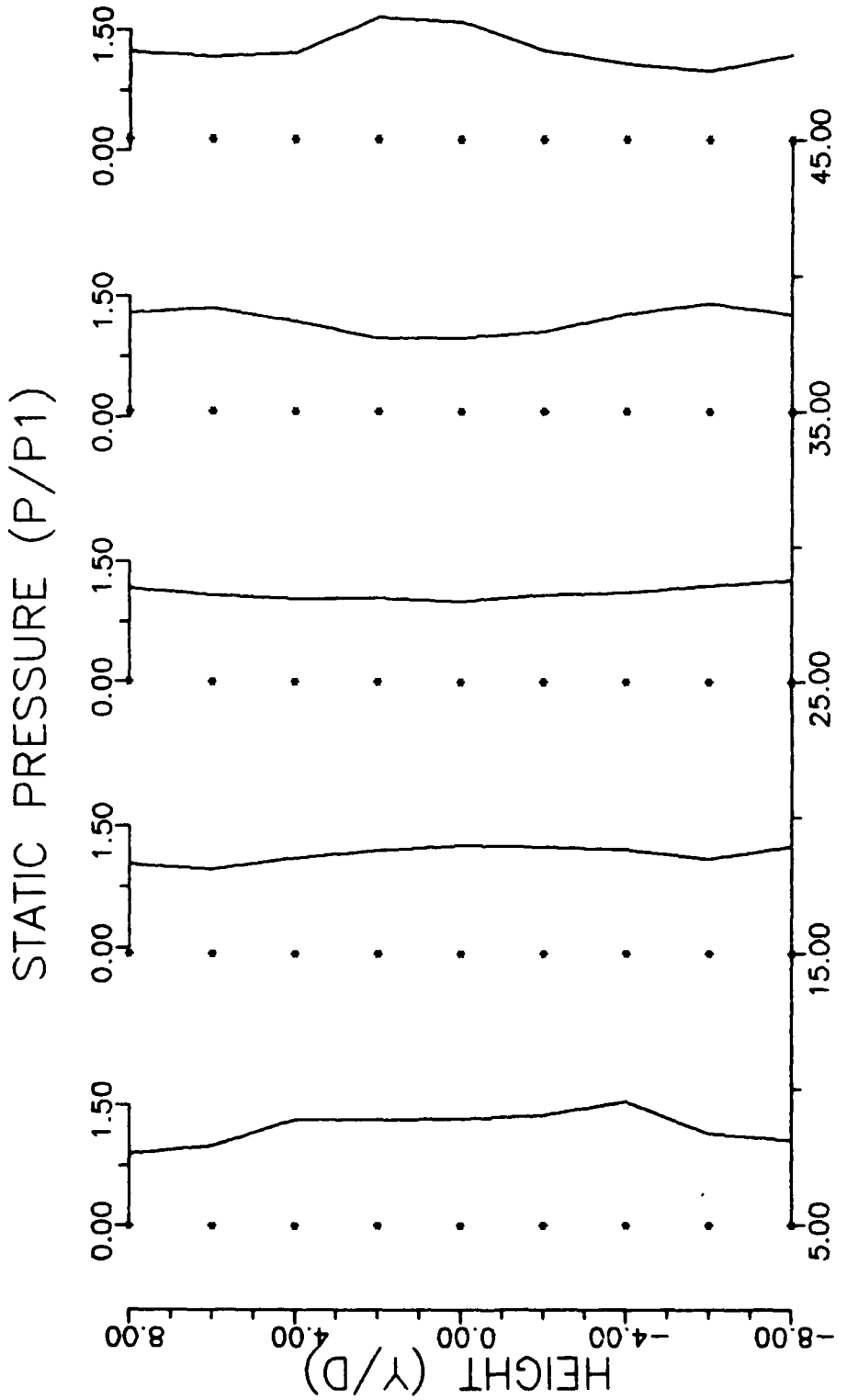

Figure 41. Static Pressure Profiles of Flow with Pressure Ratio of 0.48

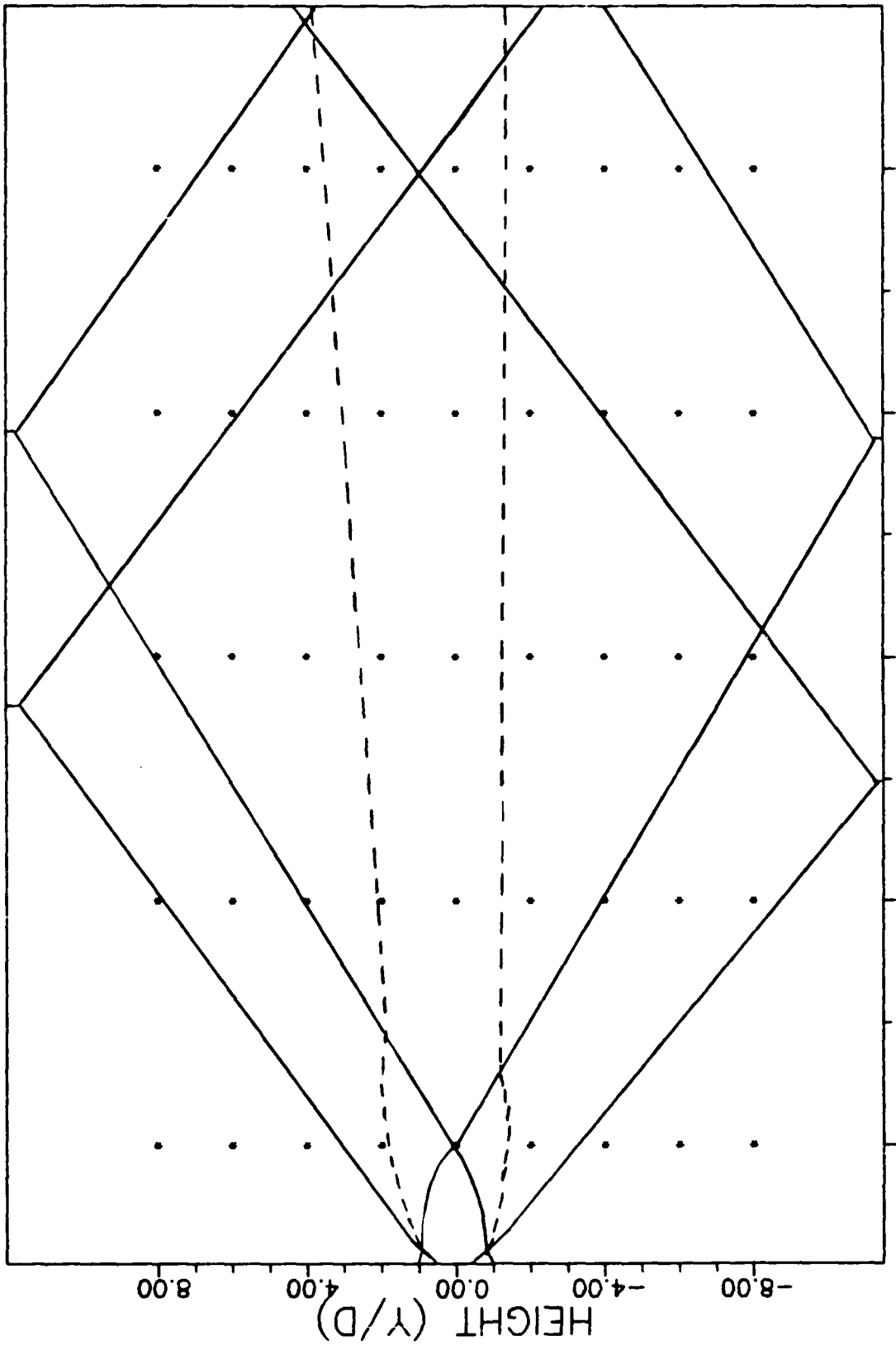

Figure 42. Template for Pressure Ratio of 0.48

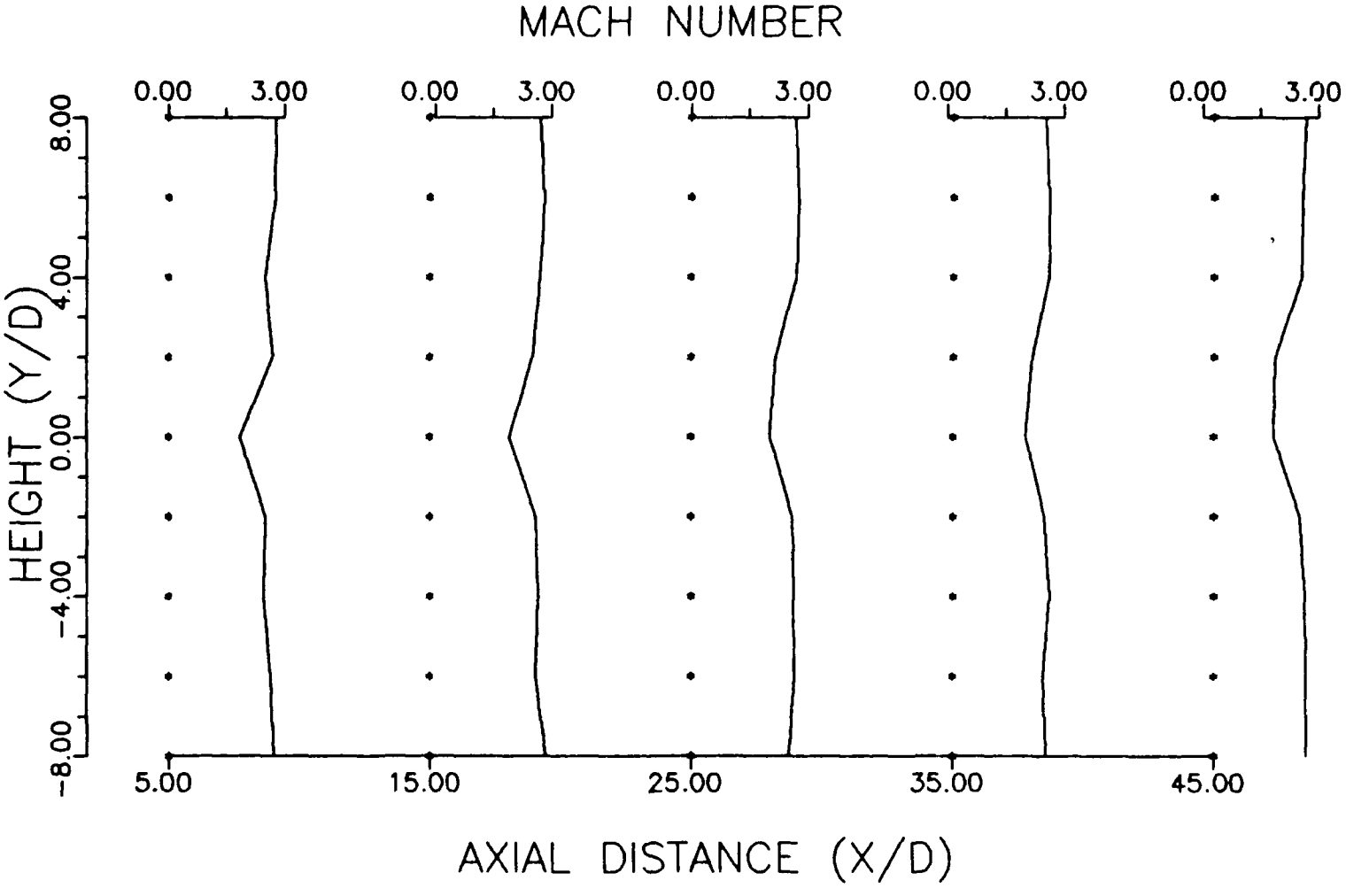

Figure 43. Mach Number Profiles of Flow with Pressure Ratio of 0.48

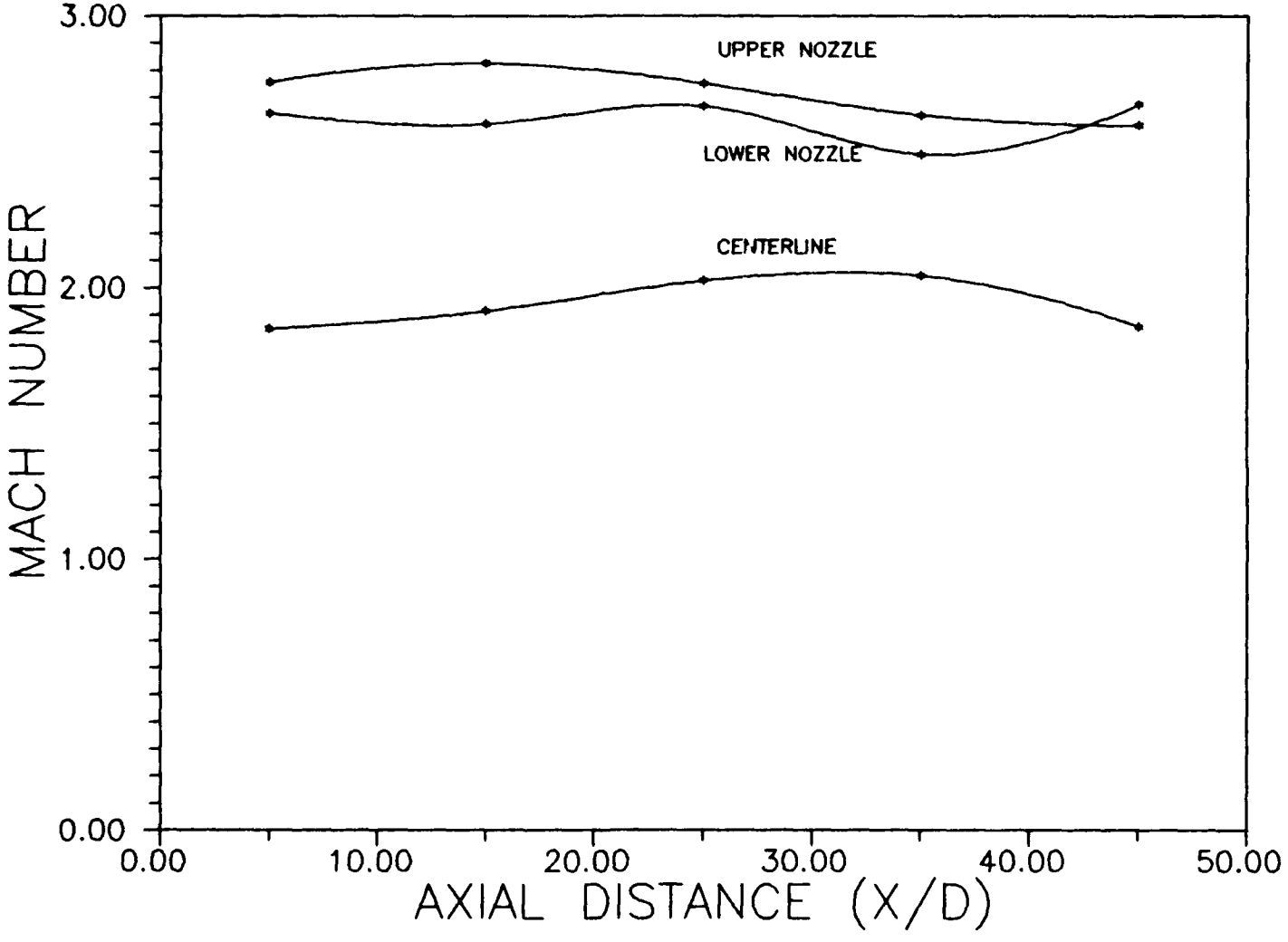

Figure 44. Mach Number VS Axial Distance on Centerlines of Flow with Pressure Ratio of 0.48

possibly due to the slight asymmetry of the test section. This means that the secondary jet may influence the outer streams for this test condition as a result of the stronger recompression shocks and shock reflections with feedback through the boundary layers.

Figure 45 represents the total pressure profiles. The same observations as for the other test conditions are made. The sharp rise in total pressure experienced at x/d = 5 and y/d = +2 could be explained by possible shock interference with the pitot probe.

Total Pressure Ratio of 0.66 and 0.73. The last test conditions were set at $P_0'/P_0 = 0.66$ and $P_0'/P_0 = 0.73$, the latter being the maximum pressure ratio attainable with the present set-up. Since no marked differences were noticed in the profile graphs, only the profiles for the pressure ratio of $P_0'/P_0 = 0.73$ were analyzed. Figures 38b) and 39b) show photographs of the flow at $P_0'/P_0 = 0.66$ and Figures 38c) and 40 are photographs of the flow at the highest pressure ratio. In both cases and as seen in Figures 38b) and 38c), recompression shock angles are larger compared to lower pressure ratios. Also, the combination of the shear layers and secondary jet has grown larger. The expansion region of the secondary flow behind the sonic nozzle is now longer and larger. Figure 46 represents the static pressure profiles for $P_0'/P_0 = 0.73$ with template shown in Figure 47. Very high pressure rises can be seen at

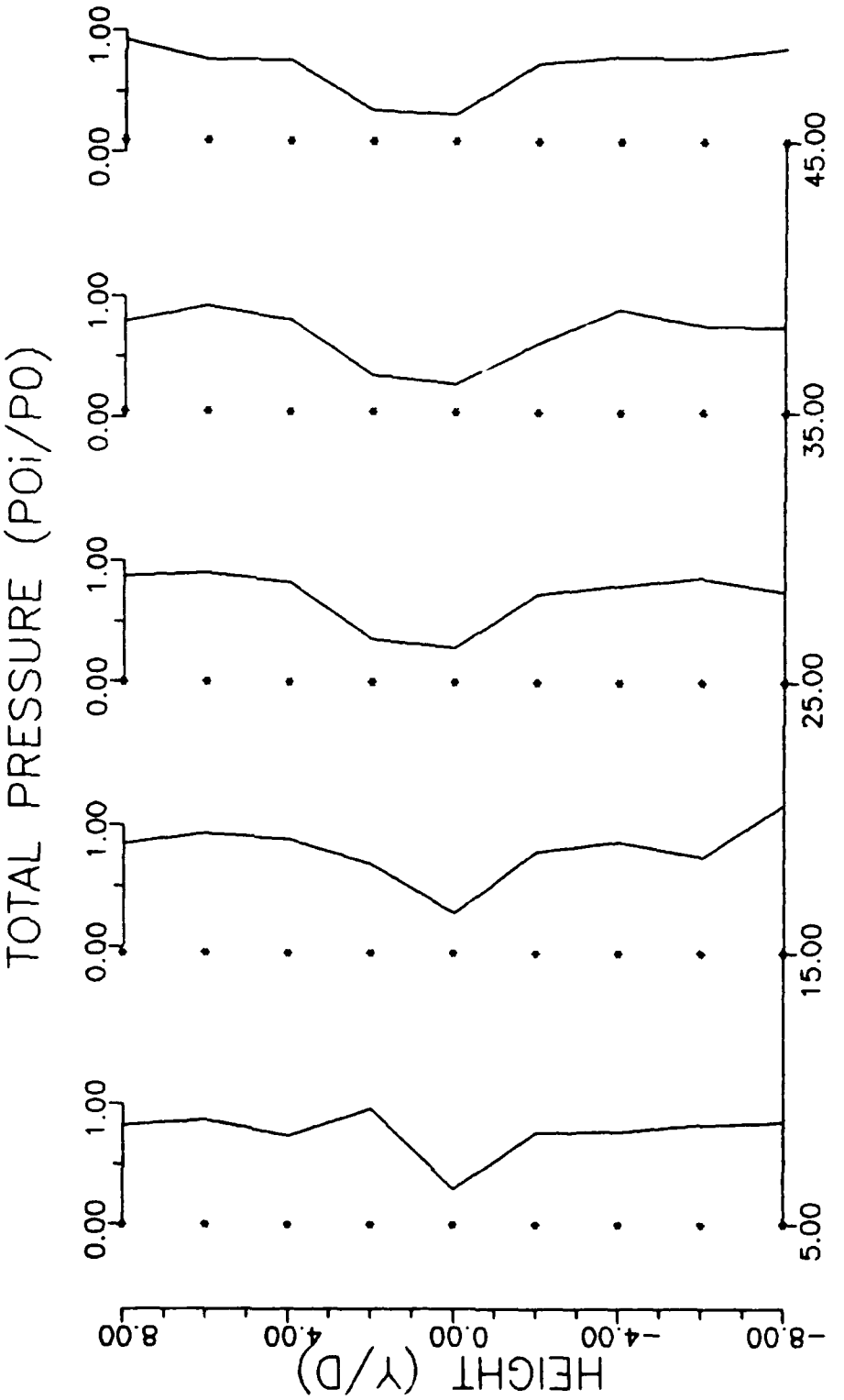

Figure 45. Total Pressure Profiles of Flow with Pressure Ratio of 0.48

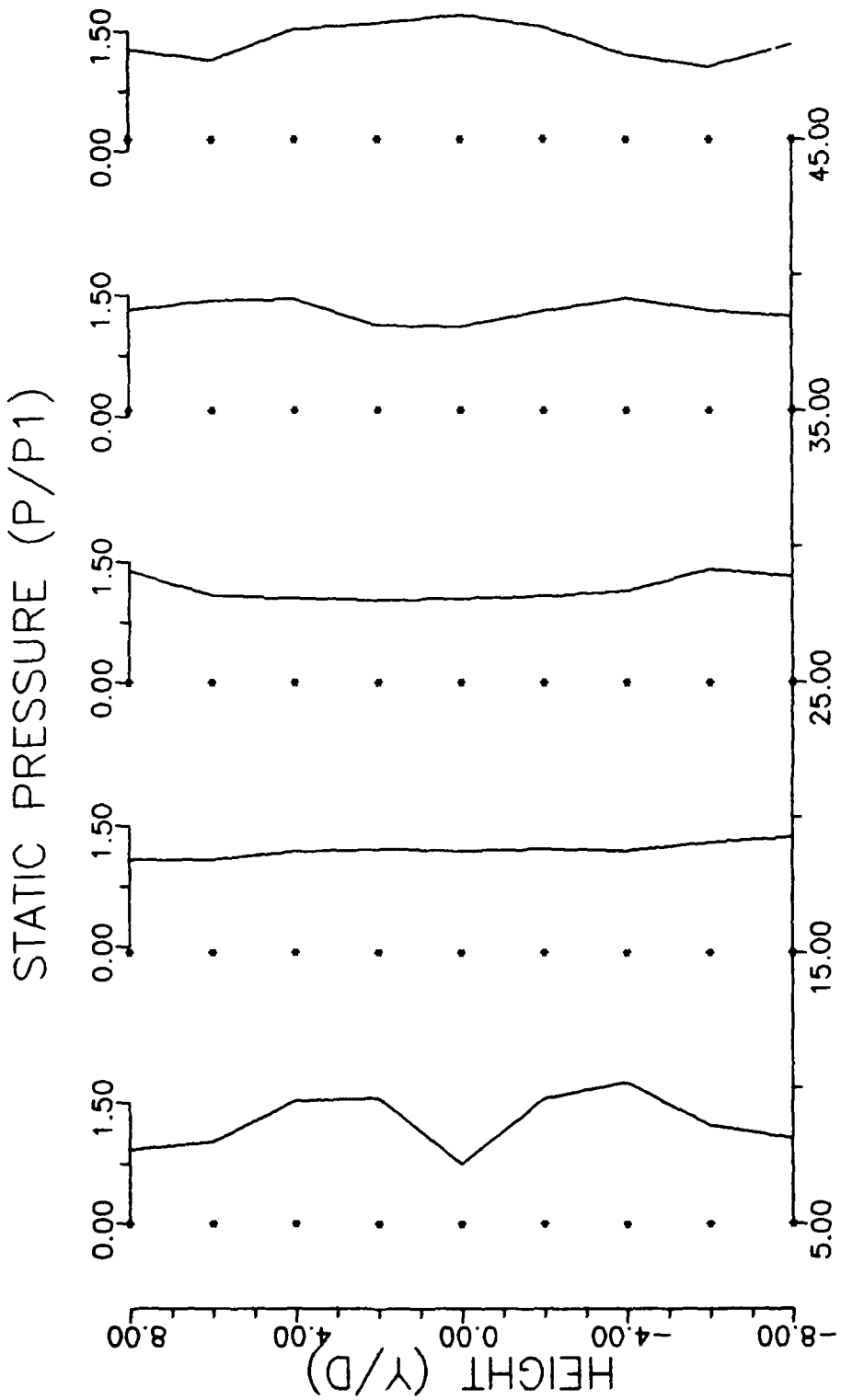

Figure 46. Static Pressure Profiles of Flow with Pressure Ratio of 0.73

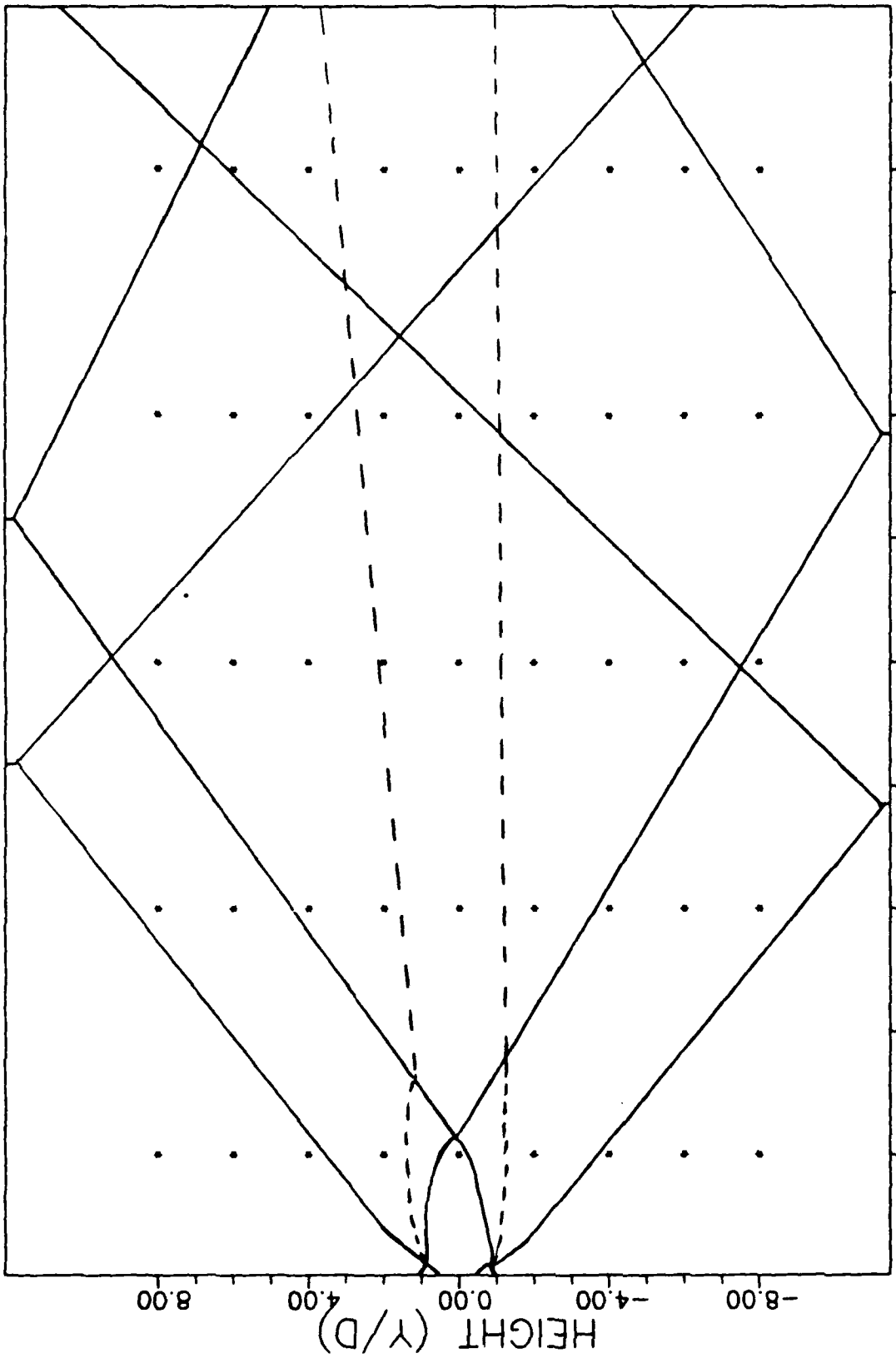

Figure 47. Template for Pressure Ratio of 0.73

x/d = 5, y/d = +2 and -2 and +4 and -4 due to the outer recompression shocks which appear to be strong. It is also shown that even at this high pressure ratio, the static pressure is fairly constant across the height of the test cavity when measured away from the shocks and far from the nozzle block.

Figure 48 represents Mach number profiles for this maximum pressure ratio. It can be seen that the profiles are nearly uniform except for a slight decrease in the secondary jet still showing a slight upward curvature from the center of the test cavity. Decreases in Mach number at x/d = 5, y/d = +2 and -2 are also experienced because of the oblique shocks. Figure 49 shows the Mach number of the primary and secondary streams for the pressure ratio of $P_0'/P_0 = 0.66$. Expected behavior of the centerline curve is observed. The center jet attained close to 88% of the Mach number of the primary stream. Figure 50 is the same type of graph but for the highest pressure ratio, $P_0'/P_0 = 0.73$ The first noticeable difference is the behavior of the centerline Mach number curve. It now starts with a higher supersonic value (2.4) compared to the lower pressure ratios. The reason for this was that the first centerline port is now located inside the expanding region of the sonic nozzle (see Figure 47). As the flow proceeds downstream, the Mach number decreases and increases again to a value close to 84% of the primary stream Mach number. This

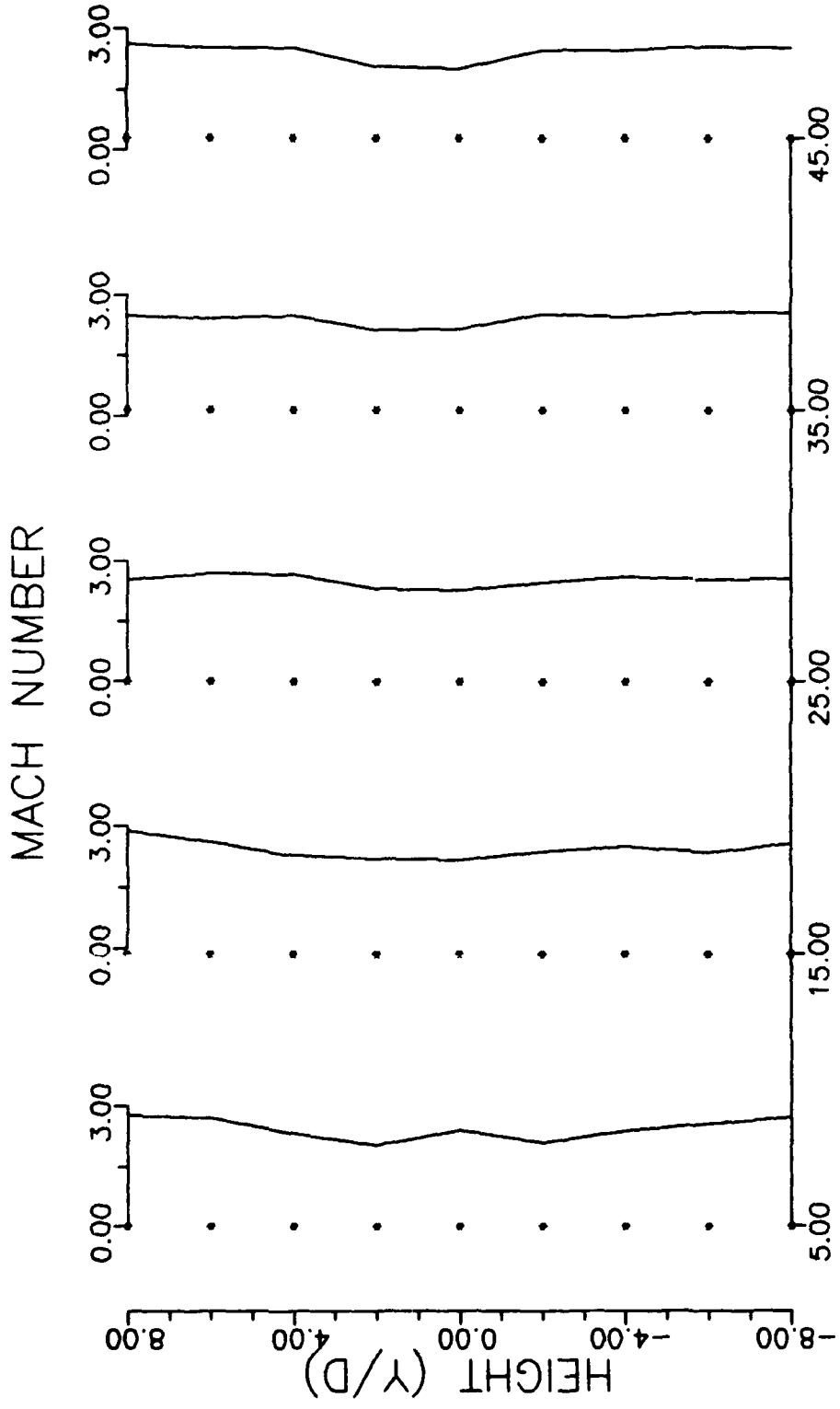

Figure 48. Mach Number Profiles of Flow with Pressure Ratio of 0.73

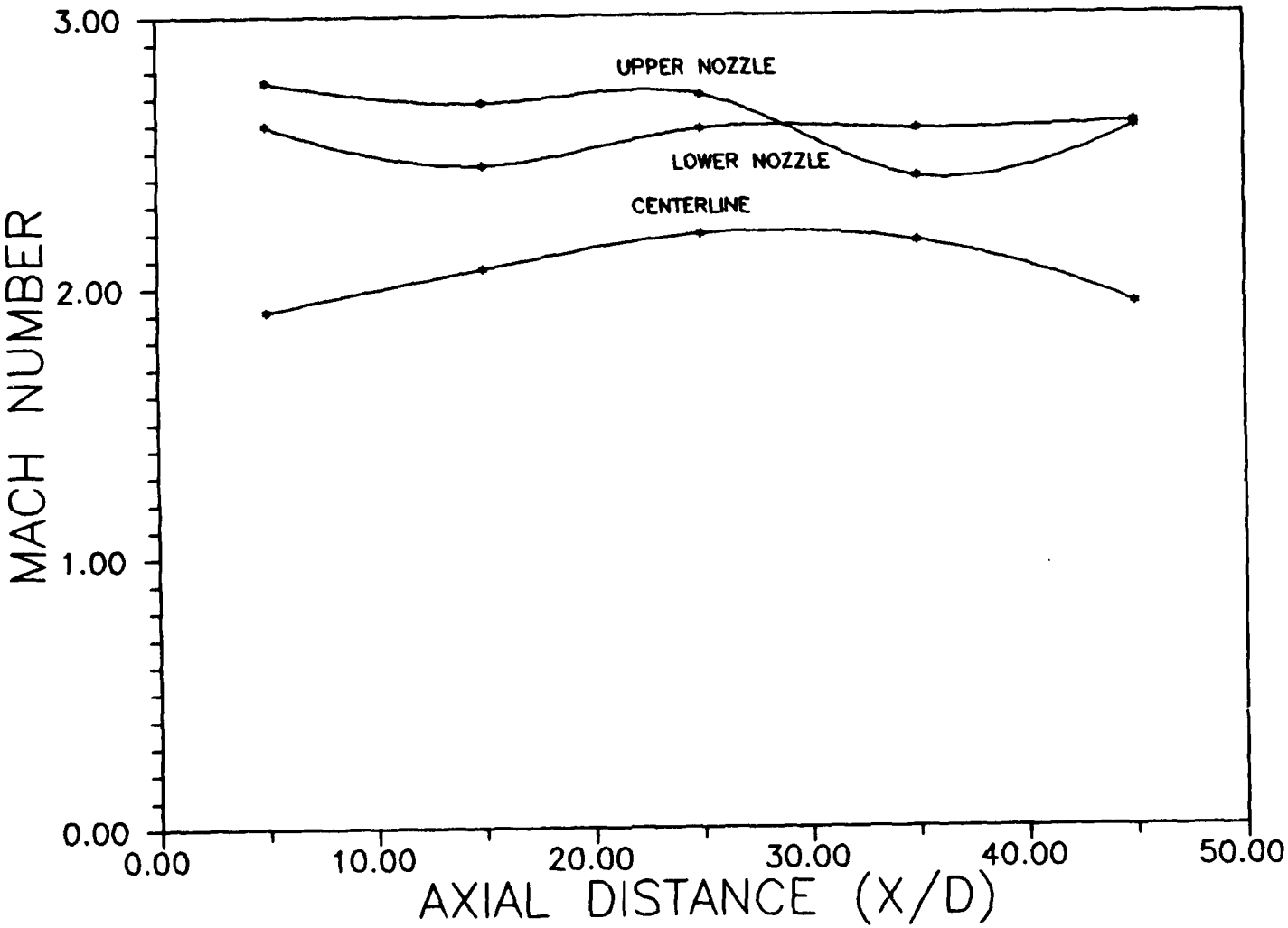

Figure 49. Mach Number VS Axial Distance on Centerlines of Flow with Pressure Ratio of 0.66

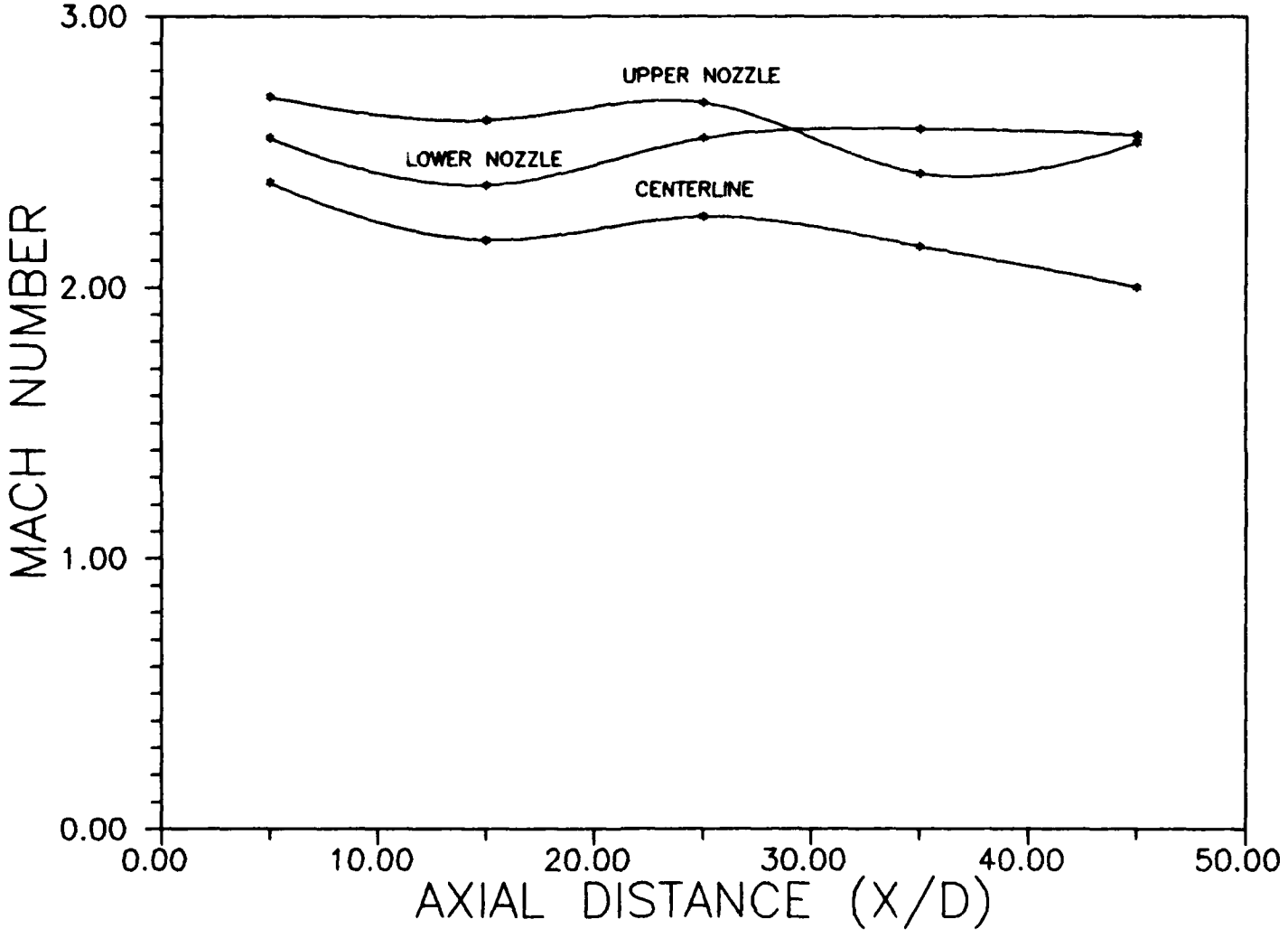

Figure 50. Mach Number VS Axial Distance on Centerlines of Flow with Pressure Ratio of 0.73

increase is attributed to the jet being accelerated by the outer streams, as was the case for the other pressure ratios. Finally, Figure 51 shows the total pressure profiles for $P_0'/P_0 = 0.73$. This figure, together with Figure 47, shows the jet corridor where the lower total pressure is experienced. Also, as the shocks grew stronger, it became more difficult to take a pitot pressure since the probe vibrated when it measured pressure close to an oblique shock. This brought a rise in pitot pressure readings and all those points are dismissed as bad data.

General Observations. Many general observations were noted throughout the flowfield discussion which are worthy of mention here. First, it was observed that the shear layer spreads on passing through an oblique shock wave. Making the shear layer larger would mean an increase in turbulence level hence a possible higher mixing rate. Note in Figures 39 and 40 the broader shear layers and more general turbulence as compared to Figure 22. An oblique shock located in a combustor could then improve the mixing process and it could be desirable even with the loss in total pressure.

As the secondary total pressure is increased, the shocks grows stronger, the shear layers are better defined and the growth of the secondary jet combined with the shear layer is more noticeable. The expansion region of the secondary flow grows larger and longer. Also, it was seen

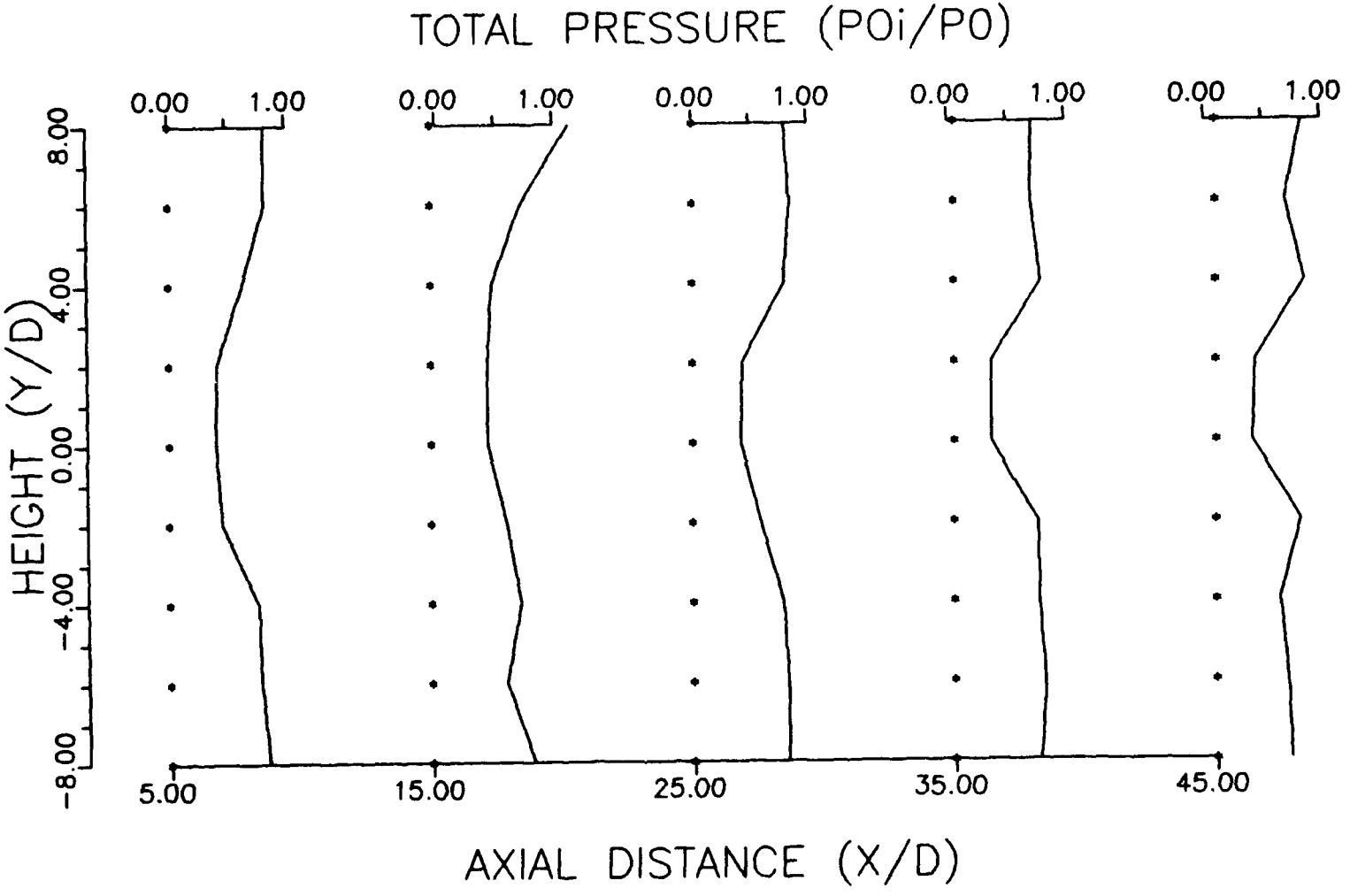

Figure 51. Total Pressure Profiles of Flow with Pressure Ratio of 0.73

that the stronger shocks have a greater effect on the flowfield directly and appenrently the mechanism of feedback through the boundary layer influence the flow upstream of the shock as well.

Using schlieren photographs of the whole test cavity, Figures 20 and 38, the shock wave angle ε was measured. The angle of the top outer recompression shock was chosen and the upstream Mach number was taken to be the value at the port closest to the shock as seen on schlieren photographs with static ports installed. Table 1 represents measured shock wave angle ε and upstream Mach number calculated with the pitot Rayleigh equation. The Mach number associated to ε for a flow turning angle of two degrees taken from a gas table (18:746) is tabulated for comparison with the calculated experimental value.

Table 1. Shock Wave Deflection Angle and Calculated Experimental Upstream Mach Number Compared to Theoritical Mach Number For Different Total Pressure Ratios.

P_0'/P_0	ε degrees	M (data)	M (table)	Difference %
0.02	21	2.838	2.98	+ 4.77
0.13	21	2.717	2.98	+ 8.85
0.30	21	2.764	2.98	+ 7.25
0.48	24	2.513	2.60	+ 3.35
0.66	28	2.379	2.24	- 6.21
0.73	29	2.312	2.16	- 7.04

Good agreement exists between experimental and theoretical Mach numbers but it is shown that a deflection angle of 2 degrees is too large for the lower values of secondary flow total pressure. As P_0'/P_0 is increased over a value of about 0.50, it was noted that the measured data was higher than the theoretical value showing that a deflection angle of more than 2 degrees exists at those higher pressures. It is obvious that the flow will have a certain angle before crossing the first shock. For example, at $P_0'/P_0 = 0.73$, if a flow turning angle of 4 degrees is assumed upstream of the top outer recompression shock (which would be realistic), an upstream Mach number of about 2.3 is found in the referenced table. This would give a difference of about 0.5% which can be associated with the experimental errors. From this table, it is also obvious that the secondary jet interaction with the outer streams slows them down. As the secondary total pressure is raised, the recompression shock wave angles enlarge and the presence of all four recompression shocks reflecting on the walls of the test cavity (combustor) also slow the flow and change its direction. However, the loss of total pressure across the axial distance is not desired if it is excessive. This is why calculations of the test cavity exit properties are important.

Table 2 lists the variations in static and total pressures and Mach number across the test cavity experienced

for different pressure ratios. The exit values averaged over all ports at x/d = 45 are compared to properties existing at the exit of the supersonic nozzles (x/d = 0). The rationale is that at the x/d = 0 location, the flow properties (P_0, P, M) can be controlled by design of combustor inlet.

Table 2. Difference in Properties Across the Length of the Test Cavity for Different Pressure Ratios.

P_0'/P_0	Difference in Static Pressure %	Difference in Total Pressure %	Difference in Mach Number %
0.02	+ 28.28	- 30.17	- 11.60
0.13	+ 33.79	- 28.39	- 13.99
0.30	+ 39.31	- 30.09	- 16.04
0.48	+ 46.21	- 29.86	- 16.04
0.66	+ 52.41	- 30.06	- 16.72
0.73	+ 56.55	- 31.74	- 17.41

With Table 2, it is clear that to minimize flow losses, a long combustor is not desirable. It first must be realized that increases or losses in properties listed in this table are experienced at a distance downstream of only 45 sonic orifice heights (4.5 inches or 11.43 cm). As the pressure ratio P_0'/P_0 is increased, a marked increase in static pressure and decrease in Mach number are observed.

These can be explained by viscous effects (friction) and also by the large number of recompression and reflected shocks in the test cavity which grow in strength as the pressure ratio is increased. The important factor to consider is the loss in total pressure: close to 32%. Also, it is noted that this value is fairly constant with variable secondary injection pressure up to $P_0'/P_0 = 0.73$. This is one reason why a higher injection pressure should be selected since the loss in total pressure is almost constant. However, no observations could be made for pressure ratios higher than the ones experienced in this investigation.

Chow's Flow Model. The geometrical similarity between Chow's two-dimensional flow model (2:176) and the set up utilized for the present investigation (see Figure 11) permits its use in the study of base pressure. As discussed earlier, a special set up was used to get the low pressure ratio data needed for comparison with Chow's model at low secondary flow conditions. A valve opened to atmosphere was connected to the secondary injection port to obtain and control the low secondary pressures.

Figure 52 shows the relation between the base pressure P_b and the secondary total pressure P_0' both normalized with the static pressure at the exit plane of the supersonic top nozzle P_1. The first observation is that our

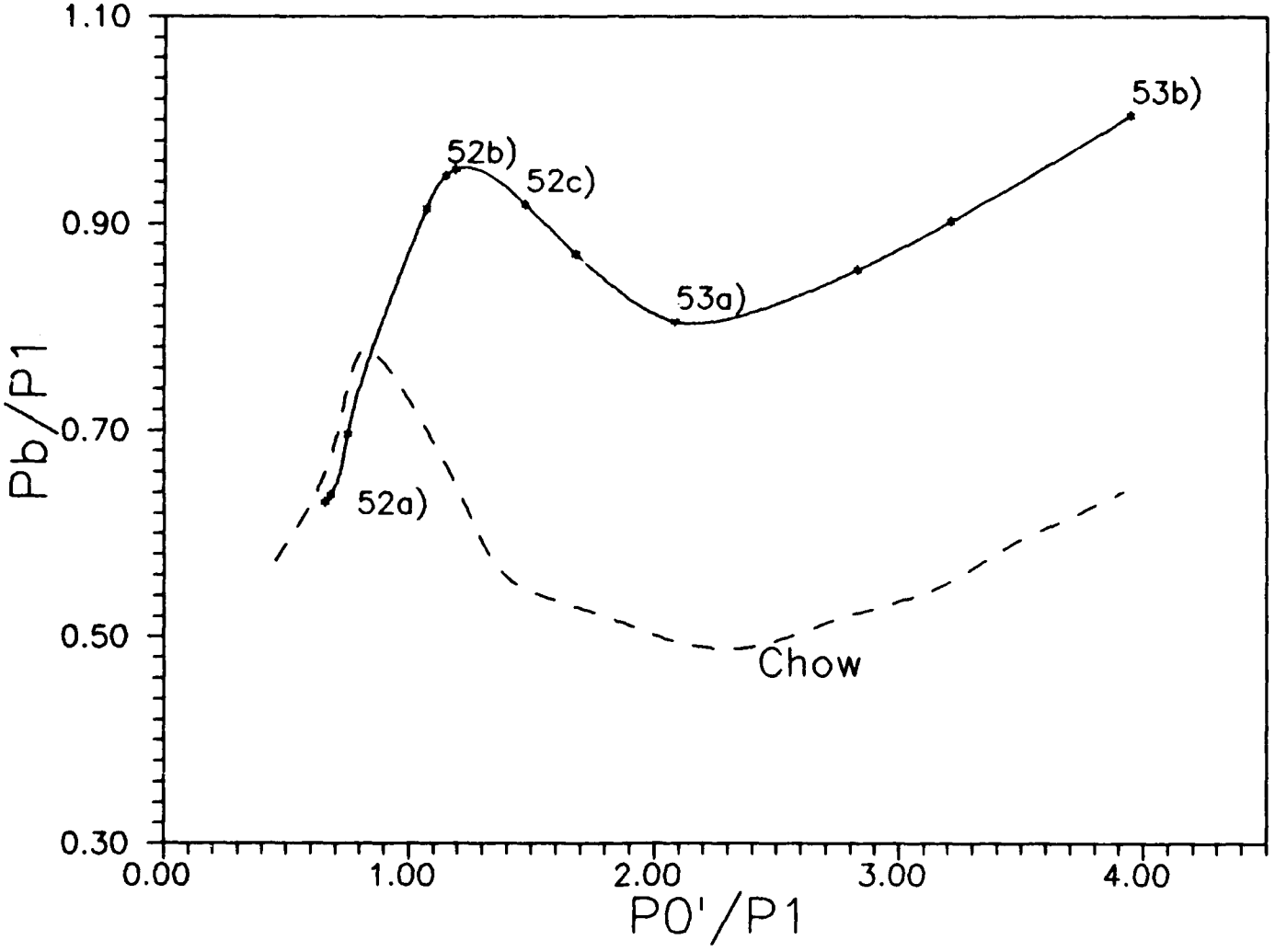

Figure 52. The Relation Between Normalized Base Pressure and Secondary Total Pressure

experimental curve (solid line on Figure 52) has the same basic trends as Chow's experimental curve (2:177) shown as a dashed line on the figure. Some differences between the two curves probably result from difference in outer stream Mach number and step height. Also, the fact that this experiment deals with two outer streams between which flows a sonic or subsonic jet (see Figure 11) may have a larger effect on experimental data. To correlate data with actual flow conditions, schlieren pictures were taken and are presented in Figures 53 and 54. Also, 5 photographs associated with the experimental curve are labeled on Figure 52.

Figure 53a) shows the magnification of the sonic orifice at the flow condition of $P_0'/P_0 = 0.02$ (no secondary flow). This was the smallest pressure ratio attainable for this set up and shows a low base pressure on Figure 52. Figure 53b) was taken at a higher pressure ratio but still low enough to prevent choking of the sonic nozzle. As can be seen on Figure 52, the base pressure increased dramatically and is now close to it's maximum value. This could be explained by the fact that the outer stream is still able to pump the mass out of the recirculation region at the same rate as it is being input by the unchoked sonic nozzle. This prevent the formation of the secondary subsonic jet, which would lower the base pressure. Those pressure ratios represent Chow's flow model I (2:178). As the pressure ratio is increased, the base pressure starts to

Figure 53. Composite Schlieren Photographs with Knife Edge Perpendicular to the Flow and Magnification Factor of 2.5 with P_0'/P_0 of:

a) 0.02 b) 0.04

c) 0.05

decrease (Figure 52). The corresponding schlieren photograph is shown in Figure 53c). The secondary jet is now visible and is subsonic close to the nozzle since choked conditions are not met yet. The pressure in the sonic nozzle and hence the secondary flow rate is now high enough to create a jet between the outer streams and it seems that the outer flow is expanding a lot less, creating weaker recompression shocks. This represent Chow's flow model II (2:178).

Next, the pressure ratio is increased to P_0'/P_0 = 0.08. This caused the sonic nozzle to choke and, as seen in Figure 54a), a normal shock is formed. This shock wave caused the supersonic expanded secondary flow to go subsonic. From Figure 52, it is seen that this condition is associated with the relative low point of the curve. This is due to the new flow configuration where the recirculation region has now the form of a closed triangle. This triangular region seen at the end of the base of the sonic nozzle (Figure 54a)) is assumed to have a constant static pressure P_b and ends with two recompression shocks. Figure 54b) shows the next pressure ratio, P_0'/P_0 = 0.12, where the control valve was fully open and that the cavity of the sonic nozzle was close to atmospheric pressure. This photograph is labeled on Figure 52 and represents the last data point taken. This condition also shows a rise in base pressure which is now almost linear with the secondary total

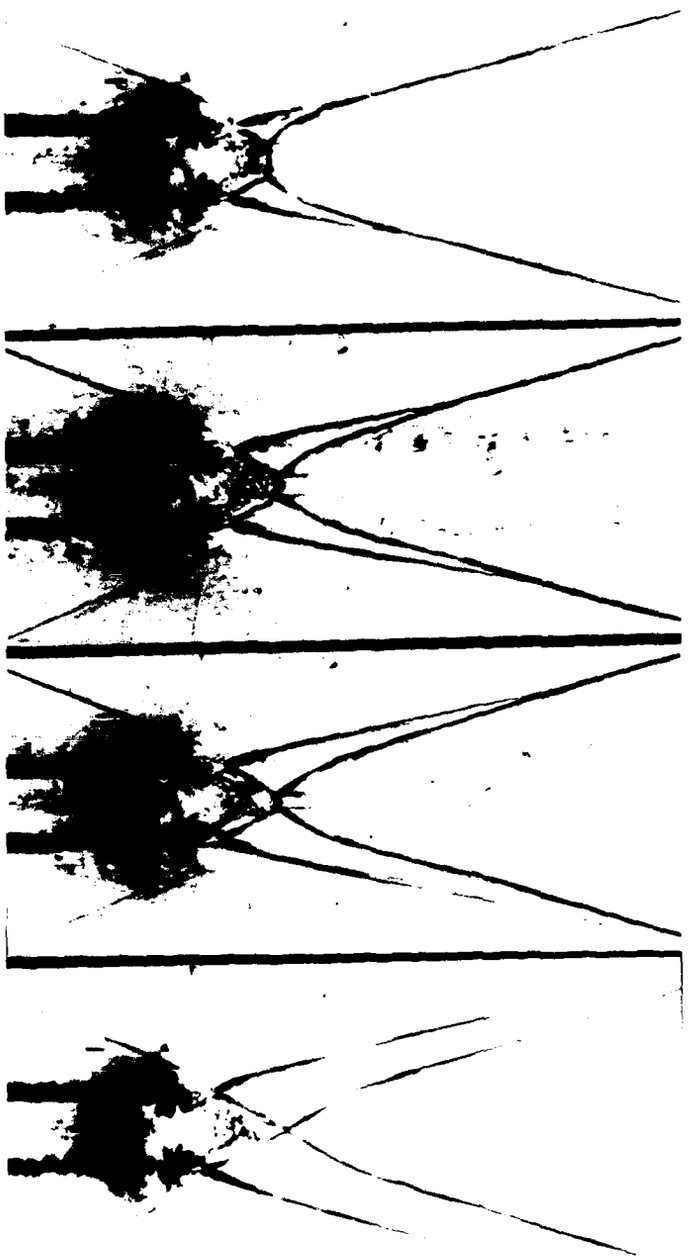

Figure 54. Composite Schlieren Photographs with Knife Edge Perpendicular to the flow and Magnification Factor of 2.5 with P_0'/P_0 of:

a) 0.08 b) 0.12

c) 0.19 d) 0.24

pressure. This represents Chow's flow model III (2:177) but nowhere in the paper did Chow mention the formation of the presently experienced normal shock wave. The fact that Chow's experimental set up used a wall as a centerline was not the case in this present investigation. This is probably the reason of the normal shocks. The formation of this normal shock could be explained by the assumption that the two primary streams expanding on each side of the expanding sonic jet will cause the flow to form converging pressure "walls" in which the normal shock will form. Also the beginning of the outer recompression shocks seen already in Figure 54a) probably allows some of the secondary flow a path out. As can be seen in Figures 54b), c) and d), the normal shock gradually reduces in cross section as the secondary flow total pressure is increased. The sonic jet expands more causing the inner recompression shocks to grow stronger, converging faster together. As can be noted on Figure 54d), a pressure ratio slightly above $P_0'/P_0 \cong 0.25$ is the right condition to have the secondary jet totally supersonic. This is when the secondary jet will start to grow and the recompression shock angles will get larger as the secondary flow total pressure is increased.

Shear Layer and Mixing Concepts. In a supersonic combustor, a shear layer is created by the supersonic airflow coming from the inlet interacting with the fuel injected through a sonic orifice (present case) and

producing a submerged jet. Complete burning of fuel is necessary for economical operation and to obtain the required performance from a hypersonic airbreathing propulsion system. If the burning of fuel takes too long, longer combustor will be required affecting the thrust-to-weight ratio of the whole vehicle.

The mixing rate correlates closely with the growth of the shear layer. A faster growing shear layer for the same mass ratio means that more mass is entrained from both co-flowing streams making mixing more efficient. Equally important is the turbulence level of the shear layer. Turbulent kinetic energy is directly linked to the mixing length (14:1270) so that higher turbulence level will mean shorter mixing length, thus a higher mixing rate.

In order to get a feel for the mixing rate, a way to measure the thickness of the shear layer at different axial location is needed. From these measurements, the shear layer growth can be examined. One way to measure the shear layer thickness is to use schlieren pictures. This proved to be difficult since demarcation between the outer streams, the center jet and the shear layers is not always easy to see. Figures 20 and 38 were used to try to measure the shear layer but for the reason mentioned, no accurate data could be obtained. However, Papamoschou (11:53) suggested that "the visual thickness, although a subjective measurement, is useful in defining the extent of the region

involved in the mixing". The measurements on the schlieren photographs (Figures 20 and 38) gave a good insight for the order of magnitude of the shear layer thickness.

Knowing that a deficit in total pressure will occur in the shear layer, a special experiment was conducted to give more detailed total pressure profiles across the height of the test section. Using a displacement transducer to monitor the vertical displacement of the pitot probe, an average of 20 data points was taken across the middle inch of the test cavity. Using the fact that the static pressure is fairly constant across the layer, total pressure was calculated from the pitot Rayleigh equation together with gas dynamic relationships. Two different pressure ratios were tested: P_0'/P_0 = 0.48 and 0.73, the latter being the maximum pressure ratio for the present experimental set up. A typical total pressure profile is shown in Figure 55. This figure represents the total pressure profile at x/d = 25, P_0'/P_0 = 0.48. The top shear layer thickness was directly measured from the total pressure profile, taking the difference between the vertical location of the outer edge of the center jet and the inner edge of the top outer stream. This can be seen on Figure 54 where constant pressure from y/d = 5 to y/d $\cong$ 2.95 gives way to a decrease in total pressure (the shear layer) down to y/d $\cong$ 2.11 where the constant total pressure across the center jet is detected. The approximate thickness of the shear layer for

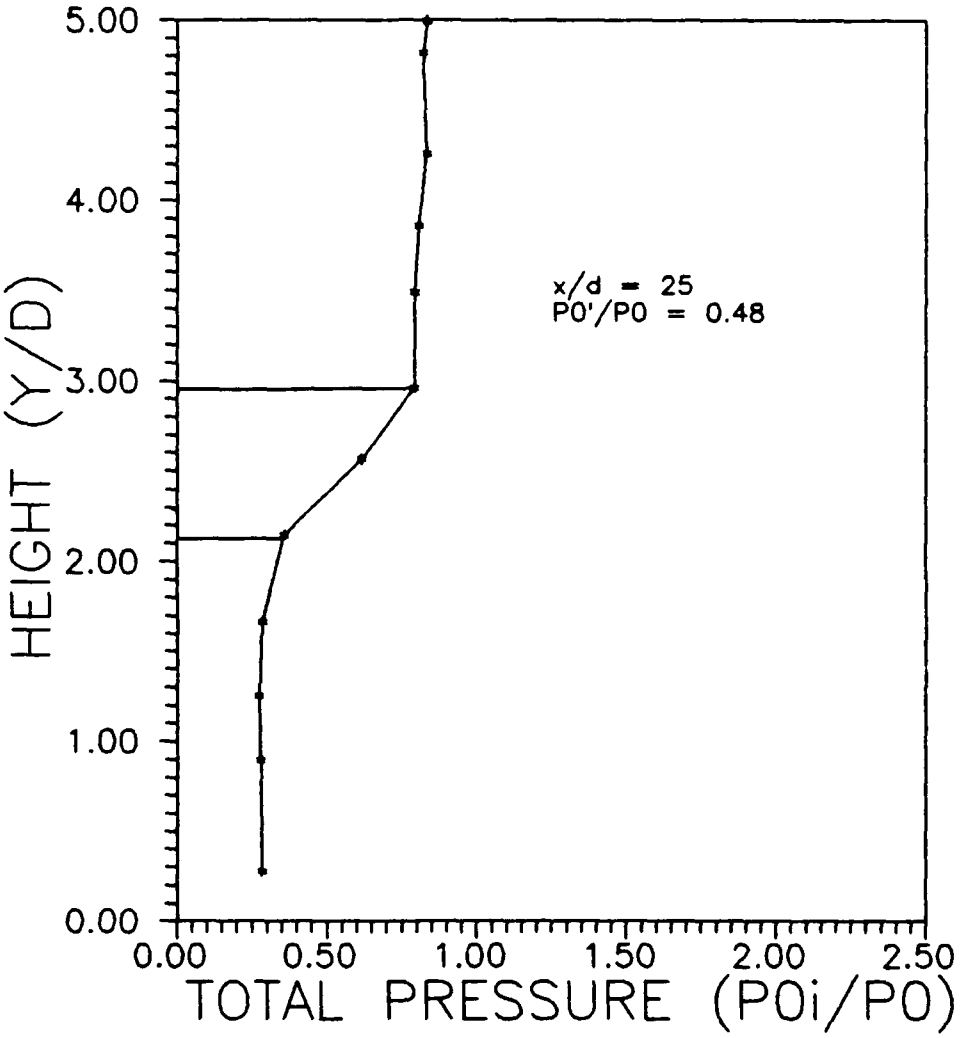

Figure 55. Selected Total Pressure Profile

this particular axial location and pressure ratio was then calculated to be 2.95d - 2.11d = 0.84d (or 0.084 inch (0.213 cm) physical dimension). This fast and apparently efficient way of measuring the shear layer thickness gives a good approximation.

The shear layer thickness obtained from the total pressure profiles was plotted against the axial direction in Figure 56 for total pressure ratios of 0.48 and 0.73. From this figure, it is evident that the shear layer grows more rapidly for a higher pressure ratio. As discussed before, this would mean that higher secondary total pressure is desired in order to accelerate the mixing rate. Different curve fitting schemes were tried for these curves and it was found that the linear fit was good and gave a shear layer thickness proportional to the axial distance times the constant 0.0332 for the lower pressure ratio (P_0'/P_0 = 0.48). Fitting the higher pressure ratio curve with the linear function gave a shear layer thickness proportional to constant 0.091 times the axial location. These results appear to be in agreement with Papamoschou (11) who investigated the growth of the shear layer formed by two co-flowing streams initially separated by a thin splitter plate. This shows that the geometry of the fuel injection system may not be an important factor for the downstream behavior of the shear layer growth rate.

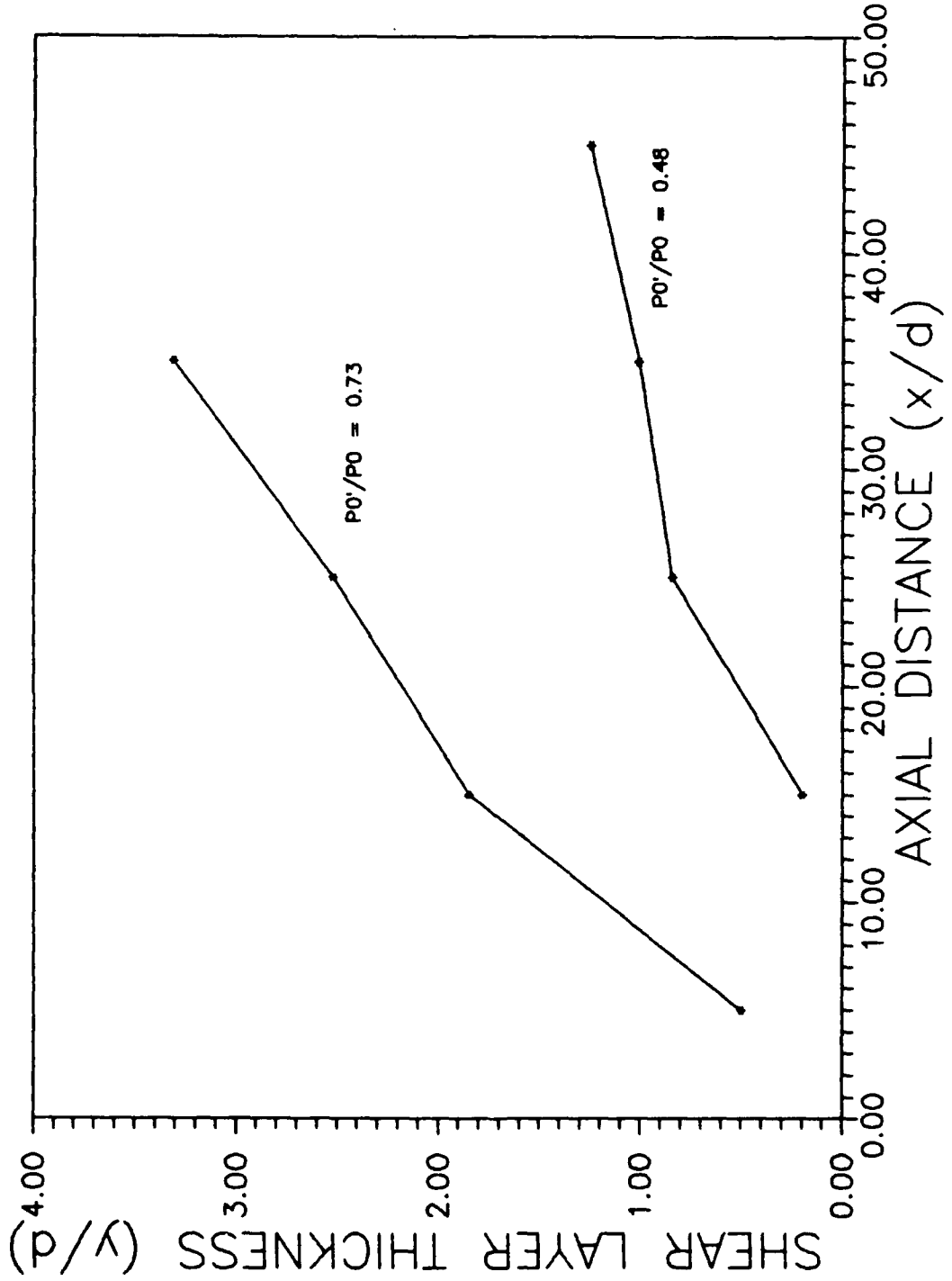

Figure 56. Shear Layer Thickness VS Axial Distance

The mathematical model for shear layer growth presented in Chapter 4 was used here to calculate the convective Mach numbers. It was found that the convective Mach numbers of the jet and outer stream were equal because both ratios of specific heats are the same (γ=1.4). The interpretation of the convective Mach number used here is basically the relative convective velocity between the shear layers and the two co-flowing streams. As the center jet accelerates due to the increase in the secondary total pressure, the relative velocity between the jet and the shear layer decreases. This caused the convective Mach number to decrease. Figure 57 shows the relation between the total pressure ratio and the calculated convective Mach number at x/d = 25. It is evident that as the pressure ratio is increased, the convective Mach number drops drastically, meaning an increase in the shear layer growth rate according to Papamoshou's theory (11).

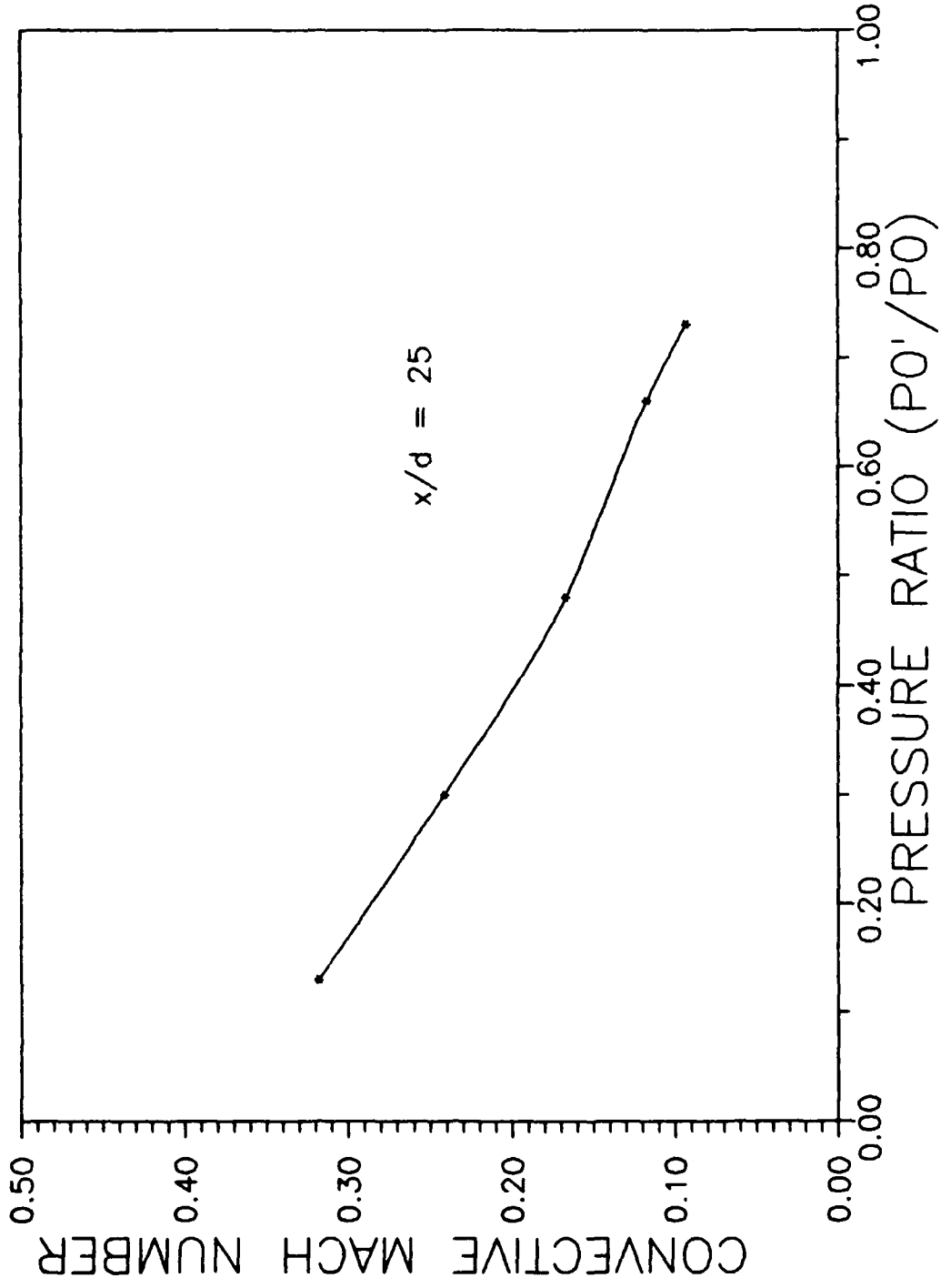

Figure 57. Convective Mach Number VS Pressure Ratio

Conclusions and Recommendations

Conclusions

This investigation analyzed the sonic parallel injection to co-flowing supersonic streams. Observations were made of the flow characteristics as a function of secondary flow to primary flow total pressure ratio. Furthermore, shear layer growth rate was analyzed in order to get a feel for mixing.

The water table is a good flow visualization tool but the recording of the flow at an acceptable standard of quality was far beyond the scope of this study.

Sonic injection with a base region between two co-flowing supersonic streams causes oblique shocks downstream of the nozzle assembly. Those shocks appear to grow in strength as the total pressure ratio is increased. However the total pressure loss across the length of the test section is independant of the total pressure ratio. Also, from visual observations, shear layers appear to spread when going through a shock wave, increasing the turbulence-affected region hence, the mixing between the flows.

Chow's relation between the secondary total pressure and the base pressure was demonstrated. Chow's theory on base pressure appears to represent the flow characteristics

near the end of the nozzle.

Mixing in the shear layer occurs at constant static pressure far from the nozzle. This theoretical assumption was demonstrated experimentally.

The convective Mach number decreases as the secondary flow total pressure is increased. The concept of convective Mach number applies to the sonic injection of secondary flow as well as the supersonic secondary injection without base region investigated by Papamoschou.

The growth rate of the shear layer increases with increase in total pressure up to $P_0'/P_0 = 0.73$ due to the sharp decrease of the convective Mach number as the total pressure ratio increases.

Recommendations

The study of flow mixing is important for the future. Eventually, the best injection system will have to be chosen and the sonic injection appears to be appropriate. Also, methods to enhance mixing should be studied to get the best performance of any supersonic combustor.

The turbulent kinetic energy is important for the mixing process. To better understand the shear layer mixing region, accurate measurements of turbulence level and velocity components with a hot film could be done.

The investigation of the flowfield created by the interaction of a supersonic jet with no base region and a

supersonic co-flowing stream must be done to compare both ways to inject fuel parallel with the flow.

Cold flow study of shear layer and mixing in the supersonic arena must continue. Changing the injected gas (for example to helium) would permit the gathering of data related to the mixing of flows with different ratio of specific heat and concentration.

Bibliography

1. Billig, F.S., and Others, "Integral-Rocket Dual-Combustion Ramjets: A New Propulsion Concept," Journal of Spacecraft and Rockets: pp 416-424, Vol. 17, No 5 , (Sept-Oct 1980)

2. Chow, W.L. "On the Base Pressure Resulting From the Interaction of a Supersonic External Stream With a Sonic or Subsonic Jet," Journal of the Aerospace Sciences: 176-180 (March 1959).

3. Curran E.T., Leingang J.L., and Donaldson, W.A., "A Review of High Speed Airbreathing Propulsion System ", Aero Propulsion Laboratory, AFWAL, ASD, WPAFB, Ohio.

4. Donaldson, I.S., "On The Separation of a Supersonic Flow at a Sharp Corner ", AIAA Journal , Vol 5, No , 1086-1088, June 1967.

5. Escher, W.J.D., Teeter, R.R., and Rice, E.E., AIAA-86-1680 Airbreathing and Rocket Propulsion Synergism: Enabling Measures for Tomorrow's Orbital Transports, AIAA/ASME/SAE/ASEE 22nd Joint Propulsion Conference, June 1986.

6. Golovichev, V.I., "Numerical Modeling of Thermal Compression of a Supersonic Stream by Combustion.", Translated from Fizika Goreniya i Vzryna, Vol. 19, No.1, pp.50-56, January-February, 1983.

7. Hamelin, S/L Gilles L., Investigation of the Mixing of Coaxial Heterogeneous Gas Jets Applied to Supersonic Combustion , M.S. Thesis, AFIT/GA/ME/65-2. School of Engineering, Air Force Institute of Technology (AU), Wright-Patterson Air Force Base OH, August 1965.

8. Ippen, A.T.,Harleman, D.R.F., and Crossley, H.E.,Jr., "Studies on the validity of the hydraulic analogy to supersonic flow," Massachusetts Institute of Technology Hydrodynamics Lab., U.S.Air Force TR 5985, Parts I and II (May 1950), Part III (October 1950), Part IV (February 1952), and Part V (December 1952).

9. John, James E.A.,Gas Dynamics, Boston: Allyn and Bacon, Inc.,1969.

10. Korst, H.H. "A Theory for Base Pressures in Transonic and Supersonic Flow," Journal of Applied Mechanics: 593-599 (December 1956).

11. Papamoschou, Dimitri, Experimental Investigation of Heterogeneous Compressible Shear Layers. PhD Thesis, California Institute of Technology, Passadina, California, 1986.

12. Shapiro, Ascher H. The Dynamics and Thermodynamics of Compressible Fluid Flow, Volume I. New York: Wiley and Sons, 1953.

13. Schetz, J.A., Billig, F.S., and Favin, S. ,"Flowfield Analysis of a Scramjet Combustor With a Coaxial Fuel Jet ", AIAA Journal , Vol 20, No 9, pp1268-1274, September 1982.

14. Schetz, J.A., Billig, F.S., "Simplified Analysis of Supersonic Base Flows Including Injection and Combustion ", AIAA Journal , Vol 14 , No 1 , Jan 1976.

15. Schlichting, Hermann. Boundary Layer Theory (Seventh Edition). New York: McGraw-Hill Books Company, 1979.

16. Traxler, Maj. John M. Interaction Between Two-Dimensional Sonic Jets and Supersonic Flow To Model Heat Addition In A Supersonic Combustor. M.S. Thesis, AFIT/GA/AA/87D-07. School of Engineering, Air Force Institute of Technology (AU), Wright-Patterson Air Force Base OH, December 1987.

17. Weber, Richard J., and Mackay John S., "An Analysis of Ramjet Engines Using Supersonic Combustion ", National Advisory Committee for Aeronautics, Technical Note 4386, September 1958, AIAA Selected Reprint Series , Volume VI , Ramjets , June 1969.

18. Zucrow, J.M., Hoffman, J.D., Gas Dynamics Volume I, New-York: Wiley and Sons, 1976.

APPENDIX A

CALIBRATION

Prior to taking data, the data acquisition system must be accurately calibrated.

Pressure Transducer Calibration

All pressure transducers were calibrated using a portable vacuum standard from MKS, type PVS-2, S/N 44362-1. A known pressure is fed to the transducer and to the vacuum standard. Transducer output voltage and pressure readings are then made simultaneously. A plot of pressure versus voltage is made and the equation of the line (if linear) is of the form $y = mx + b$ where

m = slope or sensitivity (mv/psi)

b = intercept

Depending on many variables but mainly temperature, a specific pressure transducer may have a shift of zero voltage during an experiment. Zero voltage is defined as the voltage obtained from the transducer with no pressure applied . The transducer first needs a "warm-up" period so it's temperature stays constant. A computer run was made and 2000 points were taken for each transducer and averaged. This averaged voltage at atmospheric pressure was the zero voltage. It then had to be subtracted from the readings taken during an experiment. Table 3 represents data on all

transducers.

Displacement Transducer Calibration

The displacement transducer was calibrated with a 4 foot ruler. The determination of the zero voltages also applied to this transducer and is used in this investigation. However, the zero voltage is defined here as the voltage value when the cord of the transducer is initially extended.Calibration data for this unit is included in Table 3.

Table 3. Calibration Data

Serial number	Unit of measurement	Sensitivity (mv/unit)	Measurement made
Endevco 94CL	Psia	3.184268	Primary flow total pressure
Endevco WB80	Psia	3.407688	Secondary flow total pressure
Druck PDCR 22 130595	Psig	3.027971	Test section static pressure
Endevco 29DN	Psig	4.724331	Probes pressure
Research Inc. 3593	Inch	9.734965	Vertical displacement

VITA

Captain Benoit J. Durand [redacted] He immediately joined the Collège Militaire Royal de St-Jean, Québec. He was commissioned as a Second Lieutenant upon graduation from the Royal Military College of Canada, Kingston, Ontario in 1983, with a Bachelor's degree in Mechanical Engineering. He completed a year of training in Aeronautical Engineering maintenance at Canadian Forces Base Borden, Ontario. He has served as the Armament Support Officer for the Base Aircraft Maintenance and Engineering Organization at Canadian Forces Base Greenwood, Nova Scotia. He became a registered member of the Association of Professional Engineer of the Province of Nova Scotia in 1985. He entered the School of Engineering, Air Force Institute of Technology, in May 1987. Upon graduation, he is assigned to the directorate of Fighters, Trainers and Helicopters Engineering Maintenance, Armament Engineering at National Defense Headquarters, Ottawa, Canada.

[redacted]

UNCLASSIFIED
SECURITY CLASSIFICATION OF THIS PAGE

REPORT DOCUMENTATION PAGE

Form Approved OMB No. 0704-0188

1a. REPORT SECURITY CLASSIFICATION: UNCLASSIFIED	1b. RESTRICTIVE MARKINGS
2a. SECURITY CLASSIFICATION AUTHORITY	3. DISTRIBUTION/AVAILABILITY OF REPORT: Approved for public release; distribution unlimited
2b. DECLASSIFICATION/DOWNGRADING SCHEDULE	
4. PERFORMING ORGANIZATION REPORT NUMBER(S): AFIT/GAE/AA/88D-11	5. MONITORING ORGANIZATION REPORT NUMBER(S)
6a. NAME OF PERFORMING ORGANIZATION: School of Engineering; 6b. OFFICE SYMBOL (If applicable): AFIT/ENY	7a. NAME OF MONITORING ORGANIZATION
6c. ADDRESS (City, State, and ZIP Code): Air Force Institute of Technology (AU) Wright-Patterson AFB, OH 45433-6583	7b. ADDRESS (City, State, and ZIP Code)
8a. NAME OF FUNDING/SPONSORING ORGANIZATION: AF Aero Propulsion Lab.; 8b. OFFICE SYMBOL (If applicable): AFWAL/PS	9. PROCUREMENT INSTRUMENT IDENTIFICATION NUMBER
8c. ADDRESS (City, State, and ZIP Code): Wright-Patterson AFB, OH 45433	10. SOURCE OF FUNDING NUMBERS: PROGRAM ELEMENT NO. / PROJECT NO. / TASK NO / WORK UNIT ACCESSION NO.

11. TITLE (Include Security Classification)
INVESTIGATION OF THE FLOWFIELD CREATED BY THE INTERACTION OF A SONIC JET AND A CO-FLOWING SUPERSONIC STREAM

12. PERSONAL AUTHOR(S)
Benoit J. Durand, Captain, Canadian Forces

13a. TYPE OF REPORT	13b. TIME COVERED	14. DATE OF REPORT (Year, Month, Day)	15. PAGE COUNT
MS Thesis	FROM _____ TO _____	1988 December	138

16. SUPPLEMENTARY NOTATION

17. COSATI CODES			18. SUBJECT TERMS (Continue on reverse if necessary and identify by block number)
FIELD	GROUP	SUB-GROUP	
20	04		Supersonic Combustion, Base Flow, Shock Waves, Two-Dimensional Flow, Shear layer, Flow Mixing
21	01		

19. ABSTRACT (Continue on reverse if necessary and identify by block number)

Thesis Advisor: Dr. William C. Elrod
Professor of Aerospace Engineering

12 Jan. 1989

20. DISTRIBUTION/AVAILABILITY OF ABSTRACT	21. ABSTRACT SECURITY CLASSIFICATION
☒ UNCLASSIFIED/UNLIMITED ☐ SAME AS RPT. ☐ DTIC USERS	UNCLASSIFIED

22a. NAME OF RESPONSIBLE INDIVIDUAL	22b. TELEPHONE (Include Area Code)	22c. OFFICE SYMBOL
Dr. William C. Elrod	513-255-3517	AFIT/ENY

DD Form 1473, JUN 86 — Previous editions are obsolete. — SECURITY CLASSIFICATION OF THIS PAGE: UNCLASSIFIED

The flowfield characteristics created by a sonic flow expanding freely between two supersonic streams were investigated experimentally using optical and pressure instrumentation. The base flow produced by the expansion of the streams around the base regions is compared to experimental data and theory by Chow.

Furthermore, the shear layer created between the sonic and supersonic stream is studied using schlieren photographs and pitot pressure profiles. The growth of the shear layer is examined in an effort to explain the observed flow phenomenon.

It was observed that a shear layer crossing a shock wave spreads and increases its turbulence level. However, an undesirable loss in total pressure results and this could be undesirable.

It appears that Chow's theory on base pressure approximates the characteristics of the flow near the end of the nozzle assembly where the two flows initially interact. The same trends were observed in the behavior of base pressure with increasing secondary total pressure as Chow observed during his experiment.

The convective Mach number concept was successfully applied to the sonic injection geometry and it was demonstrated that the convective Mach number decreases drastically as the secondary pressure is increased. This is an indication that the growth rate of the shear layer increases, giving a faster mixing rate.